Investigating Thermal Healing for Glass Reuse

To what extent can thermal treatment enhance the strength of naturally aged glass, affecting their potential for reuse?

Niels de Vries

Delft University of Technology

TU Delft

Investigating Thermal Healing for Glass Reuse

To what extent can thermal treatment enhance the strength of naturally aged glass, affecting their potential for reuse?

by

Niels de Vries

to obtain the degree of Master of Science

at the Delft University of Technology,

to be defended publicly on Thursday, October 9, 2025 at 16:00.

Thesis committee:	Prof. Dr. Ir. P. C. Louter,	TU Delft, Chair
	PhD. J. Cupać,	TU Delft
	Prof. Dr. M. Overend,	TU Delft
	Dr. Ir. T. Bristogianni,	TU Delft
	Dr. K. C. Datsiou,	University of Hertfordshire
Lab assistants:	J. Hermsen,	TU Delft
	F.J.P. Schilperoort,	TU Delft
	A. Thijssen,	TU Delft

Place:	Faculty of Civil Engineering and Geoscience, Delft
Project duration:	February 10, 2025 – October 9, 2025
Student number:	5169348
Cover:	Image by Slashio Photography on Unsplash

TU Delft

Acknowledgements

This thesis marks the completion of my Master's degree in Civil Engineering at Delft University of Technology. I would like to express my sincere gratitude to everyone who supported me throughout this journey.

I am deeply grateful to my chair, Christian Louter, for his invaluable guidance, support and enthusiasm throughout the project. I especially appreciated his willingness to discuss questions at every stage, his insightful feedback and his hands-on assistance in the laboratory, always making time when it was most needed.

I would like to sincerely thank my supervisors, Jagoda Cupać, Mauro Overend, Telesilla Bristogianni and Corinna Datsiou, for their constructive feedback and valuable insights during the development of this thesis. The extensive feedback and guidance provided by all of you significantly improved the quality of this report. I am particularly grateful to Jagoda for guiding me at the beginning of the project and for always making time to discuss my work. I am also thankful to Corinna, whose research inspired me to pursue this direction and continues to motivate me to follow a similar path. I also appreciate Mauro for providing the scratching and the scalp device, which were essential tools in my research. I am especially grateful to Telesilla for her practical support in the laboratory. Without her help with the thermal treatment and the post-fracture microscopy, this report would not have been as complete.

I would also like to thank the laboratory staff, John Hermsen, Fred Schilperoort and Arjan Thijssen, whose technical expertise and support were crucial in the experimental phase of the project. Their assistance made the work both efficient and safe.

I would also like to note that in preparing this report, I used AI to assist with writing. It helped me check spelling and grammar, as well as refine passages that were harder to read.

Finally, I would like to thank my parents and close friends for their steady encouragement and support throughout this process. Their belief in me helped me stay focused and motivated. I am also grateful for the many conversations we had about my work, in which their thoughtful questions often inspired me to investigate further. Talking about the study with them gave me new things to reflect on and often sparked ideas that kept me curious and engaged.

Niels de Vries
Delft, October 2025

Abstract

The construction sector is a significant contributor to the CO_2 footprint in the Netherlands, emitting greenhouse gases that harm the global environment. To mitigate these emissions, all sectors must lower their CO_2 emission. In construction, an effective strategy is reducing the use of primary materials through component reuse. However, flaws in glass components often result in the replacement of the entire panel (Overend and Louter 2015).

This research focuses on reusing glass panels to reduce waste and CO_2 emissions. Through thermal treatment, aged glass could potentially be reused without compromising structural integrity. The glass used in this study is 15-year-old annealed soda-lime silica glass. The main research question is:

To what extent can thermal treatment enhance the strength of naturally aged glass, affecting their potential for reuse?

There are three additional research questions:

- To what extent do different thermal treatments influence the morphology of surface flaws?
- To what extent do different thermal treatments affect the strength of aged glass?
- To what extent do surface flaws and strength recovery after thermal treatment differ between naturally and artificially aged glass?

Naturally aged glass, developing surface flaws over time from environmental exposure and human activity, was studied alongside artificially aged glass to assess differences in surface damage and thermal treatment effects. Microscopy and image analysis showed that naturally aged glass treated at 500°C and 600°C exhibited no clear healing trend. Some surfaces seem to show improvements, while others developed more scratches. In contrast, artificially aged glass responded more consistently. Thermal treatment at 500°C caused minimal changes apart from occasional subcritical crack growth, while at 600°C, scratch width increased due to subcritical crack growth and a yellow discolouration occurred. Energy-dispersive X-ray spectroscopy revealed chemical changes on the air side of the glass, as the metal coating oxidizes during thermal treatment, altering the surface composition.

The strength of aged glass was evaluated using a coaxial double-ring test at 20 MPa/s, with results analysed via the 2-parameter Weibull distribution and weighted least squares regression. The tests revealed clear differences between naturally and artificially aged glass. Thermal treatment reduced the strength of naturally aged glass, with the 5% fractile decreasing by 28% after heating to 500°C and by 56% after heating to 600°C. In contrast, artificially aged glass improved, with the 5% fractile increasing by 13% after heating to 500°C and by 41% after heating to 600°C. SCALP-05 measurements assess surface stress in three groups: untreated glass, and glass treated at 500°C and 600°C. The average surface stresses measured were -6.49 MPa, -2.76 MPa, and -2.30 MPa. Although thermal treatment reduced surface stress, this effect was insufficient to influence overall strength conclusions.

The influence of thermal treatment on surface flaws differs notably between naturally and artificially aged glass. Microscopy showed minimal changes in naturally aged glass despite reduced strength, while artificially aged glass appeared visually worse but showed strength improvements in ring-on-ring testing. This is likely due to the primary failure mode: artificially aged glass is strengthened by healing of dominant scratches, whereas naturally aged glass is mainly affected by overall material weakening.

This research assessed whether thermal treatment could restore the strength of naturally aged glass for reuse in the construction industry. However, the results demonstrated that thermal treatment not only failed to enhance the strength of naturally aged glass but also caused a noticeable reduction in strength. Additionally, yellow discolouration occurred during thermal treatment. In conclusion, thermal treatment, as implemented in this study, compromised both the strength and appearance of naturally aged glass, limiting its feasibility for reuse in construction.

Contents

List of Figures

List of Tables

Nomenclature

Abbreviations

Abbreviation	Definition
CO_2	Carbon Dioxide
EDS	Energy Dispersive Spectroscopy
CDR	Coaxial Double Ring
SCALP	Scattered Light Polariscope
UV	Ultraviolet Light
SLSG	Soda Lime Silica Glass
DSC	Differential Scanning Calorimetry
Tg	Glass Transition Temperature
2P	Two Parameter
PAD	Anderson-Darling Goodness of Fit
SEM	Scanning Electron Microscope

Symbols

Symbol	Definition	Unit
$\dot{\delta}$	Displacement rate	[mm/s]
D_S	Diameter of support ring	[mm]
E	Elastic modulus	[MPa]
h	Thickness of the specimen	[mm]
$\dot{\sigma}$	Stress rate	[MPa/s]
σ_f	Stress at failure	[MPa]
F	Force at failure	[N]
ν	Poisson's ratio	[-]
D_L	Diameter of loading ring	[mm]
D	Diameter of the characteristic size of the plate	[mm]
l	Average edge length	[mm]
l_1	Length of specimen's edge in dimension x	[mm]
l_2	Length of specimen's edge in dimension y	[mm]

1

Introduction

The construction sector is a significant contributor to the CO_2 footprint in the Netherlands, emitting greenhouse gases that adversely affect the global environment. On a global scale, according to Westbroek et al. (2021), the glass industry produced 150 million tonnes of glass in 2014, resulting in approximately 86 million tonnes of CO_2 emissions, about 0.3% of total global CO_2 emissions. Around 42% of this output was flat glass and it is estimated that roughly 83% of this was used in the construction sector. To mitigate these emissions, EU member states have committed to achieving climate neutrality by 2050 and reducing greenhouse gas emissions by 55% by 2030 (Ministerie van Volkshuisvesting 2024). These goals form part of the EU's contribution to the Paris Climate Agreement, which aims to limit global temperature increases (Nations 2015).

Achieving these ambitious goals requires all sectors to reduce CO_2 emissions. In the construction industry, a particularly effective strategy is to minimise the use of primary materials by reusing components such as glass panels. However, in the building industry, flaws in glass components often result in the replacement of the entire panel to ensure that the panel meets the strength requirements (Overend and Louter 2015). Although efforts to reduce waste and promote material reuse are increasing, the quality of salvaged materials is often uncertain. Without reliable information on their properties, the reuse of these materials could pose safety risks.

This research focusses on the reuse of glass panels as a means of reducing waste and could potentially minimising the CO_2 footprint. Reusing glass panels can prevent them from being discarded or recycled. Through glass repair with a process called thermal treatment, salvaged glass panels can be safely reused without compromising their structural integrity.

1.1. Problem statement

The production of flat glass, widely used in façades and windows, is one of the more energy-intensive processes in the construction materials sector (Westbroek et al. 2021). Furnaces must reach temperatures of around 1500–1600°C to melt raw materials such as sand, soda ash, and limestone, resulting in significant carbon dioxide emissions from both fuel combustion and the decomposition of carbonates in the raw materials. Although glass can be recycled multiple times without compromising its quality, it predominantly follows a linear waste model rather than a circular one, leading to continued high consumption of raw materials and energy.

According to Veer et al. (2023), the lack of knowledge about the properties of weathered glass is currently a major barrier to glass reuse, leading to many architectural glass panels being discarded rather than reused. The strength of glass is highly sensitive to surface characteristics and over time the surface becomes damaged, leading to a reduction in strength. To ensure that glass can be reused, surface damage can be repaired. A potential repairing method could be thermal treatment, which has shown the ability to repair artificially aged glass but has not yet been validated on naturally aged glass (Datsiou, Bristogianni, et al. 2025). Thermal treatment could potentially repair larger areas of glass, allowing it to regain strength and be reused in new construction projects.

1.2. Aim and objective

The aim of this research is to determine the effect of thermal treatment on the strength of naturally aged glass and to assess whether surface defects can be repaired using thermal treatment. The temperature will be varied during the study to assess its impact on the thermal treatment process and the resulting glass strength. The findings may provide valuable insights into the potential for glass repair and contribute to reducing waste from discarded glass panels.

1.3. Research question

To what extent can thermal treatment enhance the strength of naturally aged glass, affecting their potential for reuse?

Additional research questions:

- To what extent do different thermal treatments influence the morphology of surface flaws?
- To what extent do different thermal treatments affect the strength of aged glass?
- To what extent do surface flaws and strength recovery after thermal treatment differ between naturally and artificially aged glass?

1.4. Outline

This research aims to evaluate the effect of thermal treatment on naturally aged glass. Due to the limited availability of literature on this topic, artificially aged glass was also tested to allow comparison with existing studies and to validate previous findings. Naturally aged glass has been exposed to environmental conditions during the lifetime of the window, potentially developing surface defects that reduce its strength. If the glass remains in relatively good condition, the effects of thermal treatment may be less noticeable. In contrast, the artificially aged glass is intentionally scratched. By comparing artificially aged glass to naturally aged glass, this study investigates whether glass with more severe flaws responds differently to thermal treatment than glass with micro-scale surface flaws.

The specific type of naturally aged glass used in the study is soda-lime silica glass, which is the most commonly used in the building industry and is also the most representative of the glass elements currently discarded from buildings (Karlsson et al. 2023) (Sofokleous 2022).

Surface characteristics are assessed using microscopy and mechanical strength is evaluated through destructive testing to determine the glass's potential for reuse in new construction. The thermal treatment process depends on the availability of furnaces, which might be a limitation of this research.

1.5. Research gaps

Most studies have focused on artificially aged glass, where surface damage is introduced using the Vickers indentation method. In contrast, naturally aged glass has not yet been examined, representing a significant research gap in understanding its response to thermal treatment. As noted by Zaccaria and Overend (2016), previous work has relied on artificial cracks, whereas testing naturally aged glass allows evaluation of realistic flaws and provides insight into how flaw populations evolve. Unlike artificially aged samples, which contain controlled damage, naturally aged glass exhibits a distribution of flaws across its surface, necessitating adjustments in microscopy and analysis, since evaluation extends beyond a single scratch to the entire ring area of the specimen. Because the healing behaviour of naturally aged glass remains unknown and cannot be directly compared with earlier studies, unanticipated behaviours may also emerge during testing, reflecting the unique and less predictable properties of this material. Beyond addressing this gap, further research is required to maximise the potential of thermal healing across different flaw types and severities, such as surface pits (Datsiou, Bristogianni, et al. 2025), with treatment parameters like introducing water vapour during heating or approaching the glass transition temperature, potentially enhancing viscous flow and improving the healing process. At the same time, careful consideration of the thermal treatment temperature is essential, as cycles above the glass transition temperature can induce substantial morphological changes and even alter the atomic structure, directly affecting overall treatment outcomes (C. Wang, H. Wang, Gao, et al. 2021).

2

Theoretical background

This chapter provides the theoretical background on various aspects relevant to this study. It begins with general information on the production process of glass and the resulting internal stresses, before explaining its properties and recyclability. The focus then gradually narrows to the glass transition temperature, followed by a review of previous studies on thermal treatment, which can be used to develop a methodology and later compare their results with those of this study.

2.1. Production process

The production process for windows and facade glass is called float glass process. Currently, the float process is the most popular primary manufacturing method and accounts for about 90% of today's flat glass production worldwide (Haldimann, Luible, and Overend 2008).

The production process of float glass is shown schematically in Figure 2.1. The raw materials are melted in a furnace at temperatures of up to 1550°C. The molten glass is then poured continuously at approximately 1000°C onto a shallow pool of molten tin, whose oxidation is prevented by an inert atmosphere consisting of hydrogen and nitrogen. Tin is used because of the large temperature range of its liquid physical state (232–2270°C) and its high specific weight in comparison with glass. The glass floats on the tin and spreads outwards, forming a smooth, flat surface at an equilibrium thickness of 6 to 7 mm. It is gradually cooled and drawn onto rollers before entering a long oven, called a lehr, at around 600°C. The glass thickness can be controlled within a range of 2 to 2.5 mm by adjusting the speed of the rollers. The annealing lehr slowly cools the glass to prevent residual stresses from being induced within it.

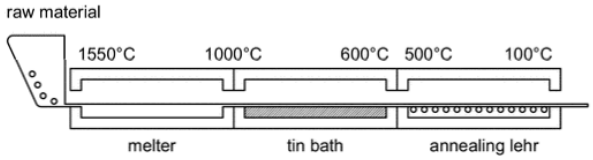

Figure 2.1: Production process for float glass (Haldimann, Luible, and Overend 2008)

As a consequence of this production process, the two faces of glass sheets are not completely identical. The strength of the tin side has been found to be marginally lower than that of the air side, due to contact with the transport rollers in the cooling area. The tin side can be identified by its bluish-white fluorescence when exposed to ultraviolet light (Haldimann, Luible, and Overend 2008).

2.2. Internal stressses

Float glass is produced at high temperatures and during cooling, the glass is slowly cooled in the annealing lehr to prevent residual stresses from being induced within the glass. If the glass is cooled too quickly, internal stresses can occur. This occurs because the surface of the glass typically cools

more rapidly than the interior, resulting in compressive stresses at the surface and tensile stresses within. These internal stresses increase the strength of the glass by resisting crack formation and propagation.

In Figure 2.2, the effect of internal stresses is illustrated. The outer surfaces of the glass are in compression, and this compressive prestress helps prevent cracks from forming or propagating. For the glass to fail, an applied load must first overcome this compressive prestress before the tensile stresses can cause fractures.

In this research, the effect of surface repair is investigated, which requires the internal stresses to remain comparable across samples. The glass used is annealed glass, which typically exhibits minimal to no surface stress. This characteristic must be considered when cooling the glass during thermal treatment, as faster cooling could unintentionally introduce surface stresses that affect the results.

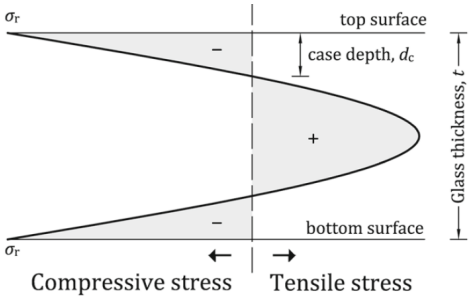

Figure 2.2: Stress profile thermal treated glass (Datsiou and Overend 2017b)

2.3. Properties

The intrinsic strength of glass is exceptionally high and may reach 32 GPa, based on the intermolecular bonds that are developed in the glass molecular network (Haldimann, Luible, and Overend 2008). However, the actual strength of glass is much lower. The engineering strength of glass is typically between 30 and 100 MPa. These strength values also correspond to measurements referred to in the EU standard EN 16612 (2019). The 5%-fractile bending strength (characteristic value) of short-term loaded glass is 45 MPa (Persson et al. 2020).

Glass is a brittle material whose strength is primarily determined by the presence of flaws on its surface (Persson et al. 2020). Naturally aged glass refers to glass that has been damaged during its service life (Datsiou and Overend 2017a). These surface flaws are created by weathering and localised damage. Damage due to weathering consists of two components: chemical corrosion and mechanical abrasion. Chemical corrosion includes the leaching of Na^+ ions from the glass by water and the breaking down of Si–O bonds by water under tension. Mechanical abrasion consists of pitting from impacts and scratches caused by the abrasion of hard particles moving over the surface (Veer et al. 2023)(Datsiou and Overend 2017b)(Rota, Zaccaria, and Fiorito 2023). A glass element fails as soon as the stress intensity, due to tensile stress at the tip of one flaw, reaches its critical value. Essentially, strength decreases as defect size increases. The size of the defect thus controls the engineering strength of annealed float glass (Veer et al. 2023).

The glass used in this research is soda-lime-silica glass. As the name suggests, it is primarily composed of soda ash (sodium carbonate, Na_2CO_3), limestone (calcium carbonate, $CaCO_3$), and silica (sand, SiO_2). A typical chemical composition of soda lime silica glass is shown in Table 2.1 and the material properties are shown in Table 2.2.

Table 2.1: Soda-lime silicate glass composition (Zaccaria and Overend 2016)

Chemical	Mass percentage (%)
SiO_2	69–74
CaO	5–14
Na_2O	10–16
MgO	0–6
Al_2O_3	0–3
Others	0–5

Table 2.2: Relevant soda-lime silicate glass properties (Haldimann, Luible, and Overend 2008)

Property	Symbol	Value
Density (kg/m3)	ρ	2500
Young's modulus (MPa)	E	70000
Poisson ratio (−)	v	0.23

2.4. Recyclability

While glass can be infinitely recycled without losing its durability, in practice only a small percentage of architectural glass is recycled. Studies on recycling of flat glass in Germany showed that almost 90% of flat glass waste generated in the building sector is recycled. However, only 11% is returned to the flat glass production, while the remaining glass is downcycled (Cupać, Datsiou, and Louter 2024). This indicates that the recycling steps within the glass lifecycle are often skipped, with most glass following a linear path toward end-of-life or transformation. As a result, the process deviates from the circular model illustrated in Figure 2.3 and resembles a more linear trajectory.

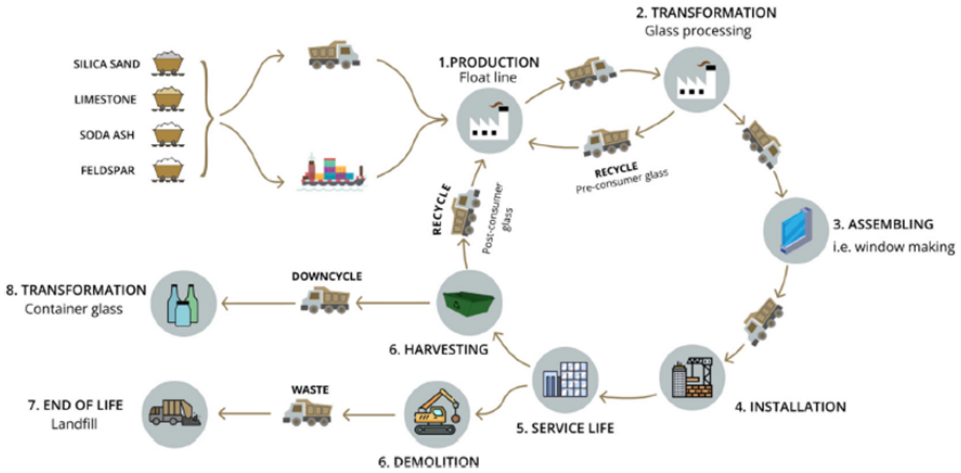

Figure 2.3: Waste cycle of glass (Teich et al. 2024)

A major barrier to glass reuse is the lack of knowledge about the properties of aged glass. The challenge of safe reuse lies in assessing the strength of glass that may be several years to several decades old. Over time, glass can become damaged due to environmental factors or human interaction, leading to a reduction in strength compared to its original condition. In order to assess the residual strength of aged glass, it is essential to quantify it in terms of defects (Sofokleous 2022).

2.5. Transition temperature

Thermal treatment is a method used to repair the surface of glass by heating it. For soda-lime silica glass, this transition typically occurs around 557°C (C. Wang, H. Wang, Gao, et al. 2021), while Haldimann, Luible, and Overend (2008) reports a slightly lower value of approximately 530°C, as shown in Table 2.3. At this point, glass begins to behave more like a viscous liquid, allowing the surface to soften and partially self-heal scratches and dents. The glass shifts from a hard, brittle state to a soft, rubbery one without melting. In the research by C. Wang, H. Wang, Gao, et al. (2021), the chosen thermal treatment temperatures were 500°C (≈0.9Tg) and 600°C (≈1.1Tg). In a more recent study by Datsiou, Bristogianni, et al. (2025), temperatures of 300 and 500 °C were used. Investigating thermal treatment both below and above this threshold can help clarify how phase transitions influence surface defect healing. Lower temperature can be used to investigate the potential of energy-saving solutions.

Table 2.3: Temperature of SLSG states (Haldimann, Luible, and Overend 2008)

State	Temperature (°C)
Working point	1040
Softening point	720
Annealing point	540
Transition temperature (Tg)	530
Strain point	506

The glass transition temperature can be determined using Differential Scanning Calorimetry (DSC), a thermal analysis technique that measures how a material absorbs or releases heat with changing temperature. DSC helps determine phase transitions such as melting, crystallisation, glass transition, and curing reactions.

2.6. Thermal treatment

Although research on thermal treatment is still developing, it shows potential for repairing the surface of artificially aged glass. Artificially aged glass meaning that controlled flaws are introduced by scratching the surface in a laboratory setting. The most common steps in these studies, apart from the thermal treatment itself, are microscopy and the ring-on-ring test. Microscopy is used to visually assess the surface condition, while the ring-on-ring test provides measurements of the glass strength. During thermal treatment, two key factors have been identified: the heating procedure and the humidity during thermal treatment. This section will review the existing literature to examine which steps are taken, how these steps have been applied and will later compare the results obtained from this study with those reported in previous studies.

Artificially aged glass

Previous studies investigated thermal healing of artificially aged glass, where controlled flaws were introduced to simulate realistic surface damage. This was typically achieved through scratching or indentation methods. For example, Datsiou, Bristogianni, et al. (2025) created artificial flaws on soda lime silica glass by scratching with a indenter before subjecting the specimens to different thermal treatments. Similarly, Blaeß and Müller (2023) introduced cracks using Vickers indentation to assess the healing effect of viscous flow at elevated temperatures. Schwind et al. (2020) prepared scratches on soda lime silicate glass using a diamond indenter to simulate production related damage before applying sub-toughening heat treatments.

Microscopy

Microscopic techniques were widely used to evaluate the evolution of cracks and subsurface damage during and after thermal treatment. Datsiou, Bristogianni, et al. (2025) showed through digital microscopy that scratches in glass treated at 300 °C exhibited only very minor changes compared to the untreated state, with features closely resembling the control samples apart from a slight rounding of crack edges which may indicate limited softening. In contrast, samples treated at 500 °C displayed clear visual improvements, with scratches appearing narrower and partially healed. Although not fully

eliminated, the reduction in scratch width indicates that viscous flow and partial thermal healing can occur even below the glass transition temperature. The extent of this improvement, however, was influenced by the initial severity of damage, with deeper flaws caused by subcritical crack growth showing little or no visual recovery.

Blaeß and Müller (2023) employed laser scanning microscopy and atomic force microscopy to characterize the geometry and depth of Vickers cracks, observing rounding and shallowing of the flaws after heating. The study further showed that healing depends on how radial and lateral cracks interact. When lateral cracks heal quickly, they prevent radial cracks from widening and bulging, allowing the overall crack system to close more efficiently. In contrast, if lateral cracks heal more slowly, radial cracks continue to widen, the surrounding material bulges, and even secondary cracks may form, which delays the healing process despite similar viscous transport conditions.

Zaccaria and Overend (2016) also used optical microscopy to assess edge flaw morphology before and after annealing, which supported their interpretation of strength increases as evidence of healing.

Ring on ring test

Several studies employed coaxial double ring tests to quantify glass strength after thermal treatment. Datsiou, Bristogianni, et al. (2025) noted that scratched glass lost up to 44% of its mean strength but regained 42% after treatment at 500 °C. It even exceeding the as-received strength at probabilities of failure = 0.008.

Zaccaria and Overend (2016) also used the ring-on-ring method to evaluate surface flaws in annealed glass, finding that annealed specimens exhibited strength recovery, with the greatest improvements observed at lower fractiles, highlighting that healing is especially relevant for design critical reliability levels.

In the study of Schwind et al. (2020), pre-damaged glass specimens subjected to heat treatment showed a clear increase in the mean fracture strength: treatment at 285°C led to an increase of approximately 12%, while treatment at 525°C raised fracture stress by about 41% compared to untreated specimens.

Heating Procedure

The heating procedure is the dominant factor in determining the effectiveness of crack healing. Datsiou, Bristogianni, et al. (2025) showed that heating scratched soda lime silica glass for three hours at 300 °C resulted in a 15% strength recovery, while treatment at 500 °C for the same duration yielded a 42% recovery. Blaeß and Müller (2023) confirmed that higher sub-transition temperatures promoted rounding and blunting of cracks, although complete healing was not achieved under their tested conditions.

In the research by C. Wang, H. Wang, Liu, et al. (2020), a detailed description of the heating process is provided. The procedure begins at room temperature, with the temperature increasing at a rate of 5°C/min. Once the target temperature is reached, it is maintained for a specific period of time. To reduce thermal stress generated during the cooling stage which may influence crack lengths, the cooling rate was set at 4°C/min. When the temperature reached 300°C, the oven was turned off, and the sample was allowed to cool to room temperature inside the furnace.

Schwind et al. (2020) tested scratched soda–lime silicate glass at around 285 °C and 525 °C, showing strength increases of 12% and 41%, respectively, indicating that higher temperatures are substantially more effective. In the study by Zaccaria and Overend (2016), a similar heating process is described. The temperature was increased from room temperature at a slower rate of 2°C/min, up to 560°C. The temperature was then held for two hours before being reduced at 2°C/min back to room temperature. It confirmed that annealing could enhance strength, particularly for polished edges, where improvements reached nearly 19% on average and 35% at the lowest fractiles.

Humidity

According to Girard, Faivre, and Despetis (2011), the viscosity of the glass surrounding cracks can be significantly reduced by water diffusion and glass hydrolysis. Hydration plays a major role in the changes observed in crack morphology during thermal treatment. According to C. Wang, H. Wang,

Gao, et al. (2021), the healing rate can be promoted by increasing both the heating temperature and water vapour pressure.

In the research by C. Wang, H. Wang, Liu, et al. (2020), water vapour pressure in the furnace was controlled by bubbling air through a deionised water bath kept at a set temperature, and then injecting it into the furnace with a steady flow. The water vapour pressure increased with the temperature of the water bath. Three different bath temperatures were used to achieve varying humidity conditions: 60°C for 150 mmHg, 80°C for 350 mmHg, and 97°C for 700 mmHg. In C. Wang, H. Wang, Gao, et al. (2021), four water vapour pressures were used, 0 mmHg, 150 mmHg, 350 mmHg, and 700 mmHg to investigate the effect on subsurface crack healing.

C. Wang, H. Wang, Gao, et al. (2021) also compared subsurface damage under dry conditions before and after the heating treatment. Even when the temperature reached 600°C, no significant healing of subsurface cracks was observed after two hours of heating under dry conditions. However, at 600°C, surface cracks did show limited healing, even without added humidity suggesting different behaviours for surface and subsurface cracks.

By contrast, Datsiou, Bristogianni, et al. (2025) observed that hydrothermal treatment, combining water soaking with thermal exposure at 500 °C, was counterproductive: it led to bubble-like defects and reduced strength gains compared to dry heat treatment. This suggests that while ambient humidity during heat treatment can aid viscous flow, prolonged pre-soaking promotes subcritical crack growth and should be avoided.

3

Research methodology

This chapter outlines the methodology followed in this research. The steps are presented in the order they were ultimately executed, although some procedures were adjusted during the course of the study. The chapter reflects the final methodology. Each section provides a detailed explanation of the step and its purpose. A brief summary of the main steps is provided below and illustrated in Figure 3.1.

1. Sample preparation & Tin side detection
2. Artificial ageing → Surface scratching
3. Microscopy and image processing (before & after treatment) → Surface defect analysis
4. Heat treatment → Thermal treatment of the surface
5. Destructive testing → Ring-on-ring strength testing
6. Statistical evaluation → Strength evaluation using the Weibull distribution
7. Energy-dispersive X-ray spectroscopy (EDS) → Surface elemental composition analysis
8. SCALP-05 → Surface stress assessment
9. Post-Fracture → Investigate the difference in glass behaviour

This research examines the effect of thermal treatment on both naturally aged (NA) and artificially aged (SC) glass. Consequently, the ageing and thermal treatment procedures vary between test groups. Panel 1 consists of four test groups, each tested on both the tin and air sides, with and without thermal treatment at 500°C.

- **P1_Tin_NA_REF** → Untreated glass tested on the tin side
- **P1_Air_NA_REF** → Untreated glass tested on the air side
- **P1_Tin_NA_500** → Glass thermal-treated at 500°C, tested on the tin side
- **P1_Air_NA_500** → Glass thermal-treated at 500°C, tested on the air side

Panel 2 includes six test groups, all tested on the tin side. Half of the samples were artificially aged, while the other half remained untreated. Each group was further divided into three subgroups: untreated, treated at 500°C and treated at 600°C.

- **P2_Tin_NA_REF** → Untreated glass
- **P2_Tin_NA_500** → Thermal-treated at 500°C
- **P2_Tin_NA_600** → Thermal-treated at 600°C
- **P2_Tin_SC_REF** → Artificially aged, untreated
- **P2_Tin_SC_500** → Artificially aged, thermal-treated at 500°C
- **P2_Tin_SC_600** → Artificially aged, thermal-treated at 600°C

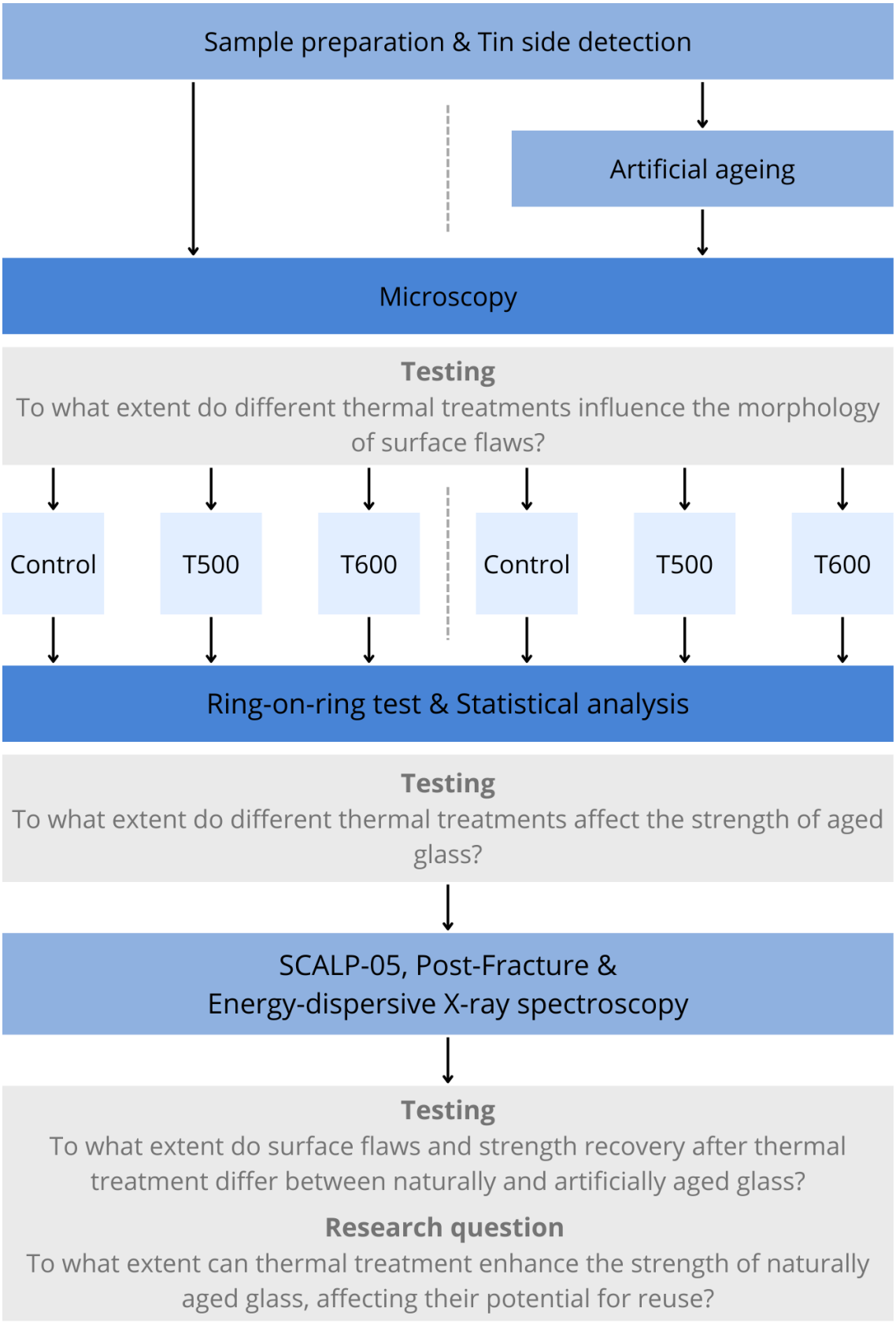

Figure 3.1: Flowchart methodology panel 2

3.1. Sample preparation

This section describes the procedures for preparing and handling the glass panels, covering their origin, dimensions, sample cutting, labelling, tin side identification and the random allocation of samples to various testing methods.

Information about the glass panel

This study is based on two glass panels retrieved from a 15-year-old building in Amsterdam provided by Christian Louter. The panels are composite units, comprising an exterior single-pane glass layer and an interior laminated glass panel. The exterior pane, a 8 mm thick Glaverbel Thermobel Energi N, was selected for analysis because it represents naturally aged glass, characterized by surface defects that developed over time due to environmental exposure and human interactions. A sketch of the glass panel is shown in Figure 3.2. The extent of surface damage depends on both the level and duration of exposure throughout the glass's service life (Datsiou and Overend 2017a).

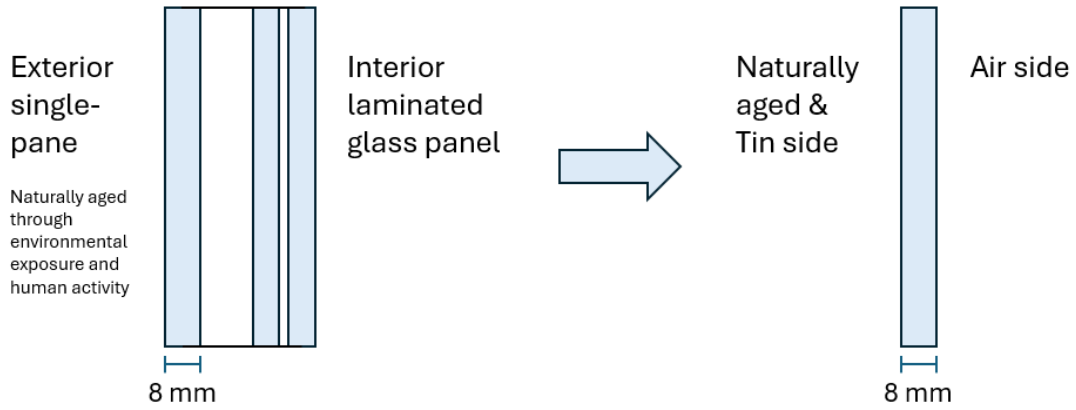

Figure 3.2: Cross section glass panel

Processing of the panel

The two glass panels were stored in a laboratory environment prior to processing. The original dimensions of panel 1 also called Amsterdam 3 and panel 2 also called Amsterdam 4 were 1.94 × 1.97 metres and 1.94 × 2.53 metres, respectively. To increase the number of test samples and to reduce the statistical uncertainty of the analysis, the glass was cut into smaller samples measuring 150 × 150 mm. Despite the reduction in size, the samples retain the essential material properties and characteristics of the original panels, and thus continue to represent real-world glass behaviour. To estimate the appropriate number of test groups, a sample size of 20 to 30 specimens per parameter was recommended by Christian Louter and Jagoda Cupać to obtain statistically reliable results. If fewer samples are taken per parameter, the likelihood of invalid tests due to a low p_{AD} or R^2 value increases.

To begin the separation process, the layered glass panels were disassembled by drilling holes at each corner. A jigsaw was then used to cut through the metal spacer and adhesive bonding the layers together. The top panel was carefully removed and the aged glass was placed on protective mats to prevent surface damage. Each panel was subsequently cut into squares measuring 15 × 15 cm. Given the brittle nature of glass, any existing weak point can lead to immediate fracture. To control the breakage, a scoring technique was employed: a straight edge was positioned across the panel, and the surface was lightly scored with a blade to establish a controlled fracture line. Different cutting methods were applied to the two panels. For the first, a light tap was delivered from beneath using a hammer following the scoring. For the second, the scored line was aligned with a support and pressed downward, allowing the glass to snap cleanly along the score. This process aimed to produce rectangular strips with a height of 15 cm, which could then be further divided into square samples. Illustrative images of the procedure are provided in Figure 3.3.

(a) Glass panel 1 **(b)** Cutting of the glass panel **(c)** Cutting squares

Figure 3.3: Samples preparation in the lab

Tin side

The mechanical strength of the tin side has been found to be slightly lower than that of the air side, due to its contact with the transport rollers during the cooling phase (Haldimann, Luible, and Overend 2008). It is therefore important to identify the tin side so that this difference in mechanical strength can be taken into account when compared with other studies.

The tin side can be identified using ultraviolet light, under which it appears as a white, milky layer. This effect is illustrated in Figure 3.4. In case of both panels, the tin side corresponds to the outer surface, which is also the naturally aged side also shown in Figure 3.2. This is the same surface on which the sample numbering has been applied.

Figure 3.4: Determining tin side

Samples results

Despite precautions, both panels did not always fracture cleanly. In many cases, cracks deviated from the score lines, resulting in smaller, irregular fragments. Where possible, these fragments were trimmed into 15 × 15 cm squares. The first panel, originally measuring 1.94 × 1.97 metres, could theoretically yield 156 samples. However, it produced only 106 usable samples, corresponding to a loss of approximately 32%. The second panel, measuring 1.94 × 2.53 metres, could theoretically yield 192 samples. It produced 170 usable samples, corresponding to a loss of approximately 11%.

Following the cutting process, each sample was numbered on the naturally aged side. Numbering began at the bottom-left corner of the panel and progressed from left to right. Each subsequent row continued sequentially from the final number of the previous row. Samples originating from panel 2 were prefixed with “2.” to indicate their source. However, cutting panel 1 proved particularly challenging, with many samples fracturing in unintended locations. As a result, a consistent numbering scheme could not be established for this panel, and its samples remained unnumbered. These unnumbered samples were later randomly distributed across different test methodologies.

The sample numbering and corresponding methodological assignments for panel 2 are illustrated in Figure 3.5. Methodologies were randomly assigned to the available samples using a Python randomisation script, as described in Appendix A. In total, 28 samples were assigned to each group, with two additional samples retained as backups.

181 - M1	182 - M5	Extra	184 - M3	185 - M5	186 - M6	187 - M3	188 - M5	189 - M5	190 - M3	191 - M6	192 - M2
169 - M6	170 - M6	Extra	172 - M4	173 - M4	174 - M3	175 - M2	176 - M6	177 - M5	178 - M6	179 - M4	180 - M1
157 - M5	158 - M5	159 - M1	160 - M3	161 - M5	162 - M1	163 - M3	164 - M1	165 - M3	166 - M3	167 - M1	Broken
145 - M1	146 - M3	147 - M2	148 - M5	149 - M1	150 - M1	151 - M6	152 - M2	153 - M5	154 - M6	Broken	156 - M2
133 - M4	134 - M4	135 - M6	136 - M6	137 - M3	138 - M1	139 - M3	140 - M2	141 - M5	142 - M4	143 - M3	144 - M2
121 - M4	122 - M1	123 - M4	124 - M3	125 - M1	126 - M6	127 - M4	128 - M5	129 - M5	Broken	131 - M6	132 - M4
109 - M5	110 - M5	111 - M4	112 - M1	113 - M2	114 - M2	115 - M6	116 - M2	117 - M3	118 - M5	119 - M6	120 - M1
97 - M6	98 - M3	99 - M3	100 - M2	101 - M4	102 - M4	103 - M2	104 - M3	Broken	106 - M3	107 - M6	108 - M4
85 - M6	86 - M6	87 - M5	88 - M4	Broken	90 - M1	91 - M1	92 - M3	Broken	94 - M5	95 - M1	96 - M1
73 - M1	74 - M5	75 - M4	76 - M1	77 - M4	78 - M1	79 - M5	80 - M2	81 - M5	82 - M2	83 - M4	84 - M2
61 - M5	62 - M5	63 - M6	64 - M1	65 - M4	66 - M3	67 - M2	68 - M3	Broken	Broken	71 - M6	72 - M3
49 - M5	50 - M4	51 - M2	52 - M6	53 - M2	54 - M4	55 - M2	56 - M3	57 - M3	58 - M2	59 - M6	60 - M2
37 - M6	38 - M3	39 - M1	40 - M4	41 - M2	42 - M1	43 - M4	44 - M3	Broken	46 - M2	Broken	Broken
25 - M4	26 - M6	27 - M4	28 - M5	29 - M3	30 - M6	31 - M2	32 - M2	Broken	Broken	Broken	36 - M2
13 - M4	14 - M1	15 - M6	16 - M4	17 - M4	18 - M5	Broken	Broken	Broken	22 - M2	23 - M6	Broken
1 - M2	2 - M5	3 - M1	4 - M6	5 - M5	6 - M1	7 - M3	8 - M1	Broken	Broken	Broken	Broken

Figure 3.5: Numbering and methodology of glass panel 2

3.2. Artificially ageing

As outlined in the methodology, some samples were subjected to artificial ageing. This step was added later to the methodology because the preliminary results from the naturally aged groups contradicted the expected outcomes based on previous studies on artificially aged glass, as stated in section 2.6. To confirm that the glass behaviour was consistent with the previously tested artificially aged samples, these specimens were also scratched to verify whether their results aligned with the literature studies.

Artificial ageing was introduced as a single controlled surface flaw using a scratching device, adapted from the one described by Datsiou, Bristogianni, et al. (2025). The scratches were applied to the exterior surface, corresponding to the naturally aged tin side of the glass samples.

The glass was placed into a custom setup, shown in Figure 3.6a, with the naturally aged side facing upwards. The scratching device was carefully positioned on the glass at the desired location. A mass was placed on top of the device to ensure that the load was consistent for every scratch. To ensure consistent placement, the scratches were made centrally on each specimen. This alignment was critical to ensure the flaw was located at the centre of loading during the ring-on-ring strength tests. A custom setup was developed in which the scratching device was guided along a wooden frame, allowing the operator to produce uniform linear scratches of 10 mm in length.

The scratching device shown in Figure 3.6b featured a 90° tungsten carbide tip with a radius of 120 µm, also used in Datsiou, Bristogianni, et al. (2025). The tip was mounted on a platform with a total load of 1.6 kg, including a 1.0 kg mass on top. The device was manually moved across the surface in a controlled sliding motion to ensure reproducibility across all scratched samples.

(a) Setup

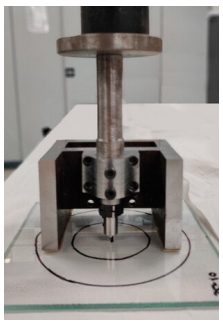

(b) Scratching device (Datsiou, Bristogianni, et al. 2025)

Figure 3.6: Scratching device and setup

3.3. Microscopy

The strength of glass is highly sensitive to surface flaws, as such flaws significantly reduce its mechanical performance. Therefore, it is essential to assess the condition of the glass surface. In this study, the Keyence VHX-7000 digital microscope at TU Delft was used to examine the test specimens. The microscopy setup is shown in Figure 3.7. This high-resolution microscope, connected to a monitor, provides live imaging of the samples under investigation and supports magnifications ranging from 20× to 3000×. It also allows for precise measurement of surface defects. Previous studies have used this microscope at magnifications of 20× and 50× (Verberg and Technology 2024).

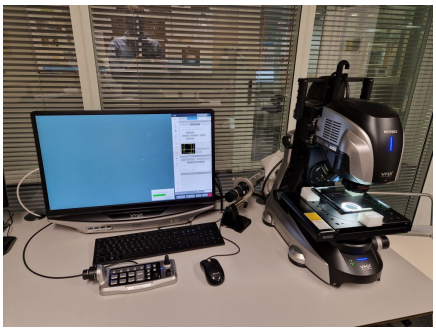

Figure 3.7: Microscopy setup

Microscopy was conducted twice during this study to examine the glass surface before and after thermal treatment. These images were used to investigate differences resulting from the thermal treatment. Due to the time intensive nature of microscopy, five samples per treatment method were selected for analysis. The sample IDs chosen for microscopy are listed in Table 3.1.

Table 3.1: Sample ID for microscopy

Methodology	sample ID				
P2_Tin_NA_500	S51	S55	S67	S113	S140
P2_Tin_NA_600	S29	S68	S92	S124	S163
P2_Tin_SC_500	S5	S74	S81	S128	S158
P2_Tin_SC_600	S15	S59	S71	S119	S154

For artificially aged samples, the focus was placed specifically on the scratch area. For naturally aged samples, the analysis concentrated on the area within the loading ring, as the locations of surface flaws were initially unknown. The area was scanned using an image stitching method supported by the microscope's software. Prior to scanning, boundaries were set to define the region of interest, allowing the microscope to capture the entire area. To accurately align the scanned region with the ring diameter, a circular paper mould was used to define the scanning boundaries. This mould was removed before scanning as the microscope captures square images of the specified area and this would results in the microscope scanning the paper otherwise. Focus was maintained on the top surface and the z-range was set to small, although this proved challenging due to the glass's transparency. In some cases, faint scratches observed on the images which may have originated from the opposite side. The microscope's autofocus function assisted in maintaining consistent focus throughout the scan. Following scanning, visible flaws were manually marked in the images. Each scan was carefully reviewed to identify significant scratches that could be monitored throughout the repair process.

Microscopy procedure

- Clean the glass samples to remove any dust or debris from the surface.
- Position the sample under the microscope using styrofoam blocks.
- Begin imaging at 50× magnification and focus on the upper surface of the sample.

- Perform a 2D serial scan using a paper mould to define the scanning area. This allows the software to automatically stitch together the full surface image. Save this unedited image under the correct filename.
- Create a duplicate of the stitched image for further analysis, such as zooming in and manually marking surface flaws.
- Use 50× magnification or higher to measure and assess individual defects.

3.4. Image processing

The glass samples were examined using a digital microscope, as described in section 3.3. The resulting images were acquired with the objective of assessing the surface condition of the glass both prior to and after the thermal treatment. For both the P2_Tin_NA_500 and P2_Tin_NA_600 groups, five samples were selected on which image processing was applied. This was necessary because the area of interest was too large to be assessed manually. In contrast, for the artificially aged glass, the area of interest was much smaller and more easily identifiable. Therefore, image processing was not applied.

Initial attempts to analyse the images were carried out using the software included with the microscope. However, this process proved to be labor intensive and susceptible to user bias and error. Consequently, alternative approaches were explored to enable more consistent, reproducible, and automated analysis.

ImageJ is used which is an open-source image processing and analysis software developed by the National Institutes of Health (NIH). In this study, ImageJ was employed to enhance image quality and detect surface defects. To ensure repeatability and efficiency, a macro was used to automate the analysis, allowing the processing of multiple microscopy images in a standardised manner. The macro used in this research is shown in section A.2.

The macro followed a series of defined steps:

1. Each image was imported and converted to 8-bit grayscale format to facilitate processing.
2. Contrast enhancement was applied to improve the visibility of surface features. This produced an initial enhanced version, although still affected by noise, revealed many of the surface flaws.
3. The enhanced image was then duplicated to preserve the contrast-adjusted version.
4. The duplicate image was further processed using thresholding techniques to generate a binary (black-and-white) image that emphasized larger defects and surface disruptions.

It is important to note that this final binary image often excluded smaller imperfections due to the loss of fine detail during thresholding. Therefore, both the contrast enhanced image and the binary version were used in the comparative assessment of the glass surface condition. An example of all the processed images is shown in Figure 3.8.

(a) S55

(b) S55 thermal treated

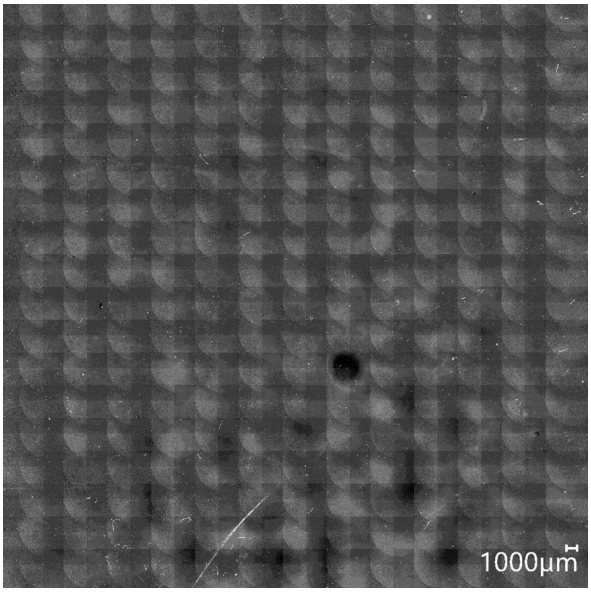

(c) S55 with contrast enhanced

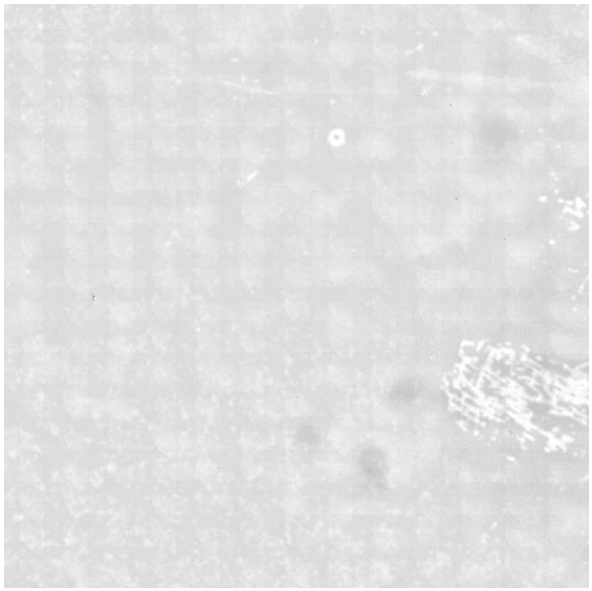

(d) S55 thermal treated with contrast enhanced

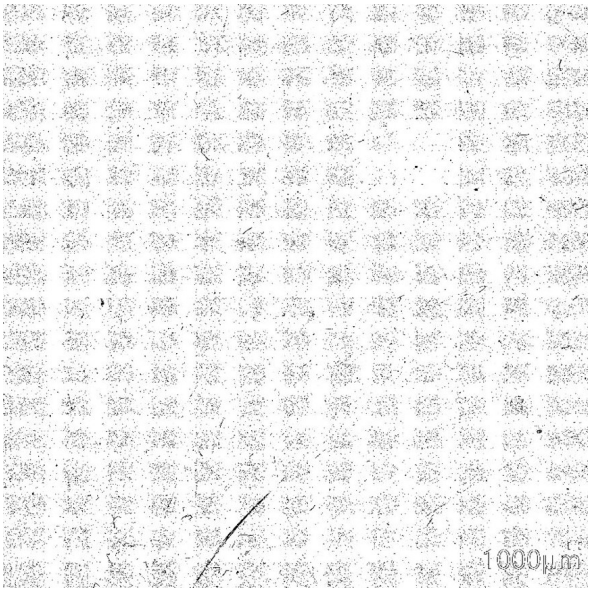

(e) S55 with image processing

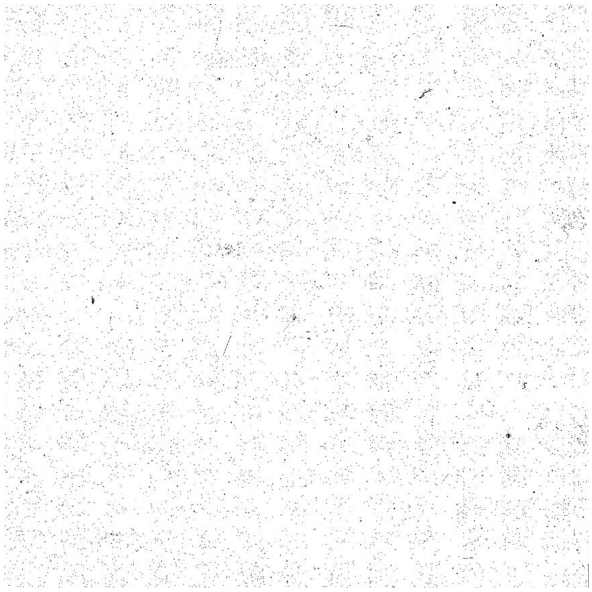

(f) S55 thermal treated with image processing

Figure 3.8: Overview of the S55 samples before and after thermal treatment with imaged processing

3.5. Thermal treatment

This section describes the thermal treatment procedure applied to the samples. The treatments were carried out using a Rohde large glass oven located in the Civil Engineering laboratory. The oven's base plate measures approximately 80 cm by 100 cm, allowing up to 30 samples to be treated simultaneously.

There are two parameters of interest to vary as explained in section 2.6 which are temperature and humidity. In this research, the temperature was varied. Controlling humidity was not possible due to limitations of the oven. Two temperature profiles were employed: 500 °C and 600 °C. The oven was programmed to follow predefined heating profiles, with heating and cooling rates chosen to minimise thermal shock and reduce the development of internal stresses caused by rapid temperature changes.

Samples were placed in the oven facing upwards with the surface undergoing healing. All samples fit within the oven, as illustrated in Figure 3.9a. Due to the elevated temperatures, surface markings were burnt off during treatment. Following thermal treatment, samples were renumbered and carefully stored to prevent surface damage.

Thermal treatment at 500 °C

For the first treatment, samples were heated to 500 °C following a three-stage profile: heating, holding, and cooling. The temperature was raised from room temperature to 500 °C at a rate of 80 °C per hour. After holding at 500 °C for three hours, samples were cooled back to room temperature at the same rate. The complete heating profile is presented in Figure 3.9b.

Thermal treatment at 600 °C

The second treatment involved heating the samples to 600 °C, exceeding the glass transition temperature. The temperature was increased from room temperature to 600 °C at 80 °C per hour. After maintaining this temperature for three hours, the samples were cooled to room temperature at the same rate.

(a) Samples in the oven **(b)** Heating profile 500°C

Figure 3.9: Oven treatment 500°C

3.6. Coaxial double-ring test

The strength of glass can be determined using a coaxial double-ring test, which is widely used to measure the biaxial flexural strength of brittle materials such as glass. The ring-on-ring tests are conducted in the Microlab using the Unitronic 50 kN universal testing machine. The machine and the controlling computer are illustrated in Figure 3.10. This press is computer controlled and is capable of recording force, displacement and time throughout the test procedure. In addition, optional sensors can be installed to monitor environmental parameters such as relative humidity and temperature.

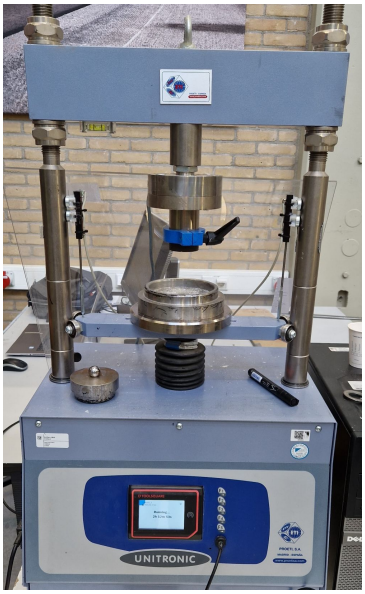

(a) Ring on ring setup

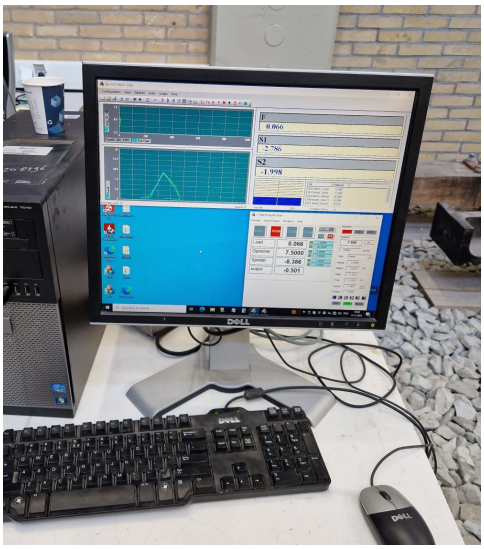

(b) Ring on ring controls

Figure 3.10: Ring on ring test

According to Datsiou and Overend (2017b), fast stress rates of 20 MPa/s were chosen for annealed glass to induce rapid fracture and thus minimise the effect of subcritical crack growth. Since the machine was operates based on displacement control, this stress rate must be converted to a displacement rate, as shown in Equation 3.1, following the guidelines provided in (International 2019).

$$\dot{\delta} \cong \left(\frac{D_S^2}{6Eh} \right) \dot{\sigma} \tag{3.1}$$

$\dot{\delta}$ [mm/s] = Displacement rate
D_S [mm] = Diameter of support ring, 60 mm
E [MPa] = Elastic modulus (for soda-lime silicate glass, 70000 MPa (NEN-EN 1288-1, 2000)
h [mm] = Thickness of the specimen
$\dot{\sigma}$ [MPa/s] = Stress rate, 20 MPa/s

Before testing, a thin adhesive foil is applied to the specimens to hold the fragments together after fracture, allowing analysis of the fracture origin. This foil is placed on the opposite side of the surface being tested. Once the foil is in place, the sample is positioned with the test surface facing downwards and the foil facing upwards.

The results are only valid when the initial crack occurs within or directly on the loading ring. This is because the stress distribution is measured inside the ring. If the failure occurs outside this region, the applied force does not correspond to the stress state measured by the machine. A reference ring is drawn onto the glass when the sample is placed in the machine. Due to the thickness of the marker used, this drawn ring is slightly larger than the actual loading ring. As a result, if failure occurs on the black line, it may in fact lie outside the loading ring. In Figure 3.11, four possible scenarios are illustrated.

(a) Inside loading ring

(b) On loading ring

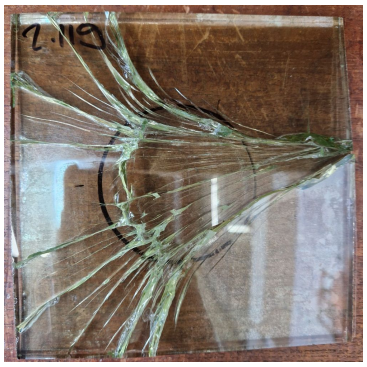

(c) Outside loading ring

(d) Not determined

Figure 3.11: Location of failure ring test

Testing Procedure for CDR Tests

The CDR tests were carried out in the same manner for each specimen, following the procedure described by Verberg and Technology (2024). Each sample was first placed on the support ring and carefully positioned so that its centre aligned with the centre of the ring. The loading ring was then placed on top of the specimen, ensuring it was centred directly above the support ring. To prevent movement, the sample was clamped between the rings. Although this clamping may have introduced a small initial load, its primary purpose was to secure the sample rather than to apply a specific preload. In practice, this also meant that the test commenced almost immediately, as the load began to increase as soon as the press was initiated.

Once positioned, the outlines of the loading and support rings were marked to verify proper alignment. The displacement was then set to zero, while force and time were automatically reset with each new measurement. Temperature and relative humidity were not controlled and therefore not reset. The measurement process began prior to activating the press to ensure complete recording of the test, with the software capturing 100 data points per second for each variable.

The press was then activated, moving at the predetermined displacement rate specified for the test series. If a specimen failed, both the press and the recording were stopped immediately. Following failure, the origin of the crack was determined and the validity of the test assessed. Crack origins were categorised as occurring inside the ring (IR), at the loading ring (LR), outside the ring (OR), or as not detectable (ND).

Analysis of the results

The stress at failure was not measured during the test so it must be calculated using Equation 3.2 from (International 2019). D needs to be calculated with Equation 3.3 and l can be calculated with Equation 3.4.

$$\sigma_f = \frac{3F}{2\pi h^2}\left[(1-\nu)\frac{D_S^2 - D_L^2}{2D^2} + (1+\nu)\ln\left(\frac{D_S}{D_L}\right)\right] \tag{3.2}$$

$$D = \frac{l}{0.90961 + 0.12652\frac{h}{D_S} + 0.00168\ln\left(\frac{l-D_S}{h}\right)} \tag{3.3}$$

$$l = 0.5(l_1 + l_2) \tag{3.4}$$

σ_f [MPa] = Stress at failure
F [N] = Force at failure
h [mm] = Thickness of the specimen
ν [−] = Poisson's ratio (for soda-lime silicate glass, 0.23 (NEN-EN 1288-1, 2000)
D_S [mm] = Diameter of support ring, 120 mm
D_L [mm] = Diameter of loading ring, 60 mm
D [mm] = Diameter of a circle which expresses the characteristic size of the plate for a rectangular
l [mm] = Average edge length (calculated as $l = 0.5(l_1 + l_2)$)
l_1 [mm] = length of specimen's edge in dimension x
l_2 [mm] = length of specimen's edge in dimension y

Experimental data

After testing, the data files can be exported and processed using a custom Python script. The force was measured directly by the testing machine, while time recording began simultaneously with the start of the measurement. Strain was monitored using two strain gauges positioned on either side of the machine. This script is shown in Appendix A in section 'Data files ring on ring test analysis'. This script extracts key parameters from each file, including the maximum force and the final recorded force. During some tests, the force displayed by the machine did not return to zero at failure, even though this should have been the case, as the machine was moving freely without resistance from the glass. This discrepancy was caused by an offset in the machine, which required correction afterwards. Consequently, any residual force recorded after testing was adjusted to ensure an accurate determination of the maximum force.

To estimate the time and strain at failure, the script identifies values at the point of maximum force as well as at a predefined threshold force earlier in the test. These points allow for linear extrapolation back to the origin of the loading curve. This method is used because the start of the test curve is often unclear with a lot of noise. However, since the loading phase generally follows a linear trend, extrapolation provides a reasonable estimate of the test duration and corresponding strain at failure.

In addition to extracting numerical values, the failure location of each sample is also assessed. If the failure occurs within or on the loading ring, the test is considered valid and the corresponding strength value is retained for analysis. Conversely, if the failure occurs outside this area, the result is excluded from the dataset.

3.7. Statistical evaluation of failure stresses

The strength of the glass samples is analysed using a Weibull distribution, a widely adopted statistical method for modelling variability in material strength. For this analysis, the *Open GLASSlab – Interactive Strength Analysis Handbook* (Cupać, Louter, et al. 2025) is used, which provides a Python script for Weibull-based evaluation. The method applied is the 2P Weibull distribution combined with weighted least squares regression. The strength of each sample is determined using the formula described in section 3.6. The Python script requires the strength values and corresponding failure times for each sample. Within the Open GLASSlab, there is an option to plot the equivalent failure stress for a selected reference period. This is also added to investigate what this reference time would do to the results. A reference time period of 5 seconds is applied.

Evaluation procedure

- Sort the stress at failure for each specimen in increasing order of magnitude: σ_i, where i is the rank number.
- Calculate the probability of failure $P_{f,i}$ for each measured value. Use the following estimator: $P_{f,i} = \frac{i-0.5}{n}$ (Hazen's probability estimator), where n is the number of tested samples.
- Put the Weibull distribution into linearized form. Enter the measured data into the Weibull mesh.
- Fit the data by Weighted Least Squares Regression. Find the slope, the intercept, and the coefficient of determination R^2, coefficient of variation COV and the Anderson Darling goodness of fit metric p_{AD}.
- Calculate the confidence interval CI.
- Determine the Weibull parameters β (shape parameter) and θ (scale parameter).
- Determine the desired fractile value of the bending tensile strength f_y using the regression line and using the confidence interval. In the case of the confidence interval, the target goal seek is used.
- Plot the cumulative distribution function $F(x)$ and the density function $f(x)$.

The input required for the code includes the names of the datasets, the measured failure strengths, and the corresponding failure times for each sample. The target stress fractile is set to 0.05, and the desired confidence interval is 0.1. Additionally, the lower and upper x-axis limits are both set to 0, allowing the script to determine appropriate values automatically based on the dataset.

The script provides detailed outputs, including calculated failure stresses, standard error and the Anderson-Darling goodness of fit metric (p_{AD}), offering insights into the strength distribution.

3.8. Energy-dispersive X-ray spectroscopy

The chemical composition of the glass samples was determined using Energy-dispersive X-ray spectroscopy, an analytical technique used to identify the elemental composition of a material. EDS operates by analysing the X-rays emitted when a sample is bombarded with a focused beam of electrons in a scanning electron microscope. Since each element emits X-rays at characteristic energies, EDS allows for accurate identification of the elements present. For this study, a FEI Quanta 650 FEG SEM equipped with EDS, located in the Civil Engineering laboratory, was used. The SEM with EDS is shown in Figure 3.12a with the results visible in Figure 3.12b.

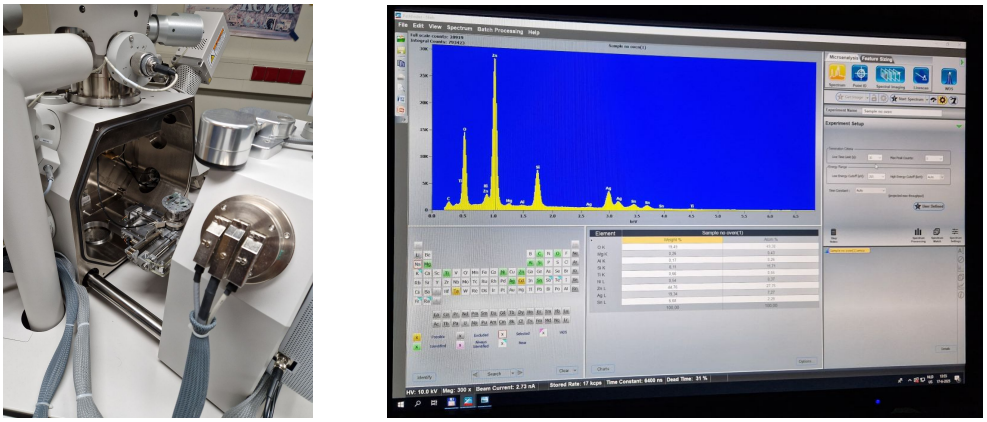

(a) EDS setup **(b)** EDS screen

Figure 3.12: Energy-dispersive X-ray spectroscopy

This step was included in the methodology due to the appearance of a yellow discolouration on the samples after thermal treatment. It was suspected that this may be related to a coating present on the glass surface. Therefore, the surface was scanned, and its elemental composition was analysed to investigate the cause of the discolouration.

The test was conducted on various glass samples subjected to the different thermal treatments used in this study, including non-treated, treated at 500°C, and treated at 600°C. Additionally, glass from a separate study was included. This uncoated glass was either non-treated or treated at 600°C, resulting in a total of five test groups. All groups were tested on both the tin side and the air side of the glass, producing ten measurements in total.

3.9. SCALP-05

This step was added later to the methodology to investigate why the preliminary results from the naturally aged groups contradicted the expected outcomes based on previous studies of artificially aged glass. Consequently, measurements were performed on the larger remaining shards, as the samples had already undergone destructive testing.

The study focused on the effect of thermal treatment on glass. Variations in the cooling phase during thermal treatment can lead to changes in internal stresses, which may influence the mechanical strength of the glass either positively or negatively. Therefore, to isolate the effect of thermal treatment, internal stresses were assessed on the samples from the groups: non-treated, treated at 500°C, and treated at 600°C.

SCALP 05 is a portable scattered light polariscope used for depth wise stress measurement in sheet glass. The device, shown in Figure 3.13, consists of a diode laser, optics and a camera. It is connected to a computer via USB, where dedicated software performs data recording and stress calculation.

Before starting the measurements, several settings need to be entered into the software. The C value, expressed in TPa(-1), was set to 2.72, which corresponds to soda lime silicate glass. The glass thickness was entered as 8 mm, and the measurement depth was set to 2 mm, to use approximately 25 percent of the total thickness. This is based on the recommendation of Dr.ir. F.A. Veer, Associate Professor at Delft University of Technology, who lend me this device. The fit type was set to a global fit using a third order polynomial.

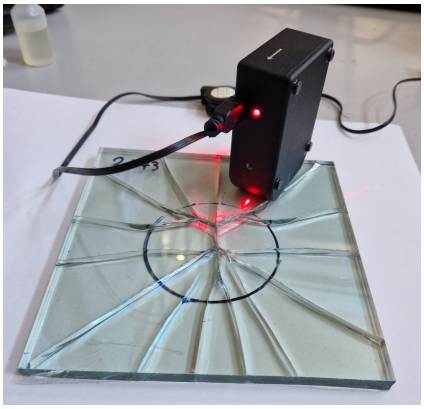

Figure 3.13: SCALP setup

The measurement process involves cleaning the glass surface, applying a drop of immersion liquid, placing the SCALP device on the measurement spot, and starting the measurement in the software. Each measurement produces a stress profile in about three seconds. Each location was measured five times, and in some cases more measurements were performed to improve the fit quality. The total amount of measurement per sample are shown in Table 4.6, Table 4.7, and Table 4.8 behind the sample ID. In total, 6 samples per thermal treatment are tested.

The device is sensitive to errors caused by slight movement during measurement, the presence of dirt or residue on the glass surface or the light present in the room. These issues can affect the quality of the data and lead to faulty readings. These effect were minimize by cleaning the sample and placing a box over the sensor to remove any light. The software displays indicators such as excluded pixels and fit error. These had to show a green status and be as low as possible to ensure reliability. Measurements with poor fit quality were excluded from the dataset.

3.10. Post-Fracture

The post-fracture step in the methodology is also added due to conflicting results after analysing the results of the ring on ring test. This section presents additional investigations into failure patterns, stiffness measurements and post-fracture microscopy. These steps aim to provide more insight into the different behaviour of the naturally aged glass compared to the artificially aged glass.

3.10.1. Failure pattern

To investigate the fracture behaviour, the broken glass samples were examined after failure. The analysis focused on identifying fracture origins and characterising the resulting crack patterns. Particular attention was given to the influence of different thermal treatments on the development of these failure features.

3.10.2. Stiffness

During this research, the ring-on-ring test was performed to evaluate the strength of the samples and assess the effect of thermal treatment. While the primary outputs for statistical analysis were force and time, the testing machine operated under displacement control and displacement data was also recorded. This data allows for the determination of the stiffness of the glass, which might be influenced by thermal treatment. Stiffness is defined as the load divided by the displacement of the sample. It should be noted that displacement is measured using two sensors on the machine itself rather than on the glass, which may influence the results and that these measurements include movement of the entire test setup. As a result, the absolute stiffness values could be less accurate. Therefore, the stiffness values in this study should be interpreted comparatively, not as precise material properties, but can be used for comparison within this study.

To analyse the stiffness, a Python script was used which is shown in Appendix A, following a procedure similar to that described in section 4.4. Load versus displacement curves were generated, and a

trendline was fitted to each dataset. These trendlines were manually reviewed to ensure an accurate fit. Since the initial portion of the test data often exhibited noise and disturbance, a minimum force threshold was applied to exclude the early, unreliable data points. The slope of the fitted trendline corresponds to the stiffness value, which was extracted for all samples.

3.10.3. Microscopy

Post-fracture microscopy is used to identify the failure origin and better understand the underlying cause. When glass fractures, it typically initiates at a weak point and propagates outward. The area surrounding this initiation point often breaks very smoothly before the crack accelerates and produces rougher fracture patterns. This smooth zone is known as the mirror region, which is clearly visible under a microscope. Adjacent to the mirror area is the mist region, which appears as a frosted or hazy zone on the fracture surface. It marks the transition from slow, stable crack growth to faster propagation and reflects the acceleration phase of the fracture process (Quinn 2020).

The mirror region always surrounds the point of fracture initiation and serves as a key indicator of the stress level at failure. Its size is inversely proportional to the applied stress: a larger mirror suggests lower fracture stress, while a smaller mirror indicates higher stress. A well-defined, circular mirror generally implies a tensile fracture, often caused by bending or uniform tension, while a distorted or asymmetric mirror may indicate mixed-mode loading, edge contact, or other complex stress conditions. The mirror region can also reveal the type of flaw that initiated the break. A single, concentrated origin often points to a pit, while a linear pattern of damage may indicate a surface scratch as the cause of failure.

Images from the post-fracture analysis are shown in Appendix D, and the experimental setup is illustrated in Figure 3.14. It is important to note that in these images, the bottom of the fracture surface corresponds to the outer surface of the glass sample, since you are viewing a cross-section.

Figure 3.14: Post fracture setup

4

Results

This chapter provides further insight into the effects of thermal treatment on both naturally and artificially aged glass. Visual differences are examined using microscopy, while mechanical strength is evaluated through ring-on-ring testing. In addition, the chemical composition and surface stress are analysed. Post-fracture results are also presented to provide a deeper understanding of glass behaviour.

4.1. Microscopy

The naturally aged and artificially scratched samples were scanned as described in section 3.3. The resulting images are presented in Appendix B. For the samples without an artificial scratch, stitched images were produced at 50× magnification. Each image was enhanced using a two-step process in ImageJ, as outlined in section 3.4, resulting in two additional images per sample: one enhanced and one defect-detection image. This produced a total of three images per sample both before and after thermal treatment, all of which are included in Appendix B. The images with artificial scratches are scanned at a zoom of 100x. This scan is only made of the area which was scratched. These image sets were visually compared to assess changes in surface condition. For each sample, observations were recorded to support the evaluation of thermal treatment effects. Table 3.1 lists the sample IDs used for microscopy, along with their corresponding methodology. The lighting conditions were consistent for all samples, provided by a full-ring light positioned above the microscope. The samples were placed on the microscope's bottom plate, which had a black surface.

4.1.1. Image processing

A custom macro for image processing was tested on untreated samples **S6**, **S73**, **S78**, **S120**, and **S150**, which served as a baseline for assessing the software's reliability and accuracy.

In several cases, the detection images revealed scratches that had been overlooked during manual inspection but were later confirmed in the original unmarked images. This suggests that the software is capable of identifying subtle surface flaws that may escape visual detection. A potential challenge is that scratches on the rear side of the glass may be misidentified as surface flaws, particularly during image processing, where differences in contrast could lead to misinterpretation of a scratch on the back as one on the front. To mitigate this effect, the depth-up function was applied with a minimal z-range. In at least one case, the software successfully filtered out rear-surface features, demonstrating its effectiveness. Because these samples had not undergone thermal treatment, they remained clean, an important factor in achieving reliable image processing. The results emphasised that sample cleanliness is critical, as dust or debris can easily be misidentified as defects.

Overall, the image processing method proved effective and shows strong potential for reducing human error in manual microscopy. It improves both accuracy and efficiency by enabling automated flaw detection. However, reliable results depend heavily on sample cleanliness. Further refinement of microscopy settings could enhance the robustness and consistency of the approach.

4.1.2. Naturally aged thermal treated samples at 500 degrees

The samples were scanned before and after the 500°C thermal treatment to assess changes in surface characteristics. Microscope images of these samples were analysed using image processing techniques explained in section 3.4 to detect and compare surface defects. Both contrast and detection images were used for analysis, as in some cases, the contrast image provided clearer results than the detection image. The samples included in this group are: **S51**, **S55**, **S67**, **S113** & **S140**. The complete set of images can be found in Appendix B: Figure B.1, Figure B.2, Figure B.3, Figure B.4 and Figure B.5.

An interesting case is illustrated in Figure 4.1 and Figure 4.2. In the detection image of sample S51, no significant scratch is visible before thermal treatment. However, after treatment, a distinct scratch appears in the bottom right region. This suggests that the scratch may have developed either as a result of the thermal treatment itself or due to handling during the process. Another plausible explanation relates to the condition of the samples after thermal treatment. The samples were sometimes dirtier and difficult to clean completely. Consequently, the microscopy images may contain spots of dirt that obstruct light transmission. This could introduce errors in the image processing, as the software may interpret these dirt spots as scratches. In contrast, sample S55 shows the opposite effect. A visible scratch in the bottom left area before treatment is no longer present after thermal treatment, indicating that the scratch may have been successfully healed. These two cases demonstrate that thermal treatment could both potentially introduce new surface flaws and contribute to the healing of existing ones, assuming the handling of the samples did not damage sample 51.

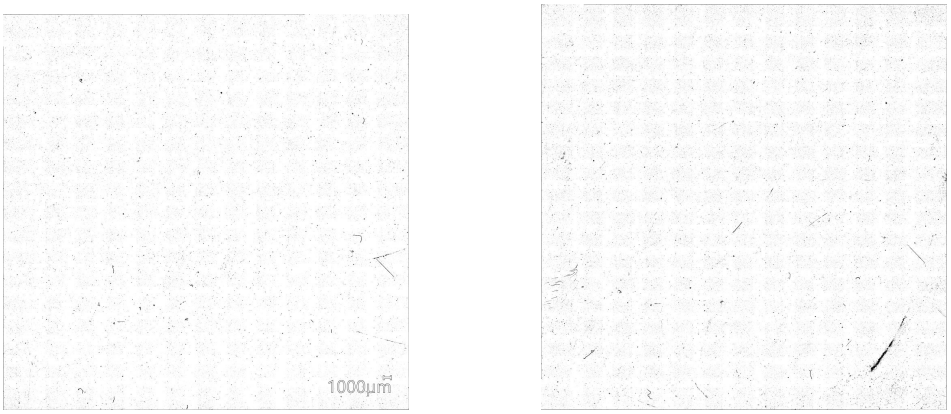

(a) S51 before thermal treatment **(b)** S51 after thermal treatment

Figure 4.1: Detection S51

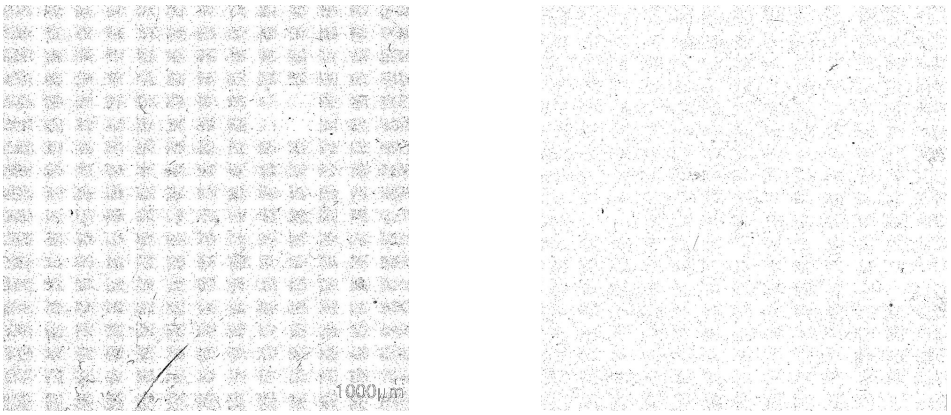

(a) S55 before thermal treatment **(b)** S55 after thermal treatment

Figure 4.2: Detection S55

In the case of sample 67 shown in Figure 4.3, an increase in surface flaws was observed following thermal treatment, suggesting that the surface was damaged during the process. This is particularly evident in the greater number of visible scratches on the surface after treatment. However, the pits present on the glass do not appear to be affected by the thermal treatment, indicating that this type of surface defect remains largely unchanged by the thermal treatment.

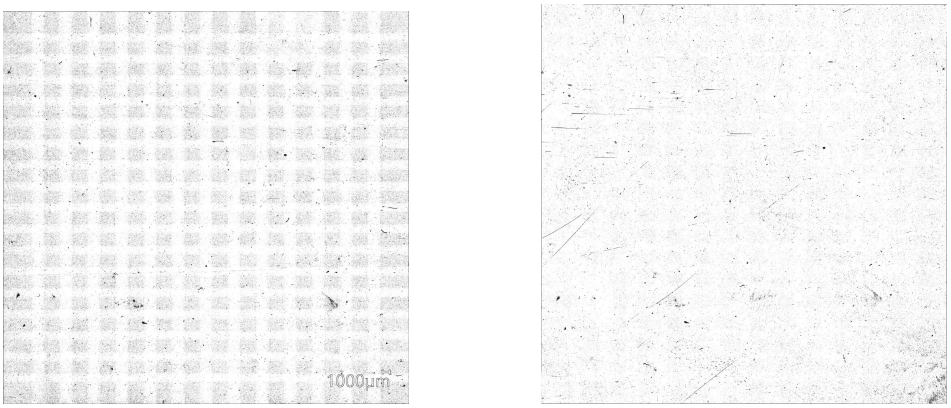

(a) S67 before thermal treatment **(b)** Sample S67 after thermal treatment

Figure 4.3: Detection S67

In the case of samples S113 and S140, shown in Figure 4.4 and Figure 4.5, the surface condition appears largely unchanged after thermal treatment. In sample S113, the surface flaw remains clearly visible, indicating no noticeable healing effect. However, some dirt appears to be visible in the top-left corner after thermal treatment. Similarly, for sample S140, there is no significant difference between the pre- and post-treatment images, with the pits appearing nearly identical in both cases. This suggests that the thermal treatment had little to no effect on these samples.

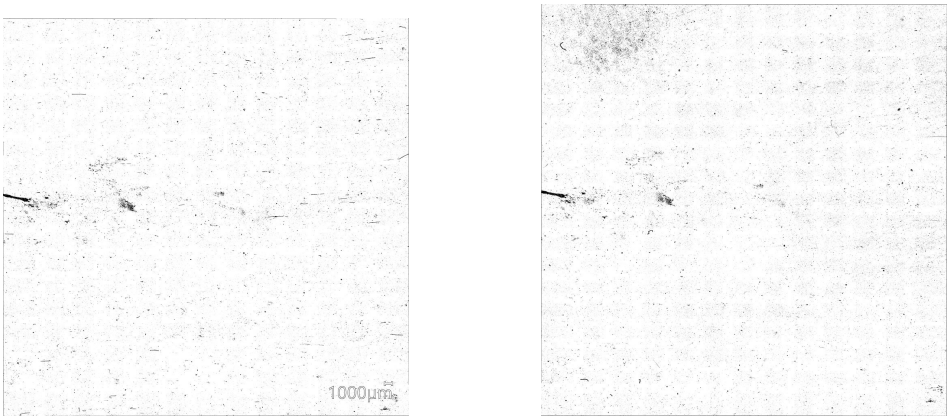

(a) S113 before thermal treatment **(b)** Sample S113 after thermal treatment

Figure 4.4: Detection S113

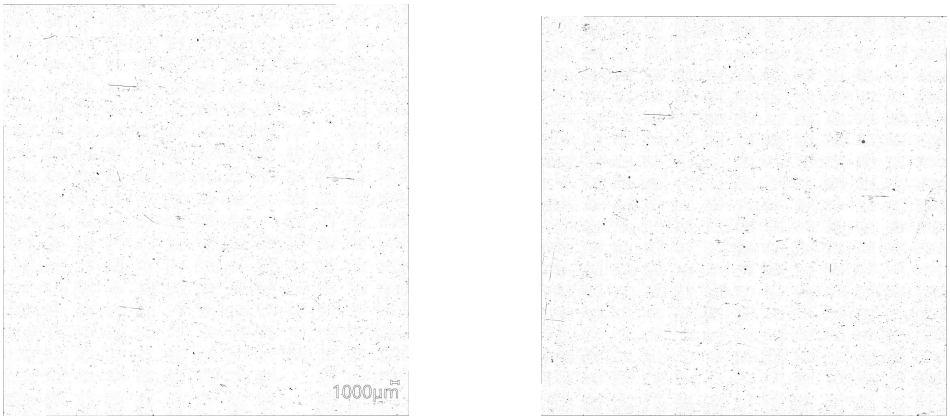

(a) S140 before thermal treatment **(b)** S140 after thermal treatment

Figure 4.5: Detection S140

The surface morphology of some samples changed after thermal treatment, with certain samples showing clear alterations while others exhibited only minor differences that could be attributed to limitations in the detection software. When evaluating all the images collectively, no consistent pattern emerged across the group. For instance, samples S51 and S67 showed an increase in visible scratches, with some existing scratches appearing to break into shorter segments. In contrast, sample S55 demonstrated signs of surface improvement, while samples S113 and S140 showed no noticeable changes. Overall, the results do not reveal a consistent trend that would support the conclusion that thermal treatment consistently heals the glass surface.

4.1.3. Naturally aged thermal treated samples at 600 degrees

The samples were scanned before and after the 600°C thermal treatment to assess changes in surface characteristics. Microscope images of these samples were analysed using image processing techniques explained in section 3.4 to detect and compare surface defects. Both contrast and detection images were used for analysis, as in some cases, the contrast image provided clearer results than the detection image. The samples included in this group are: **S29**, **S68**, **S92**, **S124**, and **S163**. The complete set of images can be found in Appendix B: Figure B.6, Figure B.7, Figure B.8, Figure B.9 and Figure B.10.

Samples S29 and S68, shown in Figure 4.6 and Figure 4.7, appear to be in worse condition after thermal treatment. There are noticeably more surface flaws visible across the entire sample area. Since these defects are spread uniformly over the surface, it is unlikely that they were caused by handling, which typically affects localized areas. Instead, the widespread distribution suggests that the damage likely resulted from the thermal treatment itself. Another possible reason, similar to that observed with the 500 °C heat-treated sample, is that residual dirt after the heat treatment affected the microscopy images. This could introduce errors in the image processing, as the software may interpret these dirt spots as scratches.

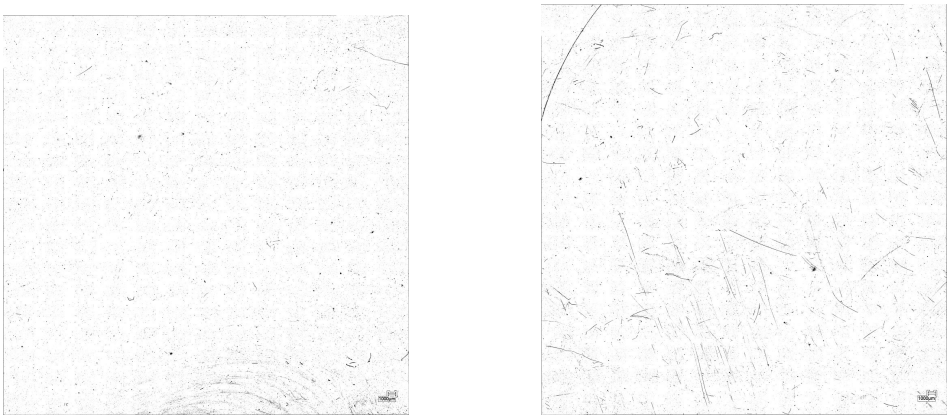

(a) S29 before thermal treatment **(b)** S29 after thermal treatment

Figure 4.6: Detection S29

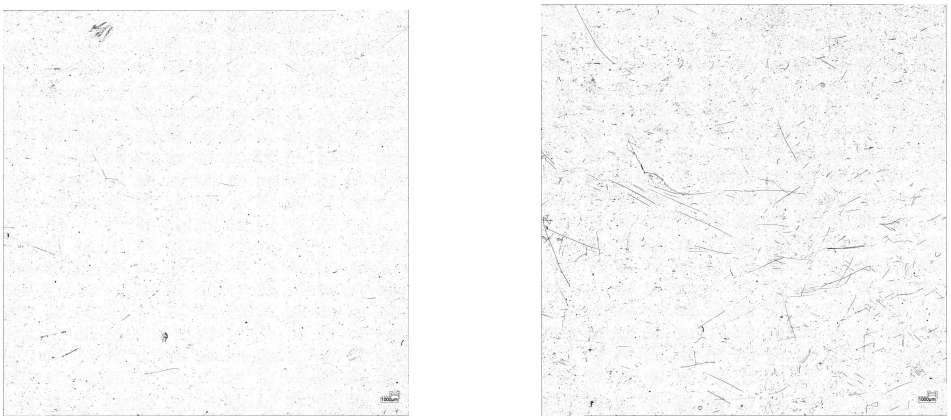

(a) S68 before thermal treatment **(b)** S68 after thermal treatment

Figure 4.7: Detection S68

Compared to the previous samples, sample S92 shown in Figure 4.8 appears largely unchanged before and after thermal treatment. The two prominent scratches on the left side remain clearly visible and show no noticeable alteration. While the right side of the sample displays slightly more detected flaws after treatment, some previously visible defects have become less distinct. Overall, the surface condition is assumed to be largely similar.

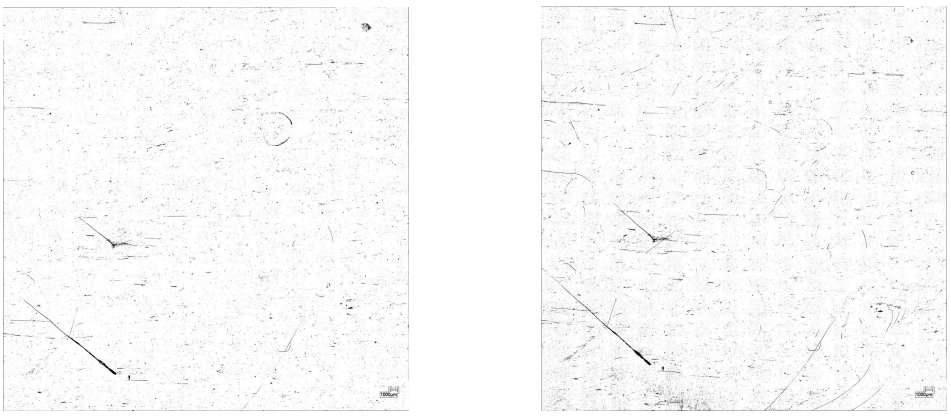

(a) S92 before thermal treatment **(b)** Sample S92 after thermal treatment

Figure 4.8: Detection S92

Sample S124, shown in Figure 4.9, appears to have fewer surface flaws than other samples initially. However, after thermal treatment, the detection images reveal an increase in visible defects, suggesting that the surface condition worsened following the treatment. In contrast, the opposite effect is observed in sample S163, shown in Figure 4.10, where scratches seem to have disappeared after thermal treatment. This indicates that in this case, thermal treatment may have successfully improved the surface condition.

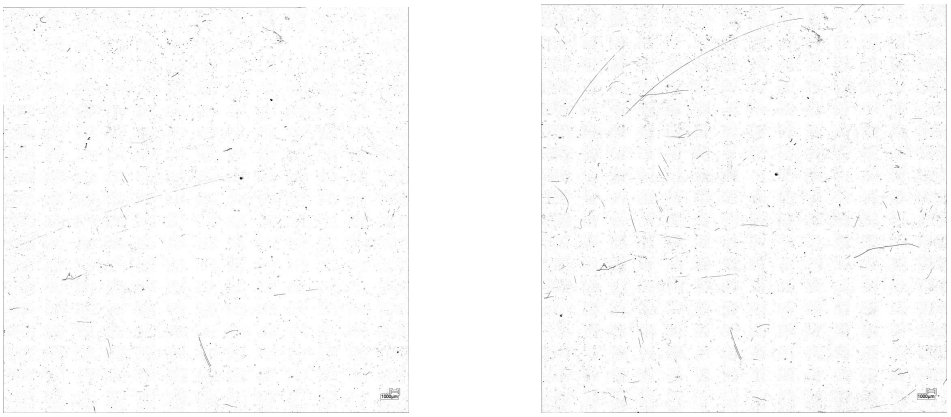

(a) S124 before thermal treatment **(b)** Sample S124 after thermal treatment

Figure 4.9: Detection S124

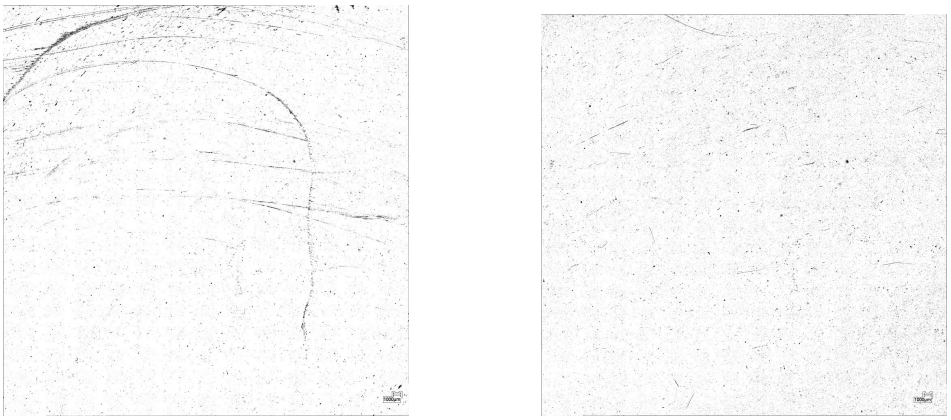

(a) S163 before thermal treatment **(b)** S163 after thermal treatment

Figure 4.10: Detection S163

A comparison of the pre- and post-treatment images for the five samples shows visible changes in surface morphology. Samples S29 and S68 appeared more damaged after thermal treatment, with no signs of surface repair. One possible explanation for this deterioration is contamination or dirt on the sample surfaces. In contrast, the images of samples S92, S124, and S163 were more consistent before and after treatment. Samples S92 and S124 showed minimal change, with no clear signs of healing. Sample S163, however, showed slight improvement, as some of the larger scratches appeared to have disappeared after thermal treatment. As observed with the naturally aged samples treated at 500°C, no consistent pattern of surface repair was identified across this group.

4.1.4. Artificially aged thermal treated samples at 500 degrees

These samples were artificially aged prior to undergoing the 500°C thermal treatment. Microscopy images were taken specifically at the location of the artificial damage. This area was marked with the software to allow for better visual comparison before and after the treatment. The samples included in this group are: **S5**, **S74**, **S81**, **S128**, and **S158**. The complete set of images can be found in Appendix B: Figure B.11 and Figure B.12.

A comparison of the pre- and post-treatment images for the five samples shows very little change in surface morphology. Neither the length nor the width of the artificial scratches appears to have altered during the 500°C thermal treatment. The width of sample 128 is illustrated by Figure 4.11b and Figure 4.11d showing similar morphology.

Despite the overall similarity, two specific changes are worth highlighting. Several scratches exhibited a thin, well-defined dark line along the groove prior to heating, as illustrated in Figure 4.11a. This feature is most likely a shadow effect. After thermal treatment, the dark line is noticeably diminished, and the scratch edges appear widened and irregular, as shown in Figure 4.11c. The same effect is also evident in sample S158. Second, in sample S5 a subcritical crack developed, becoming visible in the lower half of the image, whereas the upper half remained largely unchanged apart from the faded dark line. The average scratch width in the affected region increased from approximately 95 µm to 158 µm, suggesting that the lower region of sample S5 was negatively affected by the treatment compared to its original condition.

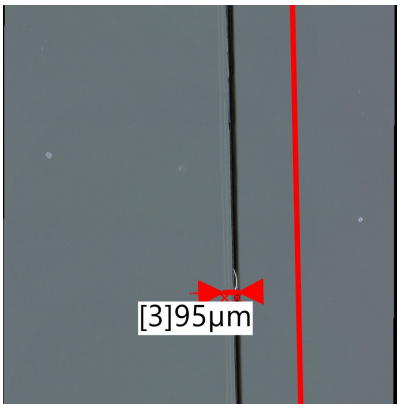

(a) Sample S5 before treatment

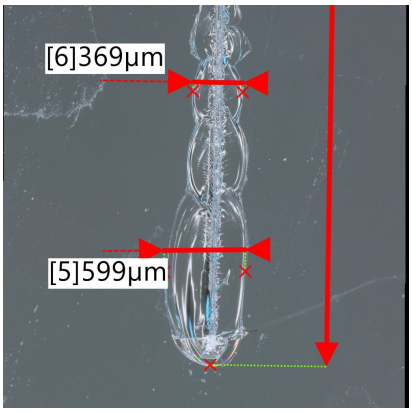

(b) Sample S128 before treatment

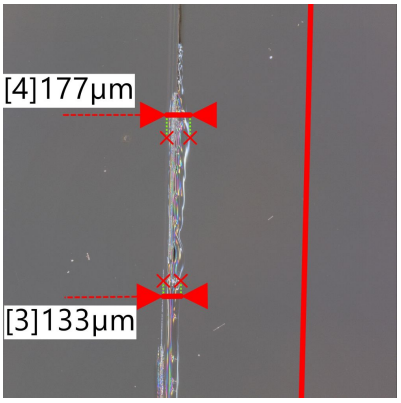

(c) Sample S5 after treatment

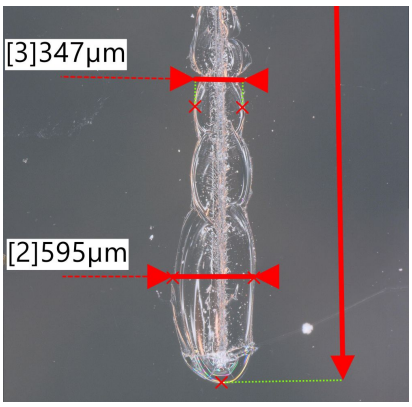

(d) Sample S128 after treatment

Figure 4.11: Artificially aged thermal treated sample S5 and S128 with 500°C treatment

4.1.5. Artificially aged thermal treated samples at 600 degrees

These samples were artificially aged prior to undergoing the 600°C thermal treatment. Microscopy images were taken specifically at the location of the artificial damage. This area was marked with the software to allow for better visual comparison before and after the treatment. The samples included in this group are: **S15**, **S59**, **S71**, **S119** & **S154**. The complete set of images can be found in Appendix B: Figure B.13 and Figure B.14.

A comparison of the pre- and post-treatment images for the five samples reveals several changes in surface morphology. While the length of the artificial scratches remained unchanged, the width increased noticeably following the 600°C thermal treatment. The central portion of the scratch created by the

indenter appeared largely unaffected. However, the formation of subcritical cracks around the scratch contributed to a significant increase in overall width. This effect is illustrated in Figure 4.12a and Figure 4.12e, where the scratch width in the affected region expanded from approximately 479 µm to 827 µm, measured at the widest point. The change in surface morphology is also evident in Figure 4.12b and Figure 4.12f. Before thermal treatment, the scratch appears clearly defined, whereas after treatment, additional lines are visible and the shape of the scratch seems altered, indicating a change in the surface structure. Additionally, all treated glass samples exhibited a yellow discoloration, which appears to have developed during the thermal treatment and will be examined further in section 4.3.

Despite the general similarity across samples, two observations are noteworthy. First, as seen with the 500 °C treatment, several scratches displayed a thin, well-defined dark line along the groove before heating, as shown in Figure 4.12c. This feature is most likely a shadow effect. After treatment, the dark line was significantly diminished, and the scratch edges appeared widened and irregular, as illustrated in Figure 4.12g. Second, in sample S154, naturally aged damage remained visible on the top left side both before and after the treatment, indicating that the scratches were not fully healed by the thermal process.

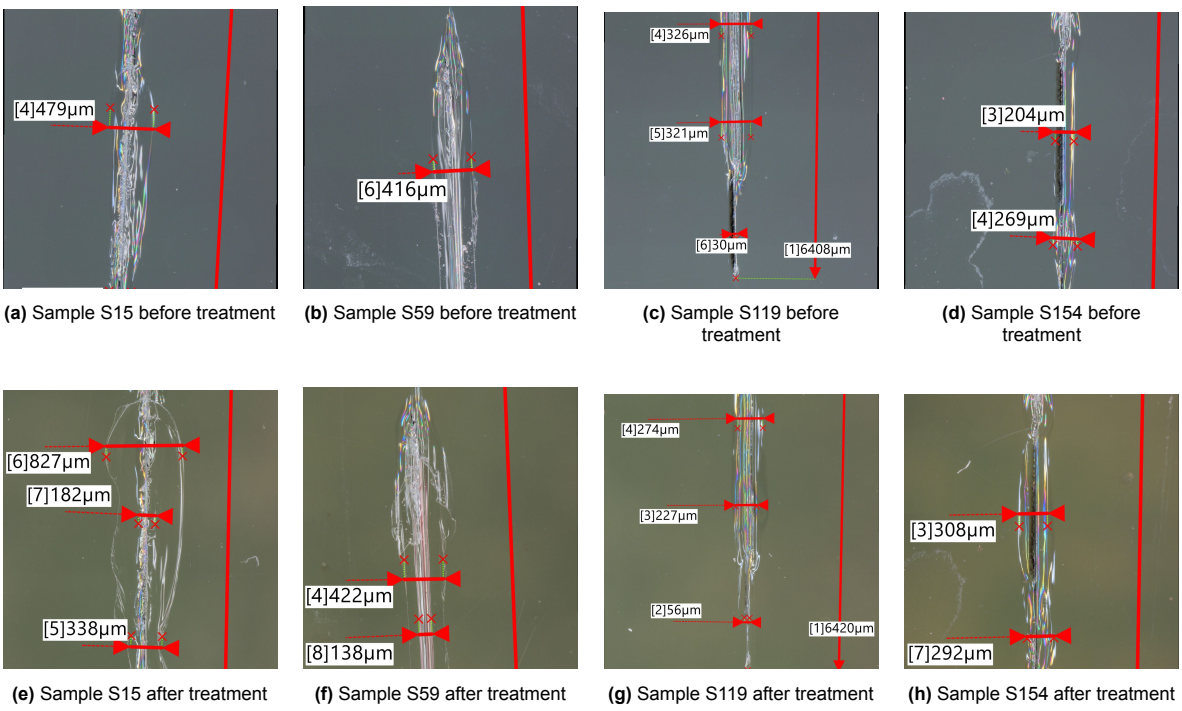

(a) Sample S15 before treatment **(b)** Sample S59 before treatment **(c)** Sample S119 before treatment **(d)** Sample S154 before treatment

(e) Sample S15 after treatment **(f)** Sample S59 after treatment **(g)** Sample S119 after treatment **(h)** Sample S154 after treatment

Figure 4.12: Artificially aged thermal treated sample S15, S59, S119 and S154 with 600°C treatment

Conclusion

An examination of the 15-year-old glass samples revealed minimal surface degradation. To the naked eye, the glass plates appeared free from visible flaws. However, microscopic analysis uncovered small pits and fine scratches on the surface. These surface defects were further analysed using image processing software, which demonstrated both accuracy and efficiency in detecting flaws. Given its strong potential for automated analysis and reduced human error, this method was adopted for the evaluation of all naturally aged glass samples.

Naturally aged glass which was thermal treatment at both 500°C and 600°C caused observable changes in the surface morphology of naturally aged glass samples. At 500°C, some samples exhibited increased scratches, while others showed a slight decrease in surface defects, indicating varied responses. At 600°C, damage appeared more pronounced in certain samples, potentially influenced by contamination during imaging, whereas others remained largely unchanged. Minor differences in some images may result from the limitations of the detection software. Although individual samples displayed visible changes in surface condition, when considering all samples collectively. These results

show no consistent evidence that thermal treatment effectively repairs surface flaws in naturally aged glass.

Artificially aged glass treated at 500°C exhibited minimal changes in scratch morphology. Most scratches maintained their original length and width. One sample developed a subcritical crack and experienced an increase in scratch width, suggesting some negative effects from the thermal process. At 600°C, the length of the scratches remained unchanged, but the formation of subcritical cracks around the scratches led to a significant increase in overall width, expanding from approximately 479 µm to 827 µm at the widest point. Before treatment, scratches appeared clearly defined, afterward, additional lines became visible and the scratch shape appeared altered, indicating changes in surface structure. The samples also exhibited yellow discolouration, likely caused by the thermal process. The samples treated at 500°C showed minimal surface changes, with signs of deterioration becoming more evident at 600°C. At the higher temperature, subcritical crack growth contributed to an increase in crack width, worsening the surface condition. These results consistently indicate that thermal treatment tends to aggravate surface flaws in artificially aged glass.

4.2. Thermal treatment

After removal from the oven, noticeable changes in surface characteristics were observed, most prominently the development of a yellow discolouration, as shown in Figure 4.13. This effect is believed to result from oxidising of the surface coating during thermal treatment. Evidence of this can be seen in Figure 4.14a and Figure 4.14b, where the coating appears to have fragmented, creating irregular patterns on the glass surface. This effect was mostly detected in the 600°C samples, but early signs of discolouration were already noticeable at 500°C.

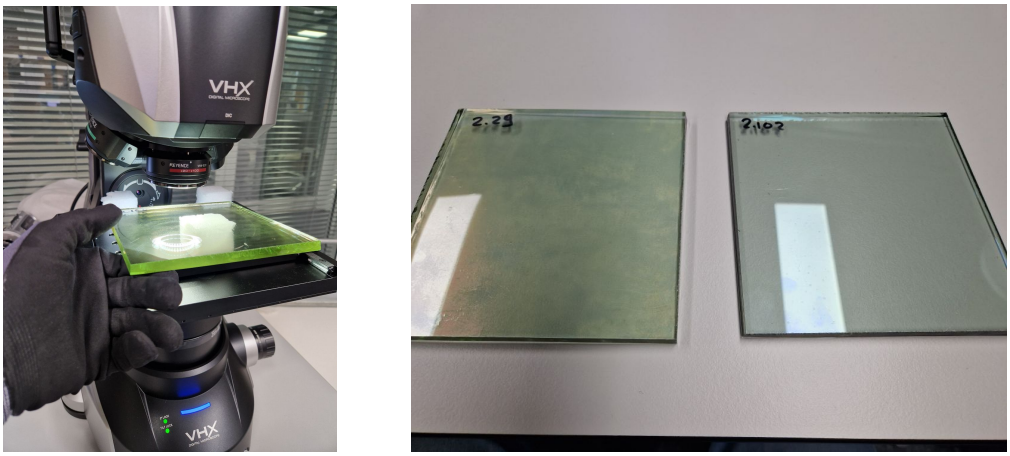

(a) Glass discolouration **(b)** Glass discolouration comparison

Figure 4.13: Glass discolouration samples

The coating on the glass is likely a soft, heat-sensitive layer composed of ultra-thin metal oxides. This is supported by the observation that areas previously covered with glue did not discolour. During manufacturing, the regions where glue was applied to assemble the glass units were cleaned, removing the coating before assembly. As a result, these areas lacked surface coating. In Figure 4.14c, the left side of the sample, which retained the coating, shows a yellow tint, while the right side, previously covered with glue, remains clear.

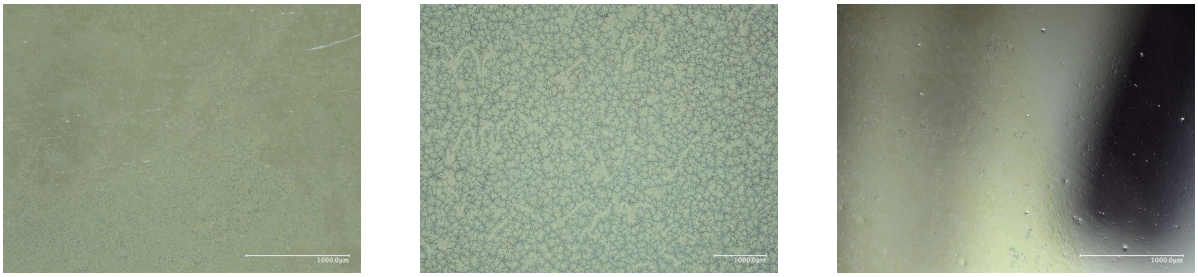

(a) Discolouration S2.7 600°C **(b)** Discolouration S2.184 600°C **(c)** Yellow discolouration

Figure 4.14: Discolouration after thermal treatment

To investigate this further, the elemental composition of the glass under various treatment conditions was analysed, as described in section 3.8, to determine whether the coating had been degraded or removed. This chapter will provide more insight in the chemical composition of the glass before and after thermal treatment.

In addition to the discolouration, the backside of the samples was found to be heavily contaminated. Cleaning cloths used after the thermal treatment showed black staining, indicating that a significant amount of residue had been removed. However, some dirt remained adhered to the surface and could not be fully cleaned off. Microscopy was used to examine the condition of the surface following the thermal treatment, as shown in Figure 4.15.

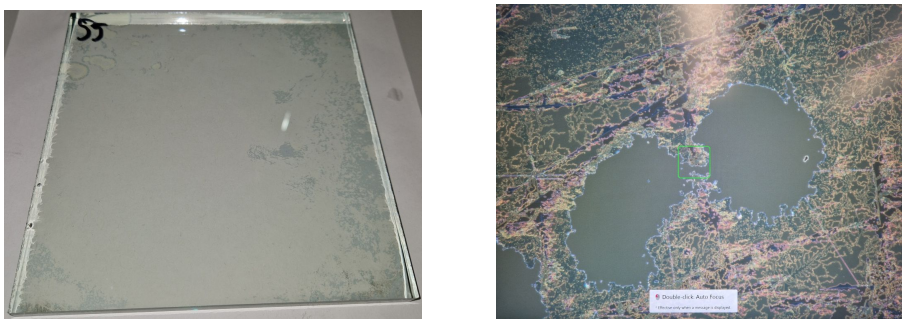

(a) Glass samples after cleaning **(b)** Dirt sample after thermal treatment

Figure 4.15: Dirt on sample after thermal treatment

Conclusion

The glass used in this research is likely to have a surface coating that degraded during thermal treatment, most likely resulting in a yellow discolouration. The effect was clearly visible at 600°C, though it was already noticeable at 500°C. This discolouration was likely caused by the oxidising of a heat-sensitive metal oxide coating. This will be further investigated in section 4.3. Interestingly, areas previously covered by glue showed no discolouration, supporting the conclusion that the coating was responsible for the colour change. Additionally, the backside of the glass was heavily contaminated after treatment, with some dirt remaining even after cleaning.

4.3. Energy-dispersive X-ray spectroscopy

Five different glass panels were investigated, with measurements taken from both sides of each panel. The naming convention reflects the properties of each sample. The first letter indicates the side of the glass: ”A” for the air side and ”T” for the tin side, as identified using a tin detector. A second letter, ”C”, denotes the presence of a surface coating. In this study, the panel labeled “Amsterdam 4” featured such a coating. Samples without coating were obtained from another studie which used new, uncoated glass. The final part of the sample name may include a number indicating the oven treatment temperature (500°C or 600°C). The results are visible in Table 4.1 and are shown in Figure 4.16 and Figure 4.17.

The composition of glass is described in section 2.3, where elements such as oxygen (O), silicon (Si), sodium (Na), and calcium (Ca) are identified as the primary constituents of glass. Trace amounts of magnesium (Mg), aluminum (Al) and potassium (K) are also present. As shown in Table 4.1, additional elements like zinc (Zn), silver (Ag), tin (Sn), nickel (Ni) and titanium (Ti) were detected, specifically on the air side of the coated glass samples. These metals are likely components of the surface coating, as they do not appear on either side of the uncoated samples. This suggests that Zn, Ag, and Sn originate from the coating layer rather than the glass itself.

Table 4.1: Chemical composition of glass (Weight percentage)

	AC	TC	AC500	TC500	AC600	TC600	A	T	A600	T600
O	19.49	47.27	21.07	47.09	27.15	46.86	47.51	47.25	46.71	46.44
Si	8.11	34.32	9.5	34.06	14.25	33.66	34.23	34.27	33.47	32.95
Na		9.28		9.94		10.24	9.57	9.69	10.14	10.1
Ca		5.86		5.83	1.91	6.08	5.81		6.9	6.53
Zn	44.76		46.32		50.94					
Ag	19.34		15.2		3.72					
Sn	6.68		6.43							1.14
Mg	0.26	2.82	0.33	2.69	0.78	2.74	2.32	2.3	2.26	2.46
Al	0.17	0.44		0.4		0.42	0.3	0.31	0.3	0.38
K							0.25	6.18	0.21	
Ni	0.54		0.54		0.62					
Ti	0.66		0.61		0.63					

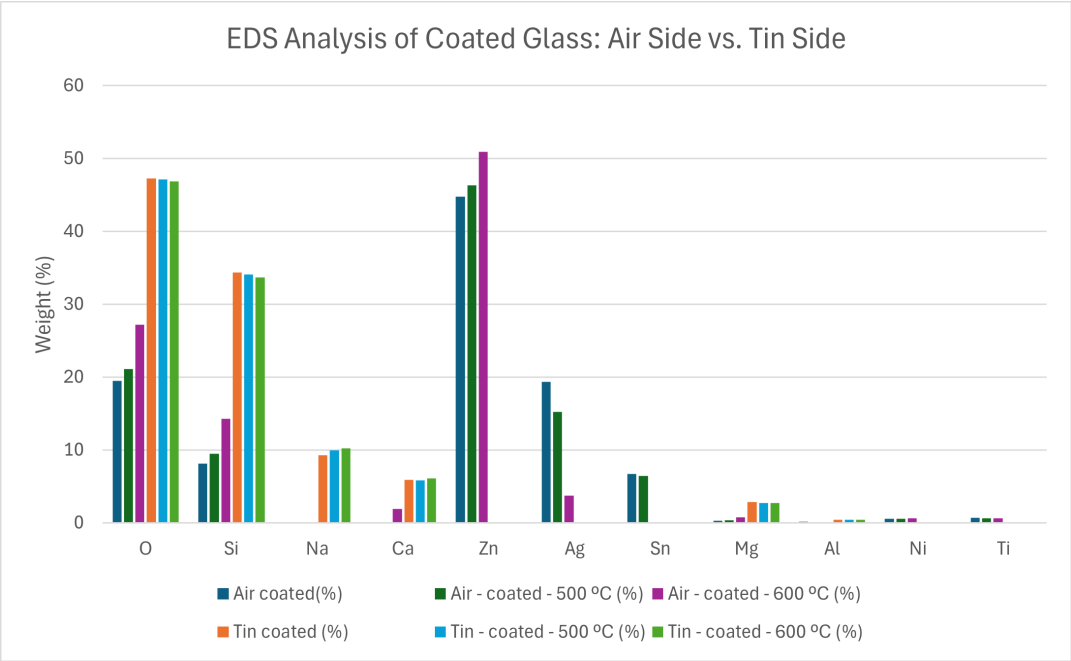

Figure 4.16: EDS Analysis of Coated Glass: Air Side vs. Tin Side

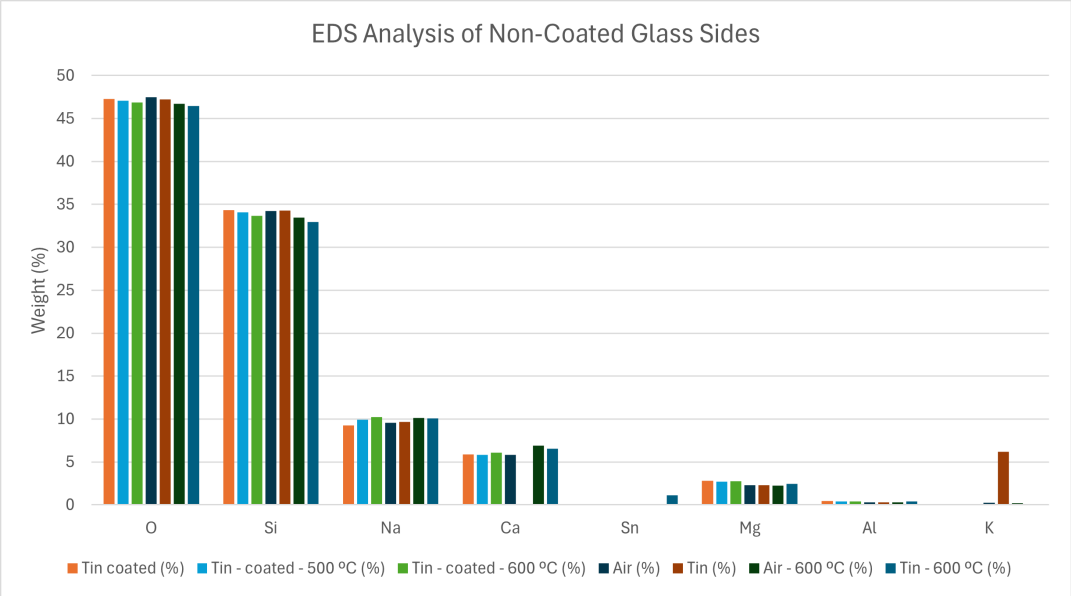

Figure 4.17: EDS Analysis of Non-Coated Glass Sides

Conclusion

The results from the EDS analysis provide valuable insights into the chemical composition of the glass, both in its untreated state and after thermal treatment. These findings are presented in Table 4.1, Figure 4.16 and Figure 4.17.

- The primary elements identified in glass samples without coating were oxygen and silicon, with notable amounts of sodium and calcium, and minor amounts of magnesium and aluminium. On the air side, it shifted a bit to oxygen, silicon zinc, silver and tin.
- The air side of the coated samples contained additional metals, primarily zinc, silver and tin, likely originating from the surface coating. Upon heating, the air side of the coated glass exhibited significant compositional changes. After heating the coated samples to 600°C, a noticeable decrease in silver content was observed, and tin was no longer detected. In contrast, the zinc content showed a slight increase.
- It was also observed that the air side of the coated glass lacked detectable levels of sodium (Na) and calcium (Ca), while these elements were present on the tin side. This could suggests that a chemical reaction involving the metallic coating on the air side may have altered the surface composition, potentially consuming or masking the presence of Na and Ca.
- The non-coated glass samples showed a consistent chemical composition across both sides and at all treatment levels. Their composition closely resembled that of the tin side of the coated glass. As shown in Figure 4.17, all non-coated glass samples display similar elemental profiles, indicating that both sides of the non-coated glass and the tin side of the coated glass share a comparable base composition.
- Despite being identified as the tin side using a UV tin detector, most samples did not show measurable tin content. An exception was observed in the “Tin No Coating 600” sample, which showed a tin content of 1.14 wt%.

These results provide greater insight into the chemical composition of the glass and its behaviour after thermal treatment. They confirm the presence of a metallic coating on the air side. Following thermal treatment, the concentrations of silver and tin were notably reduced, which may have contributed to the yellow discolouration observed on the glass surface.

4.4. Ring test and statistical evaluation

As mentioned in section 3.1, two glass panels were obtained from a building in Amsterdam, resulting in two sample sets: panel 1 and panel 2, containing 106 and 170 samples respectively.

Panel 1 was divided into four test groups and panel 2 was divided into 6 test groups resulting in 10 groups total. The name for both panels is based on the 'panel', 'side of the glass', 'Ageing method' and 'treatment condition'.

Samples panel 1

- P1_Tin_NA_REF: Untreated sample tested on the tin side.
- P1_Air_NA_REF: Untreated sample tested on the air side.
- P1_Tin_NA_500: Oven-treated (T500) sample tested on the tin side.
- P1_Air_NA_500: Oven-treated (T500) sample tested on the air side.

Samples panel 2

- P2_Tin_NA_REF: Untreated sample tested on the tin side.
- P2_Tin_NA_500: Oven-treated (T500) sample tested on the tin side.
- P2_Tin_NA_600: Oven-treated (T600) sample tested on the tin side.
- P2_Tin_SC_REF: Untreated sample with an artificial scratch tested on the tin side.
- P2_Tin_SC_500: Oven-treated (T500) sample with an artificial scratch tested on the tin side.
- P2_Tin_SC_600: Oven-treated (T600) sample with an artificial scratch tested on the tin side.

4.4.1. Statistical evaluation

The data files from the ring on ring test were processed using a Python script. The processed data is also shown in Appendix E. The data was organised and in combination with the formulas outlined in section 3.6: Analysis of the results, the stress values for all samples were calculated. The strength data was further analysed using Python code from OpenGlassLab, applying Method 2P: Weibull distribution with Weighted Least Squares Regression (Cupać, Louter, et al. 2025). The strength values were input into the program, which then performed the Weibull statistical evaluation. The results, are presented in Table 4.2 and Table 4.3. Corresponding Weibull plots are shown in Figure 4.18 and Figure 4.19. The p_{AD} Value ≥ 5 means the fit is statistically acceptable and the data is consistent with a Weibull distribution. In a ring-on-ring test, the R-squared value indicates the goodness of fit. A value of 0 indicates the model does not fit the data at all, while a value of 1 signifies a perfect fit.

Table 4.2: Weibull panel 1

Valid data	0.8% [MPa]	5% [MPa]	50% [MPa]	Min [MPa]	Max [MPa]	Var [%]	p_{AD}	R^2
P1_Tin_NA_REF	32.16	48.85	87.87	54.93	129.2	25.55	57.77	0.924
P1_Air_NA_REF	45.36	70.83	132.44	52.26	190.2	27.07	84.6	0.969
P1_Tin_NA_500	27.5	42.4	77.87	51.72	112.9	26.37	37.83	0.894
P1_Air_NA_500	18.42	36.12	93.0	50.0	158.8	39.25	9.01	0.864

Table 4.3: Weibull panel 2

Valid data	0.8% [MPa]	5% [MPa]	50% [MPa]	Min [MPa]	Max [MPa]	Var [%]	p_{AD}	R^2
P2_Tin_NA_REF	36.39	54.41	95.71	49.72	146.2	24.66	77.81	0.981
P2_Tin_NA_500	22.73	38.93	82.89	34.99	123.6	32.1	58.88	0.966
P2_Tin_NA_600	12.38	24.08	61.3	30.71	108.7	38.83	47.74	0.910
P2_Tin_SC_REF	16.29	23.72	40.2	30.82	68.97	23.19	0.12	0.724
P2_Tin_SC_500	18.9	26.88	44.05	31.78	63.73	21.83	18.01	0.863
P2_Tin_SC_600	23.38	33.41	55.16	28.33	79.03	22.12	65.25	0.977

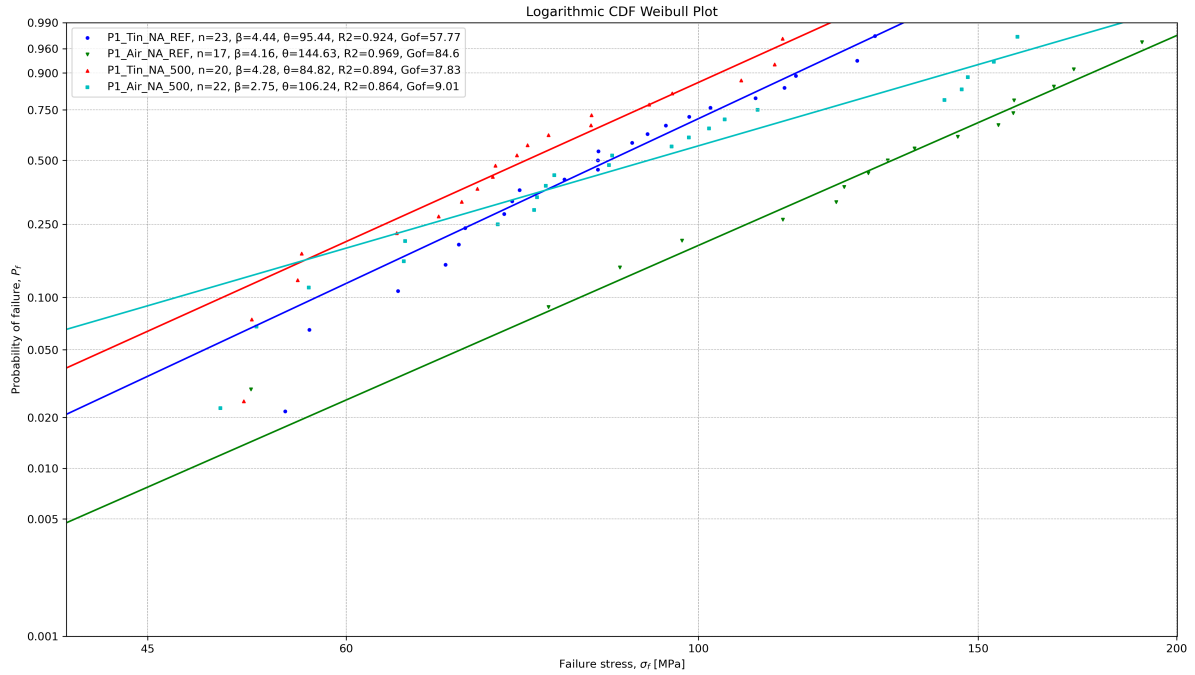

Figure 4.18: Statistical evaluation panel 1

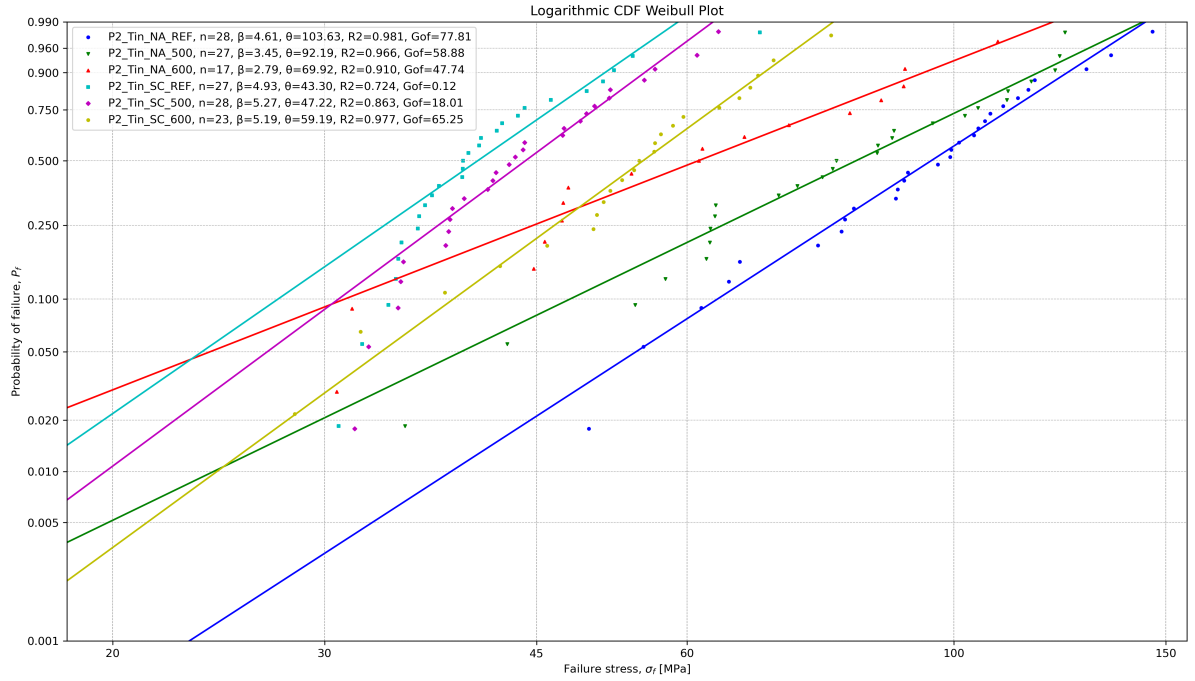

Figure 4.19: Statistical evaluation panel 2

4.4.2. Statistical evaluation of equivalent failure stress

A similar procedure is needed to analyse the strength data with a time conversion. Within the OpenGLASSlab code (Cupać, Louter, et al. 2025), the time of failure needs to be added to the python code. In this case, the data is displayed with applying a time conversion and a reference period of 5 seconds. The results of equivalent failure stress, are presented in Table 4.4 and Table 4.5. Corresponding Weibull plots are shown in Figure 4.20 and Figure 4.21.

Table 4.4: Weibull panel 1 of equivalent failure stress

Valid data	0.8% [MPa]	5% [MPa]	50% [MPa]	Min [MPa]	Max [MPa]	Var [%]	p_{AD}	R^2
P1_Tin_NA_REF	25.31	39.36	73.15	44.57	109.91	26.84	57.34	0.923
P1_Air_NA_REF	36.36	58.24	112.84	42.34	165.49	28.46	84.73	0.970
P1_Tin_NA_500	21.36	33.76	64.22	41.6	95.22	27.75	39.25	0.895
P1_Air_NA_500	13.95	28.46	77.41	40.09	136.39	41.29	8.83	0.864

Table 4.5: Weibull panel 2 of equivalent failure stress

Valid data	0.8% [MPa]	5% [MPa]	50% [MPa]	Min [MPa]	Max [MPa]	Var [%]	p_{AD}	R^2
P2_Tin_NA_REF	28.67	43.91	79.89	39.93	125.27	26.0	77.81	0.981
P2_Tin_NA_500	17.42	30.8	68.59	27.6	104.72	33.8	58.23	0.966
P2_Tin_NA_600	9.69	19.24	50.4	25.34	91.72	39.89	47.21	0.904
P2_Tin_SC_REF	12.19	18.16	31.78	23.99	56.33	24.47	0.11	0.723
P2_Tin_SC_500	14.29	20.75	35.01	25.13	51.72	23.01	16.97	0.857
P2_Tin_SC_600	18.73	27.0	45.12	23.28	65.59	22.61	71.43	0.981

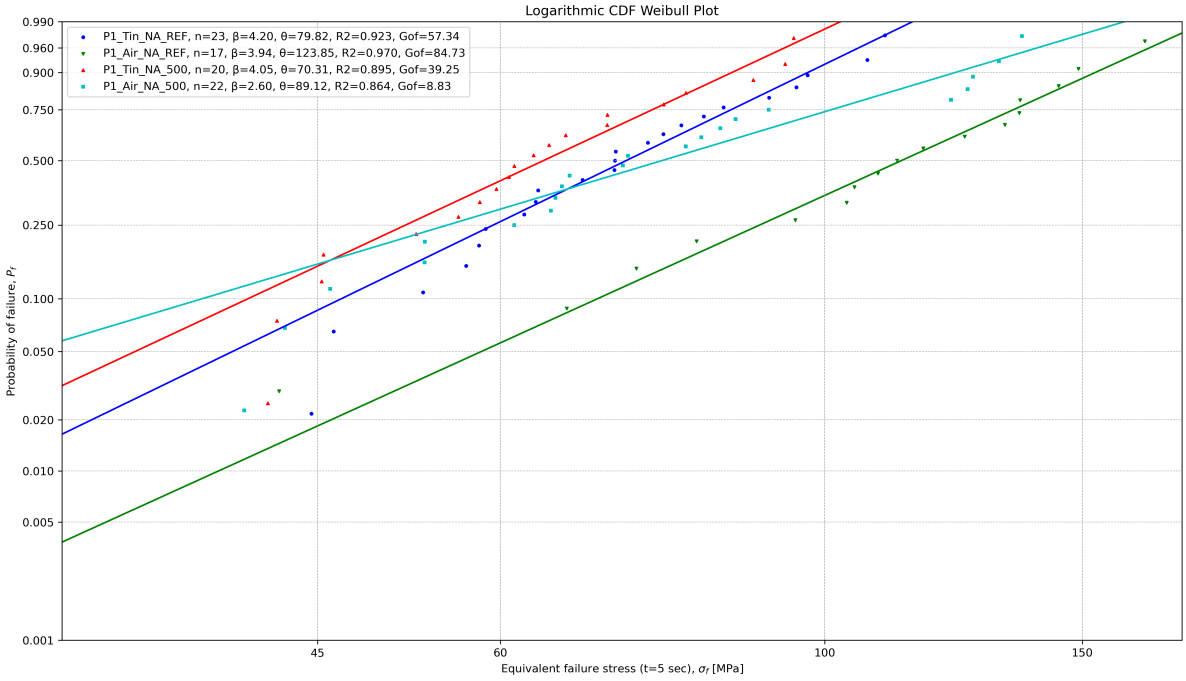

Figure 4.20: Statistical evaluation panel 1 of equivalent failure stress

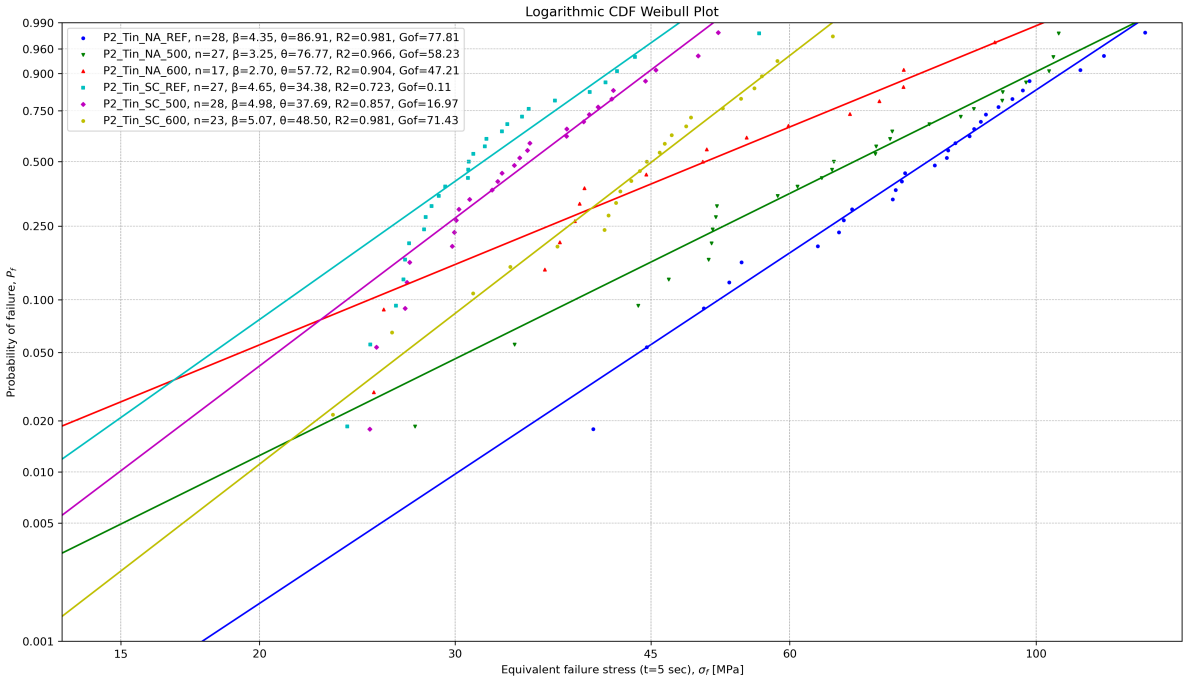

Figure 4.21: Statistical evaluation panel 2 of equivalent failure stress

Conclusion

The results without a reference period are presented in Table 4.2 and Table 4.3. The corresponding Weibull plots are shown in Figure 4.18 and Figure 4.19. These results reveal several notable trends, based primarily on the dataset without the reference period included. While the general shape and behaviour of the Weibull curves remain similar, time conversion lowers the strength values by approximately 20%.

Panel 1 contains tin and air side samples treated at 500 degrees. Several interesting conclusions can be drawn from the results in Table 4.2 and Figure 4.18:

- The 5% characteristic strength of the air side is higher than that of the tin side before treatment. Specifically, the air side exhibits a strength of 70.83 MPa, compared to 48.85 MPa for the tin side, an increase of 45%. However, after thermal treatment, this trend reverses: the tin side becomes stronger, with a strength of 42.2 MPa, while the air side drops to 36.12 MPa, representing a 15% advantage in favour of the tin side.
- A similar pattern is observed in the mean strength values of the reference samples. The air side shows a mean strength of 132.44 MPa, compared to 87.87 MPa for the tin side, an increase of 51%. After thermal treatment, the strengths decrease, but the air side remains stronger than the tin side: 93.0 MPa versus 77.87 MPa, representing a 19% increase in favour of the air side.
- In both cases, thermal treated samples show a reduction in strength compared to the untreated reference samples. This trend is clearly visible in Figure 4.18. The tin-side samples before treatment consistently outperforms the tin-side sample after treatment, and the same applies to the air-side samples. At the 5% fractile, the strength of the tin side decreases by 13%, while the air side decreases by 49%. At the 50% level, the tin side is reduced by 11% and the air side by 30%. This means that the thermal treatment reduces the strength of the air side much more compared to the tin side.
- The P1_Air_NA_500 sample shows some noteworthy deviations. Compared to the other samples, it has a low p_{AD} value of 9.01. Besides, the slope of its line in Figure 4.18 deviates from the others.

Panel 2 contains both scratched and unscratched samples. Note that P2_Tin_Na are unscratched, while P2_Tin_SC are scratched. The results can be found in Table 4.3 and Figure 4.21:

- For the unscratched samples, strength decreases with higher thermal treatment temperatures. The 5% strength of the reference sample (P2_Tin_NA_REF) drops by 28% after 500°C treatment and by 56% after 600°C treatment. At the 50% level, the reductions are 13% and 36% respectively.
- Conversely, the scratched samples improve in strength after thermal treatment. The 5% strength increases by 13% at 500°C and by 41% at 600°C compared to the reference. At the 50% level, strength improves by 10% and 37%, respectively. This indicates that thermal treatment may be more effective for samples with significant surface flaws.
- Scratching the glass has a large negative impact on strength before treatment. The 5% value drops by 56% and the 50% value by 58% compared to unscratched samples.
- Across all methods, 50% strength is consistently higher for unscratched glass. However, there are exceptions at the 5% strength for example, the P2_Tin_NA_600 sample is weaker than P2_Tin_SC_600.
- The p_{AD} of P2_Tin_SC_REF is only 0.12, well below the threshold of 5, indicating that the Weibull fit is statistically poor.
- The slopes of the Weibull lines for P2_Tin_NA_REF, P2_Tin_NA_500, and P2_Tin_NA_600 vary. While P2_Tin_NA_REF resembles the scratched sample trends, P2_Tin_NA_500 and P2_Tin_NA_600 have increasingly horizontal slopes.

The results indicate that thermal treatment has contrasting effects on artificially scratched versus naturally aged glass. For artificially scratched glass, strength improved significantly after treatment. The 5% characteristic strength increased by 13% at 500°C and by 41% at 600°C compared to the reference samples. Similarly, at the 50%, strength increased by 10% and 37%, respectively.

However, naturally aged glass exhibited a decline in performance after thermal treatment. The 5% characteristic strength decreased by 28% at 500°C and by 56% at 600°C, while mean strength dropped by 13% and 36%, respectively. A similar weakening trend was observed in Panel 1: at the 5% fractile, the tin side showed a 13% reduction in strength, and the air side dropped by 49%. At the 50% level, the tin and air sides were reduced by 11% and 30%, respectively. These findings suggest that while thermal treatment may help repair larger flaws, it negatively affects naturally aged glass.

4.5. SCALP-05

The SCALP 05 tests were performed on samples from three different groups: untreated (no thermal treatment), thermal treated at 500°C, and thermal treated at 600°C. For each group, six samples were tested to determine the effect of thermal treatment on surface stresses. The complete results from the software, including the corresponding stress profiles for each sample, are presented in Appendix C. In the graphs, each line represents an individual measurement. The average surface stress value is displayed in the center of each images to provide a clear overview of the stress distribution. The results of the tests are shown in Table 4.6, Table 4.7 and Table 4.8. Behind the samples ID is also the number of measurement shown between brackets.

Table 4.6: Surface stresses - no thermal treatment

Sample ID	Surface stress [MPa]
17 (9)	-6.01
43 (10)	-6.93
101 (13)	-7.37
123 (5)	-5.35
132 (10)	-6.71
173 (5)	-6.56
Average surface stress [MPa]	-6.49

Table 4.7: Surface stresses - thermal treatment 500 degrees

Sample ID	Surface stress [MPa]
2 (10)	-3.08
5 (10)	-3.77
141 (8)	-2.36
148 (10)	-2.33
158 (10)	-2.19
161 (10)	-2.81
Average surface stress [MPa]	-2.76

Table 4.8: Surface stresses - thermal treatment 600 degrees

Sample ID	Surface stress [MPa]
4 (10)	-2.71
15 (10)	-2.79
23 (10)	-2.38
63 (10)	-1.89
97 (9)	-2.16
115 (11)	-1.85
Average surface stress [MPa]	-2.30

The stresses of the glass samples are corrected with the surface stress and the new graphs are shown in Figure 4.22 and Figure 4.23.

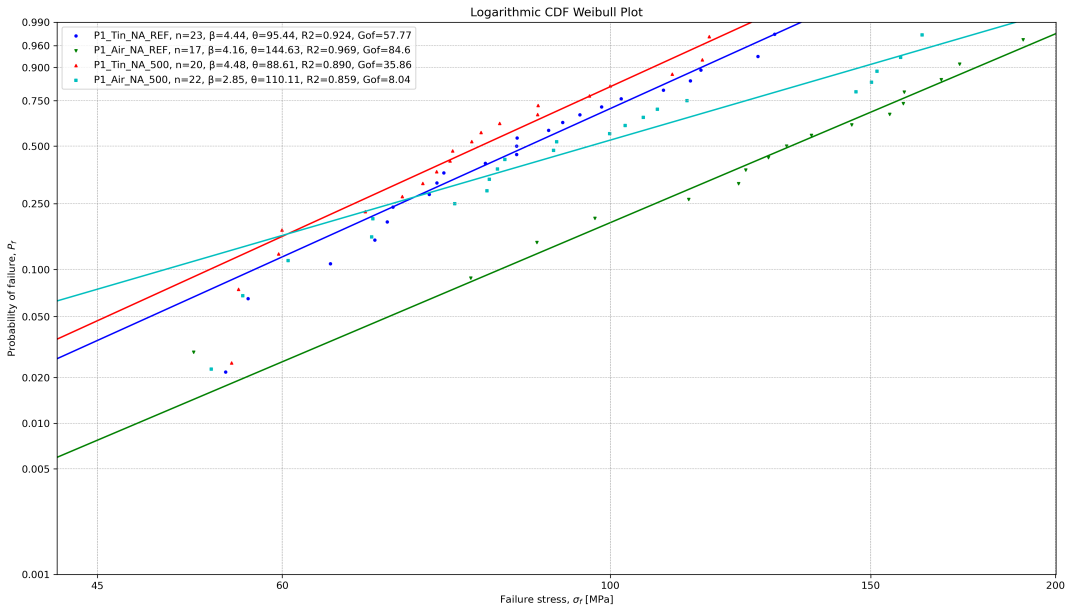

Figure 4.22: Panel 1 scalp corrected

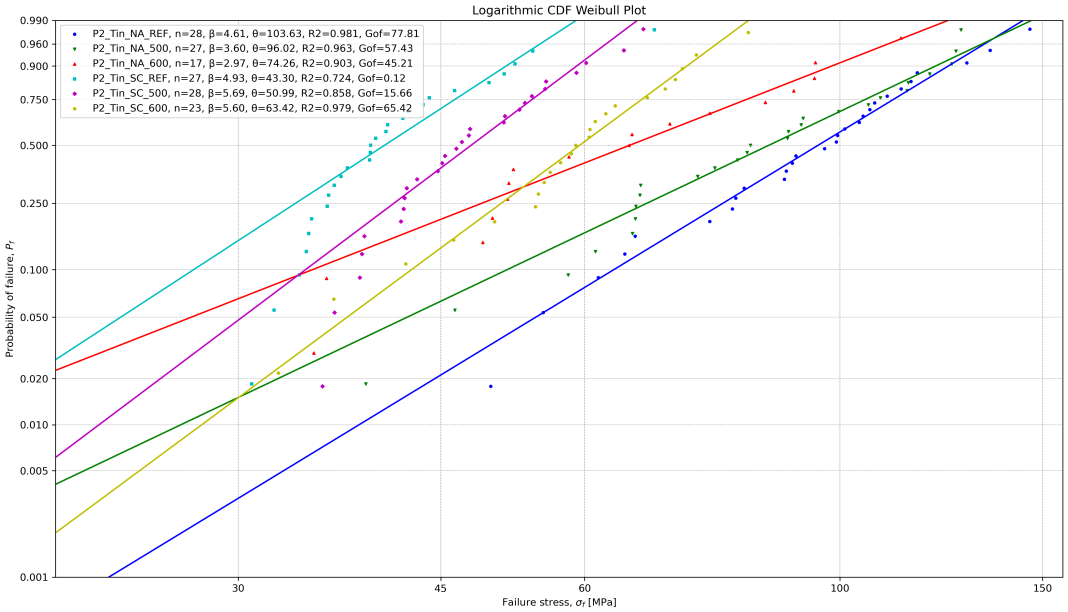

Figure 4.23: Panel 2 scalp corrected

Conclusion

The SCALP measurements were conducted on three groups: untreated (no thermal treatment), thermal treated at 500°C, and thermal treated at 600°C. The average surface stresses were -6.49 MPa, -2.76 MPa, and -2.30 MPa, respectively. These results indicate that surface stress decreases with thermal treatment. The difference between the 500°C and 600°C treatments is small and not clearly distinguishable. However, the reduction in surface stress from untreated to 500°C treated samples is 3.73 MPa, which could contribute to a decrease in the stresses measured in the ring-on-ring test.

The strength of the samples was corrected using the surface stress, as shown in Figure 4.22 and Figure 4.23. These corrections indicate that the repair process became more effective, resulting in a smaller reduction in strength. While the absolute strength values change, the overall trends and conclusions regarding the stresses remain consistent.

4.6. Post-Fracture

In this study, the difference between naturally aged and artificially aged glass is assessed. The ring-on-ring test results show that thermal treatment reduces the strength of naturally aged glass, while it increases the strength of artificially aged glass. This distinction is crucial for potential application in the construction industry, where the goal would be to repair and reuse naturally aged glass. Therefore, understanding the underlying cause of this difference in strength behaviour is essential. These steps aim to provide insight in the observed behaviour.

4.6.1. Failure pattern

The evaluation revealed several distinct fracture patterns in the artificially aged samples. These are illustrated in Figure 4.24. In total, six different failure types were identified. For clarity in the illustrations, artificially induced scratches were marked as black lines, while the resulting cracks were traced in blue. The ring is drawn in gray onto the failure pattern, but the sketches are not fully precise, showing bends in the failure pattern that are likely related to the ring without exactly aligning with it. Among them, types A to C represent the primary modes of failure, while types D to F occurred less frequently but remain of interest for understanding alternative fracture mechanisms.

Failure pattern A, shown in Figure 4.24a, features a scratch located centrally on the glass surface. A crack forms directly along the scratch and continues in a straight line even beyond the visible end of the scratch. This results in a crack that is always longer than 1 cm. Additionally, a horizontal zigzag shaped branching of cracks often appears above and below the main vertical crack, indicating further

crack propagation.

Failure pattern B, shown in Figure 4.24b is similar to A, but with a key difference. The cracks do not follow the scratch to its full extent. Instead, they divert from the scratch path before reaching its end, causing the vertical crack to be shorter than 1 cm.

Failure pattern C, shown in Figure 4.24c, the cracks appear partly unrelated to the scratch. The origin is located on the scratch, but the cracking pattern is radial propagating in all directions, typical of fracture behaviour in undamaged or new glass. Although no distinct vertical crack is visible along the scratch, the origin of failure is still located at the scratch.

Failure pattern D, shown in Figure 4.24d, is similar to pattern C in its radial layout, but the origin of failure is located at a random point on the glass surface, far from the scratch. This indicates that the scratch did not play a role in triggering the failure.

Failure pattern E, shown in Figure 4.24e, appears as a combination of pattern A and B. A crack initiates at the scratch and propagates vertically beyond the scratch's visible length, as seen in pattern A. However, the crack path turns horizontally before the scratch ends, meaning the scratch is not fully enclosed within the vertical fracture zone.

Finally, failure pattern F, shown in Figure 4.24f, involves failures that originate at the edge of the glass. Such failures typically invalidate the test, but they occurred multiple times. These edge origin failures may result from pre-existing edge damage or handling issues, highlighting the sensitivity of the test setup to edge conditions.

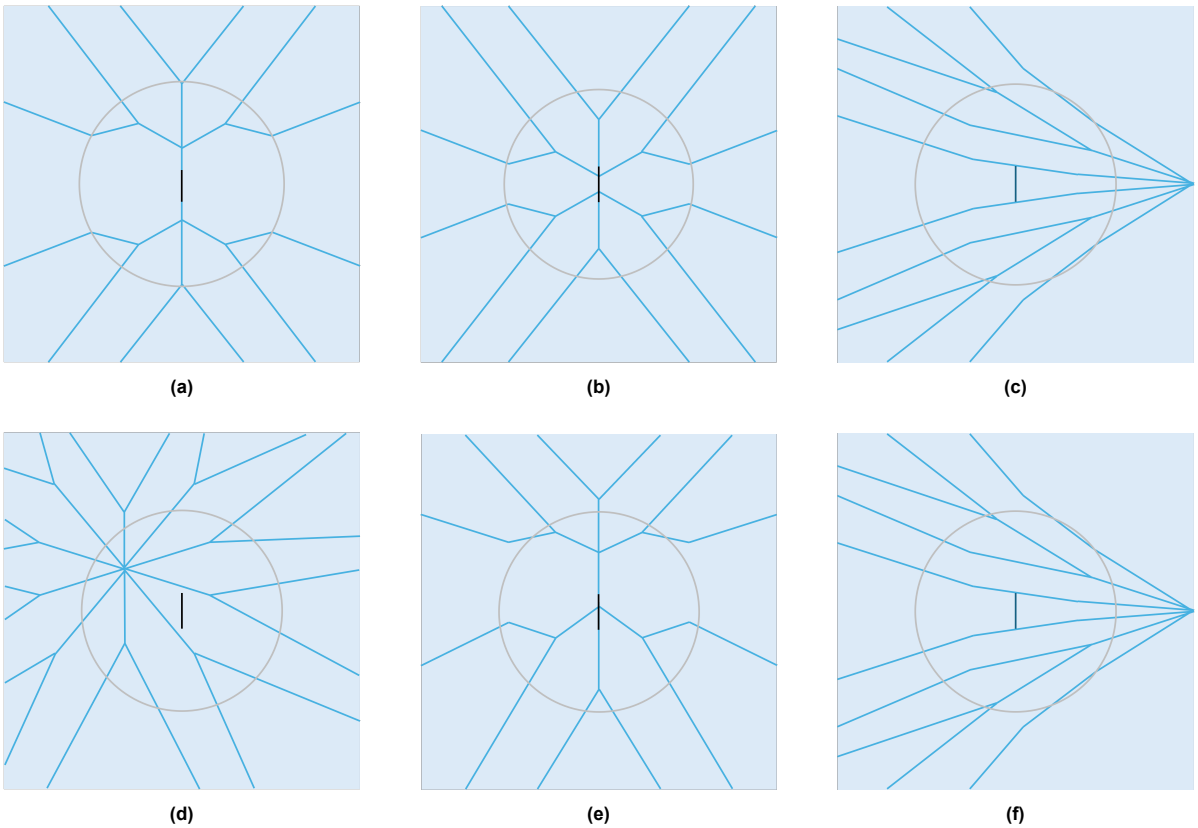

Figure 4.24: Failure pattern artificially aged glass

The failure patterns of the naturally aged glass is analysed and shown in Figure 4.25. Overall, the failure pattern for the naturally aged glass appears to be more influenced by the interaction with the ring. Inside the ring, the glass breaks into smaller fragments that seem somewhat interconnected, while outside the ring, cracks propagate toward the edge without intersecting or coming close to each other. The crack appears to initiate at a single point, suggesting that pits are more likely the governing

failure mode. A similar pattern is observed in the samples treated at 500°C. However, at 600°C, the glass exhibits a variety of failure patterns with no consistent trend. Interestingly, these diverse patterns resemble those seen in artificially aged glass treated at 600°C.

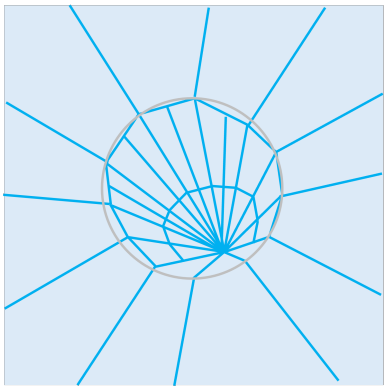

Figure 4.25: Failure pattern naturally aged glass

Some samples were examined under a microscope to analyse surface defects, and these images were compared to the failure locations observed after the ring test. However, the exact origin of failure was difficult to determine precisely, and the images did not always reveal clear defects. This made it challenging to confidently correlate specific surface flaws with the failure points.

The failure behaviour of artificially aged glass varied noticeably depending on the level of thermal treatment. In the untreated glass samples, 70% of failures followed failure mode A, where the scratch was clearly the primary cause. The cracks propagated directly along the scratch and often extended in a straight line beyond its visible end, as if compelled to follow the scratch path entirely. About 22% of failures followed failure mode B.

In contrast, the glass treated at 500°C showed signs of improvement in the area surrounding the scratch. The failure pattern shifted more frequently toward failure mode B, in which the cracks initially followed the scratch but then diverted, indicating that the scratch was no longer the weakest path throughout the entire surface. In these samples, 21% of failures followed failure mode A, while 57% followed failure mode B. This shift suggests that thermal treatment at 500 °C may have locally strengthened the glass or mitigated the severity of the scratch induced flaw.

At 600°C, the failure behaviour changed even further. 96% of the samples exhibited failure mode C, where the cracks appeared largely uninfluenced by the scratch. Although the failure typically originated near the scratch, the crack path no longer followed it. Instead, it propagated in its own direction, as though the scratch had little influence beyond the initial crack initiation. This suggests that while the scratch remained the starting point of failure, the rest of the scratch was no longer the dominant weakness, and the glass fractured in a manner more consistent with undamaged material.

The failure pattern of the naturally aged glass appears more radial, with cracks propagating in various directions. It also seems to be influenced by the interaction with the ring, as a noticeable difference can be observed between the inside and outside of the loading ring. A similar pattern is seen in the samples treated at 500°C. However, in the samples treated at 600°C, the failure behaviour becomes more varied, with no consistent pattern emerging.

Conclusion

The artificially aged glass appears to be significantly influenced by the thermal treatment. The failure pattern evolves progressively with increasing treatment temperature. Initially, cracks follow the scratch entirely, but as the thermal treatment temperature increases, they begin to follow the scratch only partially, and at higher temperatures, they originate near the scratch but no longer propagate along its path. This progression suggests that the scratch is undergoing a degree of healing during the thermal treatment. For the naturally aged samples, the failure pattern remains consistent between the untreated and the 500°C treated specimens. However, at 600°C, the failure behaviour begins to change, and the

crack patterns become more varied. This shift may indicate that the properties of the glass are being altered by the thermal treatment.

4.6.2. Stiffness

The stiffness values were extracted from all data files, and the average results are presented in Table 4.9. The stiffness of the untreated samples and those treated at 500°C were found to be similar. However, after treatment at 600°C, the stiffness decreased by approximately 21%. Additionally, it was observed that for some of the thermally treated samples at 600°C, the load-displacement curves began to deviate from linearity, becoming more curved. This behaviour suggests a potential change in the mechanical response of the glass at higher treatment temperatures.

Table 4.9: Stiffness glass samples

	Stiffness [kN/mm]
Naturally aged glass	29.4
Naturally aged glass (500°C)	29.0
Naturally aged glass (600°C)	23.2
Artificially aged glass	29.1
Artificially aged glass (500°C)	29.2
Artificially aged glass (600°C)	22.9

Conclusion

The stiffness of glass treated at 600°C was reduced by approximately 21%. This reduction may partially explain the observed decrease in strength for naturally aged glass at this temperature. However, these values should be used for comparison only, as differences could also arise from variations in failure strength or testing conditions between samples.

4.6.3. Microscopy

The images obtained from each method are shown in Appendix D and were compared, revealing several notable differences. Samples with more surface flaws, such as those with local damage or artificial scratches, generally exhibited lower strength. This confirms a clear relationship between surface defects and strength.

When comparing naturally aged glass to artificially aged glass, the area of interest around the fracture origin differed notably. Naturally aged glass required higher magnification during microscopy, typically 150×, to capture the entire mirror region and its surroundings. In contrast, artificially aged glass had larger defects, so lower magnifications (50× for untreated, 500°C for treated and 100× for 600°C treated) were sufficient. The smaller mirrors observed in naturally aged glass correspond to higher failure stresses, consistent with the known relationship between mirror size and failure stress (Quinn 2020). Conversely, the larger mirrors in artificially aged glass reflect lower failure stresses. In scratched samples, the mirror could be elongated along the scratch, making it wider, which also influenced the magnification required to observe the full fracture region.

In untreated naturally aged samples, a darker spot likely some kind of shadow was often visible in the centre of the mirror region as shown in Figure 4.26a. This effect was also noticed in other non treated samples. After thermal treatment at 500°C and 600°C, this failure origin became less localised, with damage more distributed across the surface. This could indicate that the thermal process either altered the surface characteristics or introduced additional surface degradation, possibly due to contamination in the oven. This is shown in Figure 4.26.

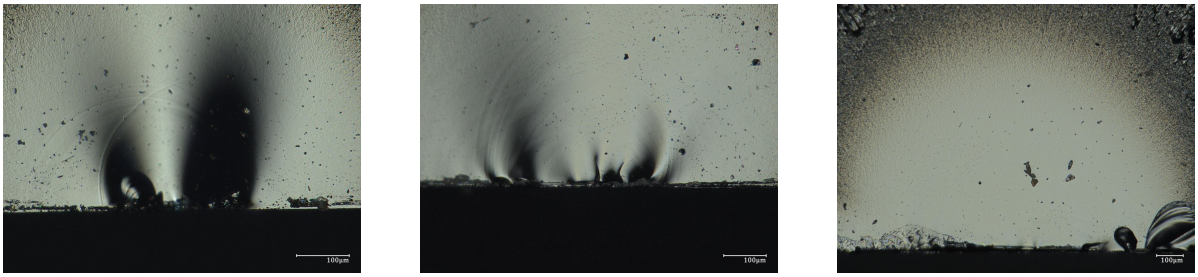

(a) S64 non treated (99 MPa) **(b)** S41 treated 500 °C (86 MPa) **(c)** S174 treated 600 °C (48 MPa)

Figure 4.26: Post fracture of naturally aged glass

In contrast, the artificially aged samples showed an inverse trend. Initially, the surface damage was broadly distributed along the scratch. After thermal treatment at 600°C, however, failures became more concentrated around a specific point rather than spreading along the entire scratch. In some 500°C-treated samples, flaws appeared shallower compared to untreated ones, suggesting partial healing. This is shown in Figure 4.27.

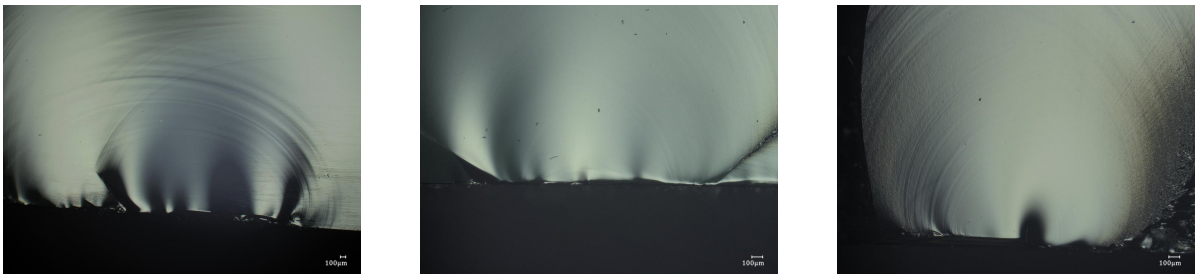

(a) S16 non treated (36 MPa) **(b)** S188 treated 500 °C (47 MPa) **(c)** S59 treated 600 °C (53 MPa)

Figure 4.27: Post fracture of artificially aged glass

Conclusion

The failure behaviour of the samples varied considerably, making direct comparisons challenging. However, a clear correlation was observed between the measured strength from the ring-on-ring test and the visible surface damage seen during post-fracture analysis. The artificially aged glass exhibited a larger damaged area compared to naturally aged glass. For the naturally aged samples, thermal treatment appeared to change the damage pattern from more concentrated flaws to more dispersed ones across the surface. In contrast, the artificially aged glass showed signs of healing, as the previously extended scratch damage became more localized. Overall, while some surface changes were observed due to thermal treatment, most differences in failure behaviour seem to relate more closely to variations in strength than to the treatment conditions themselves.

5

Discussion

This chapter discusses the results obtained in this study, interpreting both expected and unexpected observations and comparing them with previous research. Explanations for the observed behaviours and their implications are provided and limitations encountered during the experiments are highlighted.

5.1. Samples preparation & Artificial ageing

The preparation of the samples and the artificial ageing do not yield results on their own, but are necessary to prepare the samples for the methodology chosen in this study. For example, cutting the glass panels was required to increase the sample size of each group and to ensure a proper fit for the ring-on-ring test. As a result, nine out of the ten groups achieved a sufficient goodness of fit, with a p_{AD} value above 5. Some of the samples were also artificially aged due to inconsistencies in the strength results. This was done to determine whether the behaviour of the artificially aged glass was consistent with previous studies or if there were factors specific to the type of glass influencing the results. Ultimately, the artificially aged glass behaved in a manner consistent with earlier studies, increasing the reliability of the results for the naturally aged glass. However, certain limitations in these procedures were identified, which could be addressed in future research.

Limitations

The glass panels were delivered in full-size sheets and had to be cut into smaller square samples before testing could begin. Since glass is a brittle material, the cutting process required careful handling. Despite this, it is possible that some surface or edge damage occurred during processing, which may have affected the mechanical properties of certain samples.

Artificial ageing was carried out by manually scratching the glass using a controlled scratching device. While care was taken to ensure the scratches were similar in appearance and depth, microscopic inspection later showed some variation between them. This inconsistency may have influenced the comparison of healing effects between samples.

All glass used in this study was naturally aged, meaning it had been exposed to environmental conditions over time. Due to time and material constraints, artificial scratches were introduced onto this naturally aged glass instead of using completely new glass. As a result, the analysis assumes that the artificially introduced scratch is the primary failure during testing. This assumption is confirmed in subsection 4.6.1, where the failure pattern was analysed. In samples without thermal treatment, 92% failed along the scratch, either partly or along its entire length. After the 500°C thermal treatment, 78% of the failures followed or partly followed the artificially made scratch. For samples treated at 600°C, the failures no longer followed the scratch. However, in 96% of cases, the failure originated somewhere on the scratch.

5.2. Microscopy

The microscopy analysis in this study employed two distinct approaches: stitched image processing for the naturally aged glass and direct microscopy for the artificially aged glass. The types and sizes of damage differ substantially. Naturally aged glass exhibits very small defects that are difficult to detect over a large area of interest, whereas artificially aged glass displays visible scratches of approximately 1 cm, which can be observed with the naked eye.

For the naturally aged glass, stitched image processing proved to be an effective method for analysing surface defects. At 500°C, some samples exhibited an increase in scratches, while others showed a slight reduction, indicating variable responses. At 600°C, damage appeared more pronounced in certain samples, potentially due to contamination during imaging, while others remained largely unchanged, emphasising the importance of thorough sample cleaning. If the sample was dirty and blocked light, this could alter the contrast, resulting in misinterpretation of dirt as scratches. The microscopy revealed numerous small scratches, pits, and other types of damage. Some scratches or surface flaws also appeared after the thermal treatment, which could be the result of internal defects within the glass emerging at the surface. Further research is required to better understand this phenomena. The analysis considered the entire sample rather than individual flaws. Although scanning individual defects could provide additional insights, it may be time-consuming, and the microscope's resolution could limit the measuring of very small flaws. Reference studies for naturally aged glass are lacking, and the size of defects appears to respond differently to thermal treatment, indicating that naturally aged glass does not necessarily behave like artificially aged glass.

For artificially aged glass, only the area of interest was scanned, allowing higher magnification and more detailed observation of scratches. Samples treated at 500°C exhibited minimal changes in scratch morphology, with most scratches maintaining their original length and width. One sample developed a subcritical crack and showed an increase in scratch width, suggesting some adverse effects of the thermal process. At 600°C, scratch length remained largely unchanged. However, the formation of subcritical cracks around the scratches resulted in a significant increase in overall width. These observations suggest that internal stresses or heating from the oven caused crack expansion. As the images are two-dimensional, subsurface processes could not be observed, and the changes appear limited primarily to subcritical crack growth. However, microscopy revealed an increase in cracks despite an observed increase in strength. This could suggests an ambiguous role of the cracks in the glass, as they may either contribute to damage or represent a form of self-healing. Further research is required to better understand these phenomena.

Comparison with the findings of Datsiou, Bristogianni, et al. (2025) indicates some discrepancies. In that study, samples treated at 500°C exhibited visible improvements, with scratches appearing narrower and partially healed, suggesting that viscous flow and partial thermal healing occurred. In contrast, the 500°C samples in this study resemble the 300°C treated samples reported by Datsiou, Bristogianni, et al. (2025), which showed only minor changes compared to untreated controls, apart from slight rounding of crack edges. This discrepancy may be due to differences between the actual temperature experienced by the glass and the oven temperature, suggesting that the effective temperature of the glass during treatment may have been lower than intended. This difference might have something to do with the glass used in this study being 8 mm instead of the 4 mm reported in Datsiou, Bristogianni, et al. (2025).

The study by Blaeß and Müller (2023) demonstrated that healing depends on the interaction between radial and lateral cracks. In Figure 5.1, a schematic representation of crack morphology is provided. In this study, the widening of the cracks is interpreted as subcritical crack growth. However, because observations are based on 2D images, contributions from lateral and radial cracks cannot be excluded. Blaeß and Müller (2023) concluded that if lateral cracks heal slowly, radial cracks continue to widen, the surrounding material bulges, and secondary cracks may form, thereby delaying the healing process despite similar viscous transport conditions. In the microscopy samples, cracks appear to widen. However, due to the two-dimensional imaging, it is unclear which regions of the glass are affected. It is possible that, consistent with Blaeß and Müller (2023), radial cracks continue to widen because lateral cracks are healing slowly, potentially influenced by the oven's heating rate.

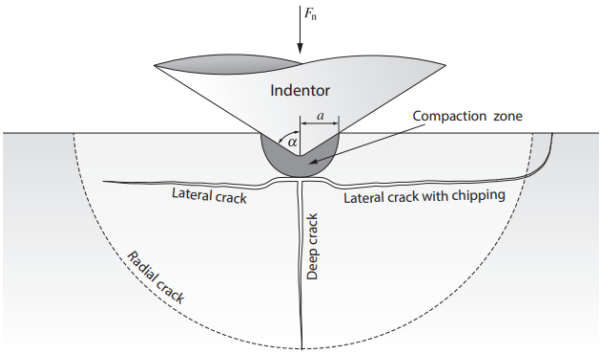

Figure 5.1: Schematic representation of the crack morphology (Prof.Dr. M. Overend)

Limitations

The samples were scanned using an automated image-stitching function within the microscope software, which allowed larger surface areas to be captured efficiently. However, due to time constraints, individual scratches were not tracked or assessed in detail to observe visual changes before and after thermal treatment.

With the microscope software, scratches or defects could be manually marked, but this process was time consuming and prone to human error. Due to the large surface area and the difficulty in identifying specific locations on the sample, it was easy to overlook some scratches. As a result, not all flaws were consistently marked in the images. To address this issue, image processing was introduced to improve accuracy and efficiency.

Proper cleaning of the samples was essential, as any residual dirt could affect the image quality and be misinterpreted as surface damage. For the oven-treated samples, it was not always possible to remove all contamination, particularly on the back side of the glass. This may have influenced some of the imaging results. Figure 4.10a shows a few curved black lines, which are likely marks left by the water used during cleaning.

The images were analysed using ImageJ, a basic but widely used image processing tool. While the software was tested on several scratched samples and generally worked as intended, not all samples were analysed in detail due to the limited scope of this research.

In this study, microscopy was used to analyse the glass in two dimensions, capturing only surface features. Consequently, the depth of cracks and any movement within them could not be observed. Incorporating three-dimensional imaging in future studies could provide a more comprehensive understanding of crack behaviour.

5.3. Thermal treatment & Energy-dispersive X-ray spectroscopy

During thermal treatment, the glass developed a yellow discolouration. This effect was clearly visible at 600°C and already noticeable at 500°C, resulting in visual distortion. The phenomenon was most likely caused by oxidation of the metallic coating, as later confirmed by EDS analysis. Since the EDS measurements were performed on a single sample, the results may have been influenced by non-uniform chemical composition across the surface. A comparison between coated and uncoated specimens provided the basis for identifying differences between the air side and the tin side, and for interpreting the changes induced by thermal treatment. Nevertheless, additional elements were detected which may also have contributed to the discolouration, leaving it unclear whether the yellow tint resulted from a combination of metals or a single element. Previous studies did not report such effects, most likely because they examined new, uncoated glass. This limitation should be addressed in future research, as the observed discolouration could have significant implications for the practical application of thermally treated glass in the construction industry.

Limitations thermal treatment

During thermal treatment, the glass samples were placed on the bottom plate of the oven. This setup may have caused uneven heating, where the top surface of the samples reached higher temperatures more quickly than the bottom.

The heating program followed a predefined temperature profile, and it was assumed that the temperature of the glass closely matched that of the oven. However, some discrepancies were noticed during cooling when the oven reached around 100°C, the samples could already be touched by hand, suggesting a lag in temperature transfer. Besides, the oven did not return to room temperature as quickly as expected. After 24 hours, it still measured around 150°C, which indicates that the cooling process was slower than the programmed profile. This could be solved by adding a thermocouple in the oven.

Finally, the humidity inside the oven was not actively controlled or monitored in this study. This was a limitation of the oven used in this research.

Limitations Energy-dispersive X-ray spectroscopy

EDS analysis was carried out on one glass shard per side for each treatment method. Since this is a point-based measurement, the results may not fully represent the overall composition of the surface, especially if local impurities or surface variations are present.

To identify the tin side of the float glass, a UV-based tin side detector was used. Interestingly, the EDS analysis failed to detect tin on this side in most cases, only one sample showed a tin signal.

5.4. Coaxial double-ring test

The ring-on-ring test was conducted on glass samples to evaluate strength after different thermal treatments. The results revealed contrasting effects between artificially scratched and naturally aged glass. For artificially scratched specimens, strength improved significantly after treatment: the 5% characteristic strength increased by 13% at 500°C and by 41% at 600°C compared to the reference group. At the 50% characteristic level, strength increased by 10% and 37%, respectively.

In contrast, naturally aged glass panel 2 exhibited a decline in performance following thermal treatment. At 500°C, the 5% characteristic strength decreased by 28% and the mean strength by 13%. At 600°C, these values declined further, by 56% and 36%, respectively. Naturally aged glass panel 1 also exhibited a decline in performance following thermal treatment. At 500°C, the 5% characteristic strength decreased by 13% and the mean strength by 11%. However, it should be noted that the results for the 500 °C treatment of panels 1 and 2 differ considerably: the 5% characteristic strength decreased by 13% and 28%, respectively, suggesting that the strength reduction may be highly dependent on the individual glass panel. Interestingly, the mean strength decreased by 11% and 13%, respectively, which are much closer to each other. These results could potentially demonstrate that glass responds differently to thermal treatment depending on the type of pre-existing damage.

Previous studies have focused primarily on artificially aged glass, limiting direct comparisons with the naturally aged samples. For artificially scratched glass, however, the findings can be checked against existing literature. Datsiou, Bristogianni, et al. (2025) reported a mean strength recovery of 42% after treatment at 500°C, while Schwind et al. (2020) observed a 41% increase after thermal treatment at 525°C. Both studies therefore demonstrated an improvement in glass strength of around 41 and 42%, which corresponds well with the 37% increase observed in the artificially scratched samples treated at 600°C in this study. Nevertheless, the mean strength increase of only 10% at 500°C was considerably lower than the values reported by Datsiou, Bristogianni, et al. (2025) and Schwind et al. (2020).

Datsiou, Bristogianni, et al. (2025) reported a 0.8% strength corresponding to 29.8 MPa for scratched glass, 38.4 MPa for heat treatment at 300 °C, and 46.4 MPa for heat treatment at 500 °C. This represents a strength increase of 29% after healing at 300 °C and 56% at 500 °C compared to artificially aged glass. In comparison, the results of this study show that the strength increase from scratched glass to 500 °C heat treatment is 16%, and to 600 °C is 44%. These results appear to diverge considerably. In this study, the 500 °C treatment corresponds more closely to the 300 °C treatment in Datsiou, Bristogianni, et al. (2025), while the 600 °C treatment aligns better with their 500 °C data.

As with the microscopy results, this discrepancy may be due to differences between the actual temper-

ature experienced by the glass and the nominal oven temperature, potentially influenced by the heating rate. Furthermore, differences in sample thickness (8 mm in this study compared with 4 and 6 mm in the cited studies) may also have contributed to the variation in results.

Limitations coaxial double-ring test

The testing machine is controlled via displacement sensors located on the sides of the device. However, because these sensors are not positioned directly at the point of loading, there may be a slight reduction in measurement accuracy.

Each sample was mounted in the setup with a small preload. When the test began, the force did not increase immediately in a linear fashion. Instead, there was a brief period of disturbance before the load was applied consistently. This could have influenced the early phase of the loading curve and should be considered when interpreting the failure data.

5.5. SCALP-05

The heating profile was selected to ensure that the internal stresses remained comparable to those of the reference group, thereby isolating the effect of thermal healing without additional stress influencing the results. SCALP measurements indicated that surface stress decreased with thermal treatment. To assess whether internal stress influenced the results, the data were corrected accordingly. Although the absolute strength values changed after correction, the overall trends and conclusions regarding stress behaviour remained consistent. This underlines the importance of carefully controlling the heating process. In the present study, the differences were too small to affect the outcome.

Limitations SCALP

The surface stress values obtained using the SCALP-05 device were relatively low, which may influence the accuracy of the results. The device has a minimum measurable surface stress of 1 MPa, with a precision of ±1 MPa for surface stress below 4 MPa, and within ±5% for surface stress above 4 MPa. This level of precision should be considered when interpreting the results, particularly for the samples treated at 500°C and 600°C, where the measured surface stresses are close in value.

Since the original panels had already been tested destructively, SCALP measurements were performed on leftover glass shards. While surface stress is generally uniform across a glass pane, using fragments instead of whole panels may have influenced the results slightly, especially if stress variations exist across the surface. The shard could also impact the results due to light scattering, which is used to measure the internal stresses.

5.6. Post-Fracture

The post-fracture is later added and aims to explain why the strength of artificially aged glass improves after thermal treatment, while the strength of naturally aged glass decreases. This is based on the data already discussed but also on the crack pattern, stiffness and the post fracture. Based on these findings, a theory is proposed to account for these differences.

Thermal treatment had a strong influence on artificially aged glass. With increasing temperature, the failure pattern progressed from cracks fully following scratches, to partially following them, and eventually to initiating near scratches without propagating along them. This behaviour indicates changes in the scratch damage during treatment. In naturally aged glass, failure patterns remained similar between untreated and 500 °C specimens, but at 600 °C the behaviour changed, with more varied crack patterns and a shift from concentrated flaws to a more dispersed distribution. At the same temperature, a reduction in stiffness of about 21% was measured, which corresponds with the observed decrease in strength for naturally aged glass. Post-fracture analysis showed that artificially aged samples generally exhibited larger damaged areas, but also evidence of localized healing of scratches, whereas naturally aged samples displayed a redistribution of damage across the surface. The measured strength from the ring-on-ring tests correlated closely with the observed fracture damage.

Healing vs. Degradation: a proposed theory

Based on these findings, it appears that cracks in artificially aged glass undergo a healing process during thermal treatment. This conclusion is supported by the crack pattern analysis in subsection 4.6.1, which shows that at first, cracks follow the scratch entirely. As the thermal treatment temperature increases, cracks begin to deviate from the scratch path, and at higher temperatures, they originate near the scratch but no longer propagate along it.

Conversely, the glass itself seems to lose strength during thermal treatment. In Figure 4.5, surface stress measurements show reductions of 3.73 MPa and 4.19 MPa after treatment at 500°C and 600°C, respectively. Additionally, the stiffness of glass treated at 600°C decreases by approximately 21%. Structural relaxation may also contribute to this weakening, as it involves molecular rearrangements that reduce internal tensile stresses, which initially made the glass appear slightly harder or more brittle.

It is likely that multiple processes are occurring simultaneously, but their effects differ depending on the type of glass. In artificially aged glass, the primary failure mode is the scratch. As a result, thermal treatment can partially heal this flaw, reducing its severity and thereby increasing the overall strength of the glass. In contrast, naturally aged glass may not have a single dominant surface flaw. Instead, it typically contains many smaller flaws scattered across the surface. Because there is no clear flaw to heal, thermal treatment has limited effect in strengthening the material.

Meanwhile, both types of glass experience a general reduction in intrinsic strength due to thermal exposure. However, this reduction influences the two types of glass differently. In naturally aged glass, where the surface itself becomes the primary failure origin, any decrease in intrinsic material strength directly reduces the overall strength. In artificially aged glass, the scratch remains the dominant flaw, so weakening of the surface plays a lesser role. The scratch remains the critical point of failure, not the surface itself. A visual representation is illustrated in Figure 5.2 which shown the effect of the healing and degradation for the different groups.

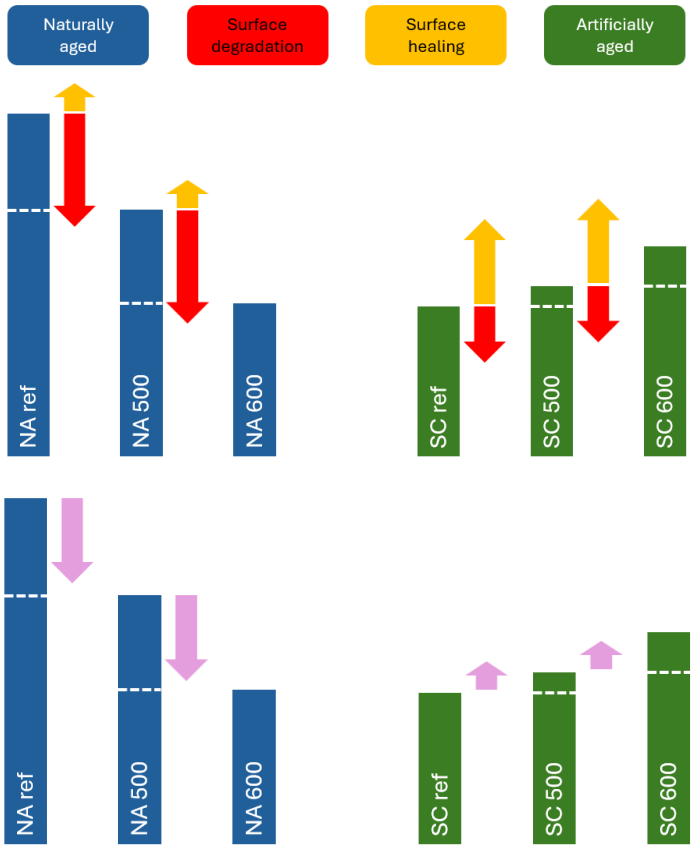

Figure 5.2: Visualisation of the healing effect

The gap in strength is not fully quantifiable because two processes appear to act simultaneously. Surface strength could be assessed through SCALP measurements and stiffness, which both reflect surface behaviour. However, the healing effect of the scratch cannot be directly measured. In naturally aged glass, surface degradation is the primary cause of failure and can be estimated, but in scratched glass this effect may be obscured because the scratch weakens the glass significantly, causing failure from the scratch rather than from the surface strength.

Ultimately, the net effect of thermal treatment depends on the balance between crack healing and strength reduction, which is influenced by the dominant failure mode. Artificially aged glass benefits because scratch healing outweighs the material weakening, while naturally aged glass deteriorates because minimal healing cannot compensate for the strength loss.

Inconsistencies with the proposed theory

Several factors may explain the differing behaviour observed between naturally aged and artificially aged glass, but one aspect does not fully align with the proposed theory. According to this theory, naturally aged glass loses strength due to surface deterioration, while artificially aged glass gains strength because of scratch healing. This suggests there should be a point where the effects of scratch healing and surface deterioration balance out, resulting in no net change in strength.

After thermal treatment at 600°C, the artificially aged glass P2_Tin_SC_600 shows in Figure 4.19 a notable increase in strength, while the naturally aged glass P2_Tin_NA_600 exhibits a decrease. Intuitively, the naturally aged glass should have similar or higher strength compared to the artificially aged glass if such a balance point exists. However, in this case, the artificially aged glass has higher strength than the naturally aged glass. This could suggests that smaller surface cracks in naturally aged glass might worsen during thermal treatment, indicating that the thermal process affects different types of surface flaws in distinct ways. It could also be influenced by the condition of the glass itself. As described in the methodology, the naturally aged glass was intentionally scratched, thereby transforming it into artificially aged glass. This approach assumes that the introduced scratch represents the primary failure mode. However, due to the heat treatment, this assumption may no longer hold, as the surface characteristics could change.

Another possible explanation lies in the analysis of the strength data. A box plot of the strength data shown in Figure 5.3, reveals a similar trend as the Weibull distribution plots but also highlights the differences in spread between groups. The naturally aged glass exhibits a much wider spread in strength values compared to the artificially aged glass. Looking more closely at the P2_Tin_NA_600 and P2_Tin_SC_600 methods, both thermally treated at 600°C, the groups have similar minimum values and comparable averages. However, their spreads and maximum values differ significantly. This nuance is harder to discern in statistical evaluations, so exploring alternative data analysis methods may provide further insights into the differing glass behaviours.

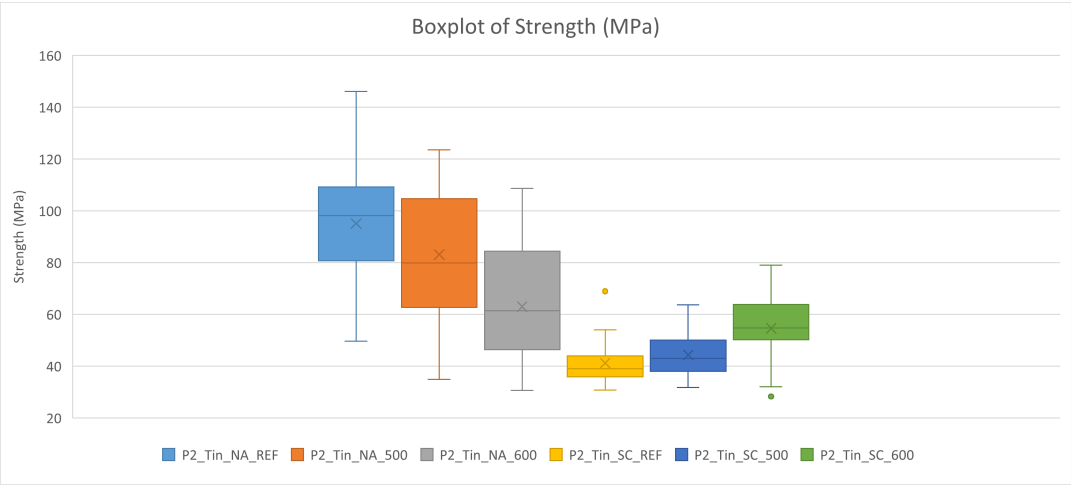

Figure 5.3: Box plot strength

This effect can also be confirmed by examining the shape factor (β) of the Weibull distribution, which characterizes the scatter of failure strengths. For the naturally aged glass, the calculated shape factors are 4.61, 3.45, and 2.79, while the artificially aged glass exhibits higher values of 4.93, 5.27, and 5.19. The shape factor corresponds to the slope of the Weibull probability plot, a higher value produces a steeper slope, meaning that failures occur within a narrower range of strength values. This reflects a more uniform and predictable failure behaviour. In contrast, lower shape factors result in a flatter slope, indicating a wider spread of strength values and greater variability in the failure process. Thus, the naturally aged glass demonstrates a broader distribution of failure strengths, while the artificially aged glass shows more tightly clustered failures, suggesting that artificial ageing produces more consistent degradation.

Additional considerations

In addition to the three subjects already explained, several other possible explanations could be interesting to discuss in this section and explored further in future research. Surface stress and stiffness have already been investigated, but structural relaxation could also play a role in influencing the strength of the glass. Structural relaxation in glass refers to the rearrangement of atoms or molecules toward a more stable, lower-energy configuration. This typically occurs near or below the glass transition temperature, where the glass is rigid but still exhibits some molecular mobility. An important consequence of this process is the gradual loss of pre stress. As the glass structure relaxes, compressive stresses are reduced, which can alter the apparent hardness or brittleness of the material. Recent work by (Hamada et al. 2023) confirmed that when soda lime silicate glasses were annealed 50 K below the glass transition temperature, they underwent structural and volume relaxation involving reorganization of the SiO_2 network and migration of Na^+ ions, changes that are consistent with the release of internal stresses and the reduction of pre stress in the glass.

Besides scratches, other types of flaws such as pits were observed during microscopy. These pits could react differently to thermal treatment, potentially influencing the degradation seen in naturally aged glass. This effect has not been investigated in this study and could be an important factor contributing to the deterioration of naturally aged glass.

Another factor to consider is the size and nature of surface flaws. Artificially aged glass have larger flaws due to the intentionally made scratch, which may respond differently to thermal treatment. Larger flaws generally have lower stress concentrations at their tips compared to sharp micro-cracks. During heating, the increased viscosity of the glass allows viscous flow at the edges of these flaws, partially “rounding” the defects and reducing the stress intensity factor. This mechanism can improve the strength of artificially scratched glass. In contrast, naturally aged glass typically contains numerous small but sharper cracks that have higher stress intensities. These sharp cracks are less likely to blunt significantly during thermal exposure and can remain critical flaws. This rounding mechanism has been experimentally confirmed by (Blaeß and Müller 2023), who studied the thermal healing of Vickers indentation, induced cracks in different silicate glasses. They observed that during annealing, initially sharp cracks undergo tip blunting and edge rounding, often widening into oval or cavity, like shapes before gradually smoothing and filling through viscous flow. This process lowers the stress concentration at the flaw tip and can delay or suppress further crack growth. Importantly, their results show that larger indentation flaws are more prone to this rounding and partial healing, whereas smaller, sharper cracks remain critical and heal less effectively

6

Conclusion & Recommendations

This chapter addresses the additional research questions posed at the beginning of the study, using the findings gathered throughout this research. It also provides a final answer to the main research question, bringing the investigation to a conclusion. Lastly, recommendations are provided to guide future research in this area.

6.1. Research question

To what extent can thermal treatment enhance the strength of naturally aged glass, affecting their potential for reuse?

Additional research questions:

- To what extent do different thermal treatments influence the morphology of surface flaws?
- To what extent do different thermal treatments affect the strength of aged glass?
- To what extent do surface flaws and strength recovery after thermal treatment differ between naturally and artificially aged glass?

To what extent do different thermal treatments influence the morphology of surface flaws?

In this research, both naturally and artificially aged glass were investigated. Naturally aged glass showed minimal surface degradation, with only small flaws detectable. In contrast, artificially aged glass was intentionally scratched to create larger, visible surface flaws for analysis.

Thermal treatment of naturally aged glass led to observable but inconsistent changes in surface morphology. At 500°C, some samples developed additional scratches, while others showed a slight reduction in surface defects, reflecting varied responses. At 600°C, the damage became more pronounced in certain samples, potentially due to contamination affecting image interpretation, while others remained relatively unchanged. Although individual samples showed visible changes, there was no consistent trend across the entire group. These findings suggest that thermal treatment does not reliably repair surface flaws in naturally aged glass.

Artificially aged glass showed a more consistent pattern. At 500°C, changes in scratch morphology were minimal. Most scratches retained their original shape, though some showed a fading of the dark groove line or developed subcritical cracks. At 600°C, subcritical crack formation around existing scratches led to a significant increase in overall crack width. Scratches became less defined, and their shapes appeared altered, indicating a degradation of surface structure. These results consistently show that thermal treatment, particularly at higher temperatures, tends to aggravate surface flaws in artificially aged glass.

In summary, thermal treatment produces inconsistent and partly negligible effects on the surface flaws of naturally aged glass, whereas in artificially aged glass it consistently aggravates existing scratches, particularly at higher temperatures.

To what extent do different thermal treatments affect the strength of aged glass?

In this research, both naturally and artificially aged glass were tested to assess the effect of thermal treatment on mechanical strength.

For artificially aged glass, strength improved significantly after thermal treatment. The 5% characteristic strength increased by 13% at 500°C and by 41% at 600°C compared to the reference samples. Similarly, the mean strength increased by 10% and 37%, respectively. These results suggest that thermal treatment can positively affect the strength of artificially aged glass.

In contrast, naturally aged glass exhibited a decline in strength following thermal treatment. The 5% characteristic strength decreased by 28% at 500°C and by 56% at 600°C, while the mean strength dropped by 13% and 36%, respectively. A similar trend was observed in panel 1, where thermally treated naturally aged glass also showed reduced strength. These findings indicate that thermal treatment tends to negatively affect the performance of naturally aged glass.

To isolate the effect of thermal treatment from surface stress, SCALP-05 measurements were conducted. These results showed a reduction in surface stress due to thermal treatment by 3.73 MPa at 500°C and by 4.19 MPa at 600°C. This reduction in surface stress may have contributed to the lower strength values observed in the ring-on-ring tests.

Overall, when accounting for the reduction in surface stress, the improvement in artificially aged glass becomes larger, while the decrease in strength for naturally aged glass appears less severe. However, the SCALP-05 measurements do not alter the general trends or the main conclusions regarding the effects of thermal treatment on glass strength.

In summary, thermal treatment significantly increases the strength of artificially aged glass while simultaneously decreasing the strength of naturally aged glass, with the magnitude of these effects growing at higher temperatures.

To what extent do surface flaws and strength recovery after thermal treatment differ between naturally and artificially aged glass?

The difference between naturally aged and artificially aged glass begins with the type of surface damage. Naturally aged glass deteriorates over time, exhibiting mostly small scratches and pits, whereas artificially aged glass is intentionally scratched in the laboratory, creating a larger, visible flaw. Consequently, the approaches for investigating surface flaws differed. In artificially aged glass, a 1 cm scratch was placed in the center, making it easy to detect and compare before and after thermal treatment. In contrast, naturally aged glass contained numerous smaller flaws at unknown locations, requiring the entire ring area to be scanned to assess changes.

The effects of thermal treatment on surface flaws also differed between the two types. Naturally aged samples showed inconsistent responses: some surfaces improved slightly, others deteriorated, and some remained unchanged. Artificially aged glass, however, consistently exhibited visually worsened surface defects after heating, primarily due to subcritical crack growth.

Strength recovery mirrored these differences. Naturally aged glass showed a reduction in strength after thermal treatment, while artificially aged glass demonstrated improved strength. Failures in naturally aged glass could originate anywhere on the surface, whereas in artificially aged glass, failures typically initiated at the scratches.

Based on these observations, a theory is proposed to explain the contrasting effects of thermal treatment on naturally and artificially aged glass, where the primary failure mode largely determines the outcome. In artificially aged glass, the dominant scratch acts as the critical flaw, and thermal treatment allows partial healing, reducing its severity and increasing overall strength. Crack pattern analysis shows that at lower temperatures, cracks follow the scratch, while at higher temperatures they initiate near the scratch without propagating along it. Although the surface itself experiences some intrinsic weakening, the scratch remains the primary failure point, so the net effect is strengthening. In naturally aged glass, failure arises from numerous small surface flaws, leaving no dominant crack to heal. As a result, thermal treatment cannot significantly improve strength, and the glass experiences overall weakening due to surface degradation and intrinsic material loss.

These results highlight the contrasting outcomes of thermal treatment on naturally aged versus artificially scratched glass. Microscopy revealed minimal visible changes in naturally aged glass despite the reduction in strength, while artificially aged glass appeared visually worse but showed strength improvements in ring-on-ring testing. This suggests a transition point at which thermal treatment becomes ineffective or even detrimental, depending on the characteristics of the surface flaws.

To what extent can thermal treatment enhance the strength of naturally aged glass, affecting their potential for reuse?

This research assessed the potential of thermal treatment to restore the strength of naturally aged glass. Naturally aged glass develops surface defects over time due to environmental exposure and handling. The goal was to determine whether thermal treatment could recover the glass's strength for reuse in the construction industry. However, the results showed that thermal treatment did not improve the strength of naturally aged glass. Instead, it caused a noticeable reduction in strength.

The glass used in this study had a metallic surface coating that degraded during thermal treatment, likely resulting in the observed yellow discoloration. This discoloration was probably caused by the oxidising of a heat-sensitive metal oxide coating. The effect was clearly visible at 600°C, though it was already noticeable at 500°C. These findings indicate that for thermal treatment to be a viable option for glass reuse in construction, surface coatings must either be thermally resistant or removed prior to processing. Such aesthetic changes are undesirable in the building industry and therefore limit the potential for reuse.

Overall, thermal treatment as applied in this study reduced both the mechanical performance and visual quality of naturally aged glass. Consequently, it cannot be considered a suitable method for restoring naturally aged glass for reuse in construction.

6.2. Recommendations

Based on this research, several recommendations can be made to support future investigations and enhance the reuse potential of glass. The process of thermal treatment was carried out on naturally aged glass, but this category is quite broad and lacks clear definition. It remains unclear when glass can be formally classified as ”naturally aged” and how its condition should be assessed. There may be a threshold in the ageing process beyond which thermal treatment becomes more effective, but further research is needed to identify such a point.

To better simulate the micro-scale damage in naturally aged glass, a Berkovich nanoindenter can introduce fine surface flaws in a controlled, reproducible manner. (Moayedi and Wondraczek 2017) used an instrumented microindenter (G200, Agilent) with a Berkovich diamond tip to scratch silica glass under gradually increasing loads, recording forces and later examining the marks microscopically. This allowed them to pinpoint the onset of cracking and microabrasion, showing that this can quantitatively reproduce and accelerate natural surface wear, making them well suited for artificial ageing tests.

An interesting extension of this work would be to explore the role of oven parameters. Experiments could be conducted using different temperatures and investigating the effect of humidity during the healing process. It may also be worth exploring active cooling methods to achieve a faster cooling rate, which could increase surface stress and potentially improve the mechanical strength of the glass.

Furthermore, the actual glass temperature may not have matched the oven set temperature, which could have significantly influenced the healing process, as healing depends directly on the glass temperature. Some results in this study appear to resemble outcomes from samples treated at lower temperatures, suggesting such discrepancies. This issue could be addressed by using a thermal coupling in the oven to ensure that the glass temperature corresponds to the desired treatment temperature.

The image processing method proved to be an effective and accurate approach for analysing larger glass surfaces, with strong potential to reduce human error in manual microscopy. By enabling automated flaw detection, it improves both accuracy and efficiency. Further research, including refinement of microscopy settings and optimization of processing parameters, could enhance the robustness, consistency, and overall effectiveness of the method for assessing extensive glass areas.

To improve the comparability of data, the development of a standardised test procedure, with a fixed loading rate and controlled conditions, would be beneficial. Naturally aged glass is not only limited in availability but also varies significantly depending on its exposure to environmental conditions. A standardised approach would help generate more consistent results and provide a clearer picture of glass degradation over time.

More attention should be given to the coatings commonly found on architectural glass. This study suggests that such coatings degrade or burn off at elevated temperatures, leading to discolouration. Since discoloured glass is often undesirable in the construction industry, this effect could limit the practical reuse of thermally treated glass.

Further research is needed to investigate the proposed theory in section 5.6: ’Healing vs. Degradation: a proposed theory’ and deepen understanding of how thermal treatment affects glass. One possible approach is to use Differential Scanning Calorimetry to study how the material relaxes strain at different temperatures, which would provide valuable insight into the thermal behaviour of glass during treatment. Complementing this, experiments with new, untreated glass could help to isolate the direct impact of the oven environment itself and reveal whether thermal treatment introduces contamination.

Beyond thermal considerations, greater attention should be given to the role of flaws in determining glass behaviour. Studying artificially introduced defects, such as micro-scratches or surface pits, would allow more systematic comparisons between different flaw types and their response to treatment. While the effect of scratches has mainly been assessed through 2D imaging, extending this work to 3D analysis could provide a more complete picture of how subsurface flaws evolve after treatment. Interestingly, microscopy revealed an increase in cracks despite an observed increase in strength, suggesting that cracks may not solely be damaging but could also contribute to a form of self-healing. In addition, new scratches or surface flaws appeared after thermal treatment, possibly resulting from internal defects emerging at the surface. These phenomena require further investigation to better understand their implications for glass behaviour.

References

Blaeß, Carsten and Ralf Müller (2023). “Viscous healing of Vickers indentation–induced cracks in glass”. In: *Journal of the American Ceramic Society* 106.10, pp. 5795–5805. DOI: https://doi.org/10.1111/jace.19245. eprint: https://ceramics.onlinelibrary.wiley.com/doi/pdf/10.1111/jace.19245. URL: https://ceramics.onlinelibrary.wiley.com/doi/abs/10.1111/jace.19245.

Cupać, Jagoda, Kyriaki Corinna Datsiou, and Christian Louter (Aug. 2024). “Reuse potential of architectural glass: experimental study on the strength of used window glazing”. In: *Glass Structures & Engineering* 9.3, pp. 321–337. DOI: 10.1007/s40940-024-00267-y. URL: https://link.springer.com/article/10.1007/s40940-024-00267-y.

Cupać, Jagoda, Christian Louter, et al. (2025). *Open GLASSlab – Interactive Strength Analysis Handbook*. Source files at TUDelft-books/open-GLASSlab. URL: https://oit.tudelft.nl/open-GLASSlab/.

Datsiou, Kyriaki Corinna, Telesilla Bristogianni, et al. (2025). “Influence of thermal and water treatment on strength recovery for soda lime silica glass”. In: *Glass Structures & Engineering* 10.3, p. 14. ISSN: 2363-5150. DOI: 10.1007/s40940-025-00298-z. URL: https://doi.org/10.1007/s40940-025-00298-z.

Datsiou, Kyriaki Corinna and Mauro Overend (Mar. 2017a). “Artificial ageing of glass with sand abrasion”. In: *Construction and Building Materials* 142, pp. 536–551. DOI: 10.1016/j.conbuildmat.2017.03.094. URL: https://www.sciencedirect.com/science/article/pii/S0950061817304592.

— (July 2017b). “The strength of aged glass”. In: *Glass Structures & Engineering* 2.2, pp. 105–120. DOI: 10.1007/s40940-017-0045-6. URL: https://link.springer.com/article/10.1007/s40940-017-0045-6.

Girard, Rémi, Annelise Faivre, and Florence Despetis (2011). “Influence of water on crack self-healing in soda-lime silicate glass”. In: *Journal of the American Ceramic Society* 94.8, pp. 2402–2407. DOI: 10.1111/j.1551-2916.2011.04517.x. URL: https://ceramics.onlinelibrary.wiley.com/doi/10.1111/j.1551-2916.2011.04517.x.

Haldimann, Matthias, Andreas Luible, and Mauro Overend (2008). *Structural Use of Glass*. International Association for Bridge and Structural Engineering (IABSE). ISBN: 978-3-85748-119-2. URL: https://app.knovel.com/hotlink/khtml/id:kt008RYOD1/structural-use-glass/front-matter.

Hamada, Yuya et al. (Feb. 2023). “Volume relaxation of soda-lime silicate glasses below glass transition temperature”. In: *AIP Advances* 13.2, p. 025353. ISSN: 2158-3226. DOI: 10.1063/5.0131705. eprint: https://pubs.aip.org/aip/adv/article-pdf/doi/10.1063/5.0131705/16760572/025353_1_online.pdf. URL: https://doi.org/10.1063/5.0131705.

International, ASTM (2019). *Standard Test Method for Monotonic Equibiaxial Flexural Strength of Advanced Ceramics at Ambient Temperature*. ASTM C1499-19. DOI: https://doi.org/10.1520/C1499-19.

Karlsson, S. et al. (May 2023). “Non-destructive strength testing of microindented float glass by a nonlinear acoustic method”. In: *Construction and Building Materials* 391, p. 131748. DOI: 10.1016/j.conbuildmat.2023.131748. URL: https://www.sciencedirect.com/science/article/pii/S0950061823014617.

Ministerie van Volkshuisvesting, Ruimtelijke Ordening en Milieubeheer (Apr. 2024). *Voortgang klimaatdoelen*. URL: https://www.rijksoverheid.nl/onderwerpen/klimaatverandering/voortgang-klimaatdoelen.

Moayedi, Elham and Lothar Wondraczek (2017). “Quantitative analysis of scratch-induced microabrasion on silica glass”. In: *Journal of Non-Crystalline Solids* 470, pp. 138–144. ISSN: 0022-3093. DOI: https://doi.org/10.1016/j.jnoncrysol.2017.05.003. URL: https://www.sciencedirect.com/science/article/pii/S0022309317302521.

Nations, United (2015). *PARIS AGREEMENT*. Tech. rep. United Nations. URL: https://unfccc.int/files/essential_background/convention/application/pdf/english_paris_agreement.pdf.

Overend, Mauro and Christian Louter (Apr. 2015). “The effectiveness of resin-based repairs on the inert strength recovery of glass”. In: *Construction and Building Materials* 85, pp. 165–174. DOI: 10.1016/j.conbuildmat.2015.03.072. URL: https://www.sciencedirect.com/science/article/pii/S0950061817304592.

Persson, Kent et al. (Sept. 2020). “Non-destructive testing of the strength of glass by a non-linear ultrasonic method”. In: *Challenging Glass Conference Proceedings* 7. DOI: 10.7480/cgc.7.4498. URL: https://proceedings.challengingglass.com/index.php/cgc/article/view/281.

Quinn, George.D (Sept. 2020). “NIST Recommended Practice Guide: Fractography of Ceramics and Glasses, 3rd edition”. en. In: *NIST*. DOI: https://doi.org/10.6028/NIST.SP.960-16e3.

Rota, Angelica, Marco Zaccaria, and Francesco Fiorito (Aug. 2023). “Towards a quality protocol for enabling the reuse of post-consumer flat glass”. In: *Glass Structures & Engineering* 8.2, pp. 235–254. DOI: 10.1007/s40940-023-00233-0. URL: https://link.springer.com/article/10.1007/s40940-023-00233-0.

Schwind, Gregor et al. (Nov. 2020). “Double ring bending tests on heat pretreated soda–lime silicate glass”. In: *Glass Structures & Engineering* 5.3, pp. 429–443. DOI: 10.1007/s40940-020-00129-3. URL: https://doi.org/10.1007/s40940-020-00129-3.

Sofokleous, E. (2022). *Methodology for the prediction of the strength of naturally aged glass based on surface flaw characterization*. URL: https://resolver.tudelft.nl/uuid:b6ad7619-da9c-448c-aaf4-10cd065bbe14.

Teich, Martien et al. (Aug. 2024). “Reuse and remanufacturing of insulated glass units”. In: *Glass Structures & Engineering* 9.3, pp. 339–356. DOI: 10.1007/s40940-024-00276-x. URL: https://link.springer.com/article/10.1007/s40940-024-00276-x.

Veer, Fred et al. (Jan. 2023). “A Novel Method for the Non-Destructive Assessment of Strength Degradation and Re-Use Potential of Weathered Float Glass From Facades: A Proof of Concept Study”. In: *International Journal of Structural Glass and Advanced Materials Research* 7.1, pp. 1–15. DOI: 10.3844/sgamrsp.2023.1.15. URL: https://thescipub.com/abstract/10.3844/sgamrsp.2023.1.15.

Verberg, Boy and Delft University of Technology (2024). *Enhancing the design strength of weathered float glass: Experimental study into scanning and tempering techniques*. Tech. rep. TU delft.

Wang, Chu, Hongxiang Wang, Rui Gao, et al. (2021). “Experimental investigation on thermal healing of subsurface damage in borosilicate glass”. In: *Ceramics International* 47.12, pp. 17128–17138. ISSN: 0272-8842. DOI: 10.1016/j.ceramint.2021.03.022. URL: https://www.sciencedirect.com/science/article/pii/S0272884221006854.

Wang, Chu, Hongxiang Wang, Zhichao Liu, et al. (2020). “Kinetic model and effect of surface impurities on the crack healing of BK7 glass”. In: *Ceramics International* 46.11, Part B, pp. 19069–19077. ISSN: 0272-8842. DOI: 10.1016/j.ceramint.2020.04.239. URL: https://www.sciencedirect.com/science/article/pii/S0272884220311962.

Westbroek, Coenraad D. et al. (2021). “Global material flow analysis of glass: From raw materials to end of life”. In: *Journal of Industrial Ecology* 25.2, pp. 333–343. DOI: https://doi.org/10.1111/jiec.13112. eprint: https://onlinelibrary.wiley.com/doi/pdf/10.1111/jiec.13112. URL: https://onlinelibrary.wiley.com/doi/abs/10.1111/jiec.13112.

Zaccaria, Marco and Mauro Overend (2016). “Thermal Healing of Realistic Flaws in Glass”. In: *Journal of Materials in Civil Engineering* 28.2, p. 04015127. DOI: 10.1061/(ASCE)MT.1943-5533.0001421. URL: https://ascelibrary.org/doi/abs/10.1061/%28ASCE%29MT.1943-5533.0001421.

A

Appendix A: Python scripts

A.1. Random method assignment

```
import numpy as np
import matplotlib.pyplot as plt
import pandas as pd

np.random.seed(1)

N = 6
group_size = 28
Mic_samples_size = 7

samples = list(range(1, 193))
broken = {9, 10, 11, 12, 19, 20, 21, 24, 33, 34, 35, 45, 47,
48, 69, 70, 89, 93, 105, 130, 155, 168}
extra = {171, 183}
samples_after_cutting = [num for num in samples if num not in broken]
samples_total = [num for num in samples_after_cutting if num not in extra]

data = pd.DataFrame(samples_total, columns=['Sample'])

random_numbers = []
for i in range(1, (N + 1)):
    random_numbers.extend([i] * group_size)

np.random.shuffle(random_numbers)
data['Method'] = random_numbers

data["Microscopy"] = ""
for group in range(1, (N+1)):
    group_rows = data[data["Method"] == group]
    random_sample_indices = group_rows.sample(n=Mic_samples_size, random_state=12).index
    data.loc[random_sample_indices, "Microscopy"] = "Yes"

# pd.set_option('display.max_rows', None)
print(data)
```

A.2. Image processing

```
open();
imgName = getTitle();
run("8-bit");
rename(imgName + " - Contrast");
run("Gaussian Blur...", "sigma=1.0");
run("Enhance Contrast", "saturated=0.50");
run("Duplicate...", "title=[" + imgName + " - Detection]");
run("Find Edges");
setAutoThreshold("Triangle dark");
setOption("BlackBackground", false);
run("Convert to Mask");
run("Dilate");
showMessage("Complete", "Finished with:\n" + imgName);
```

A.3. Data files ring on ring test analysis

```
import pandas as pd
import numpy as np
import os
from glob import glob

def analyze_file(file_path, force_threshold=2):
    df = pd.read_excel(file_path)

    force_start_idx = df.index[(df['Load']) > force_threshold][0]
    start_row = df.loc[force_start_idx]
    max_idx = df['Load'].idxmax()
    max_row = df.loc[max_idx]

    max_force = max_row['Load']
    end_force = df['Load'].iloc[-1]
    corrected_force = max_force - end_force

    segment = df.loc[force_start_idx:max_idx]
    a_time, b_time = np.polyfit(segment['Time'], segment['Load'], deg=1)
    zero_time = (end_force - b_time) / a_time
    max_time = max_row['Time']
    total_time = max_time - zero_time

    a_strain, b_strain = np.polyfit(segment['Avg_S1_S2'], segment['Load'], deg=1)
    zero_strain = (end_force - b_strain) / a_strain
    max_strain = max_row['Avg_S1_S2']
    total_strain = max_strain - zero_strain

    stiffness = corrected_force / total_strain
    loading_rate = total_strain / total_time

    H = df['H'].mean() if 'H' in df.columns else None
    T = df['T'].mean() if 'T' in df.columns else None

    return {
        "filename": os.path.basename(file_path),
        "max_force": round(max_force, 3),
        "end_force": round(end_force, 3),
        "corrected_force": round(corrected_force, 3),
        "loading_rate": round(loading_rate, 3),
        "total_time": round(total_time, 2),
        "total_strain": round(total_strain, 3),
        "Stiffness": round(stiffness, 3),
        "H": round(H, 2) if H is not None else None,
        "T": round(T, 2) if T is not None else None
    }

folder_path = "."
files = glob(os.path.join(folder_path, "*.xlsx"))
results = []

for file_path in files:
    try:
        result = analyze_file(file_path)
        results.append(result)
```

```
    except Exception as e:
        print(f"Error processing {file_path}: {e}")

df_results = pd.DataFrame(results)
df_results.to_csv("Results.csv", index=False)
print(df_results)
```

A.4. Stiffness plots

```
import pandas as pd
import numpy as np
import os
from glob import glob
import matplotlib.pyplot as plt

def analyze_file(file_path, force_threshold=2):
    df = pd.read_excel(file_path)

    # Determine starting point where load exceeds threshold
    force_start_idx = df.index[(df['Load']) > force_threshold][0]
    start_row = df.loc[force_start_idx]

    max_idx = df['Load'].idxmax()
    max_row = df.loc[max_idx]

    # Force values
    max_force = max_row['Load']
    end_force = df['Load'].iloc[-1]
    corrected_force = max_force - end_force

    # Segment used for trendline
    trendline_segment = df.loc[force_start_idx:max_idx]

    # Linear fits
    a_time, b_time = np.polyfit(trendline_segment['Time'],
    trendline_segment['Load'], deg=1)
    zero_time = (end_force - b_time) / a_time

    a_strain, b_strain = np.polyfit(trendline_segment['Avg_S1_S2'],
    trendline_segment['Load'], deg=1)
    zero_strain = (end_force - b_strain) / a_strain

    max_time = max_row['Time']
    max_strain = max_row['Avg_S1_S2']

    # Calculations
    total_time = max_time - zero_time
    total_strain = max_strain - zero_strain
    stiffness = corrected_force / total_strain
    loading_rate = total_strain / total_time
    time_over_load = corrected_force / total_time

    # Optional columns
    H = df['H'].mean() if 'H' in df.columns else None
    T = df['T'].mean() if 'T' in df.columns else None

    return {
        "filename": os.path.basename(file_path),
        "max_force": round(max_force, 3),
        "end_force": round(end_force, 3),
        "corrected_force": round(corrected_force, 3),
        "loading_rate": round(loading_rate, 3),
        "total_time": round(total_time, 2),
        "total_strain": round(total_strain, 3),
```

```
        "Stiffness": round(stiffness, 3),
        "H": round(H, 2) if H is not None else None,
        "T": round(T, 2) if T is not None else None
    }

folder_path = "."  # Or specify your folder
files = glob(os.path.join(folder_path, "*.xlsx"))
results = []
trendline_stiffness_list = []  # NEW: collect trendline slopes

# Make sure plot folder exists
plot_folder = "plots4"
os.makedirs(plot_folder, exist_ok=True)

for file_path in files:
    try:
        # Analyze file
        result = analyze_file(file_path)
        results.append(result)

        # Load data again for plotting
        df = pd.read_excel(file_path)
        force_start_idx = df.index[(df['Load']) > 2][0]
        max_idx = df['Load'].idxmax()
        trendline_segment = df.loc[force_start_idx:max_idx]

        # Actual data
        x = trendline_segment['Avg_S1_S2']
        y = trendline_segment['Load']

        # Fit line
        a_strain, b_strain = np.polyfit(x, y, deg=1)
        x_fit = np.linspace(x.min(), x.max(), 100)
        y_fit = a_strain * x_fit + b_strain

        # Save slope for this file
        trendline_stiffness_list.append({
            "filename": os.path.basename(file_path),
            "trendline_stiffness": round(a_strain, 3)
        })

        # Plot
        plt.figure(figsize=(8, 6))
        plt.plot(df['Avg_S1_S2'], df['Load'], label='Full Data', alpha=0.4)
        plt.plot(x, y, 'o', label='Trendline Segment', color='orange')
        plt.plot(x_fit, y_fit, '--', label='Trendline Fit', color='red')

        # Title and labels
        filename = result["filename"]
        plt.title(f"{filename}")
        plt.xlabel("Avg_S1_S2 (Strain)")
        plt.ylabel("Load (Force)")
        plt.legend()
        plt.grid(True)

        # Add stiffness text (from trendline slope)
```

```
        stiffness_text = f"Stiffness = {a_strain:.3f}"
        plt.text(
            0.05, 0.95,
            stiffness_text,
            transform=plt.gca().transAxes,
            fontsize=10,
            verticalalignment='top',
            bbox=dict(boxstyle="round,pad=0.3", facecolor="white", edgecolor="gray")
        )

        # Save plot
        plot_path = os.path.join(plot_folder, f"{filename}.png")
        plt.savefig(plot_path)
        plt.close()

    except Exception as e:
        print(f"Error processing {file_path}: {e}")

# Convert to DataFrames
df_results = pd.DataFrame(results)
df_trendline_stiffness = pd.DataFrame(trendline_stiffness_list)

# Merge both into one file if desired
df_combined = df_results.merge(
    df_trendline_stiffness,
    on="filename",
    how="left"
)

print(df_combined)

# Save to Excel
df_combined.to_excel("All_Results_with_Trendline_Stiffness.xlsx", index=False)
```

B

Appendix B: Microscopy images

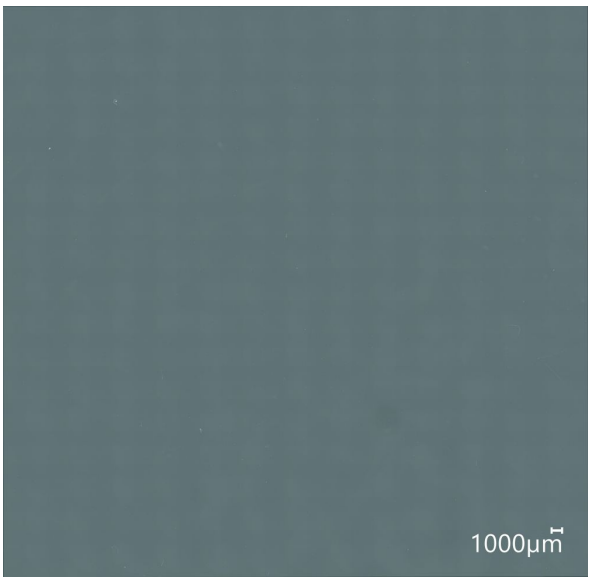

(a) S51

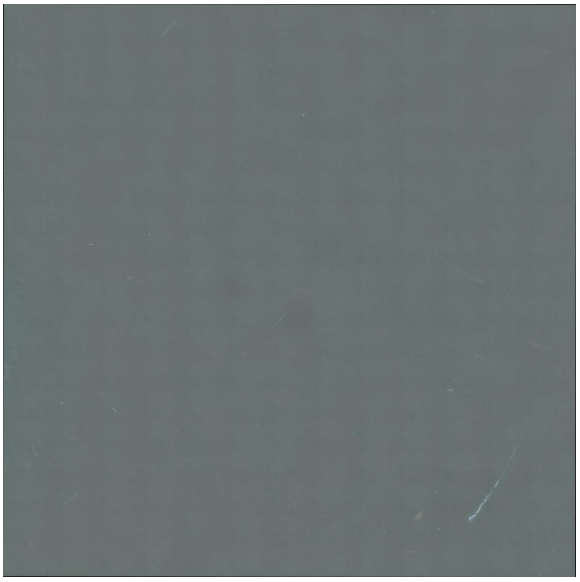

(b) S51 thermal treated

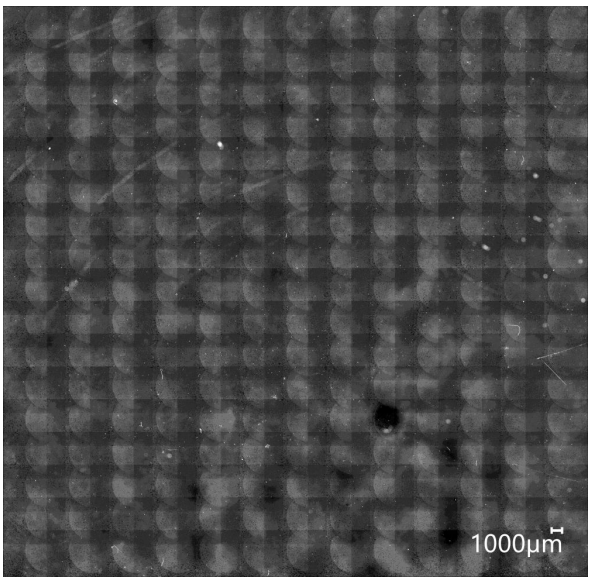

(c) S51 with contrast enhanced

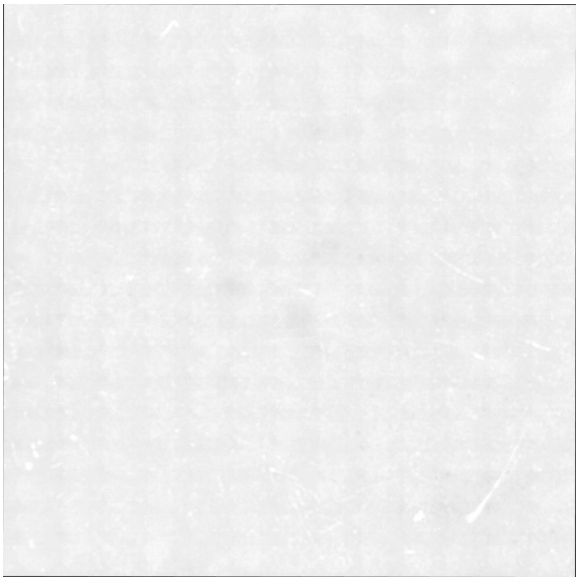

(d) S51 thermal treated with contrast enhanced

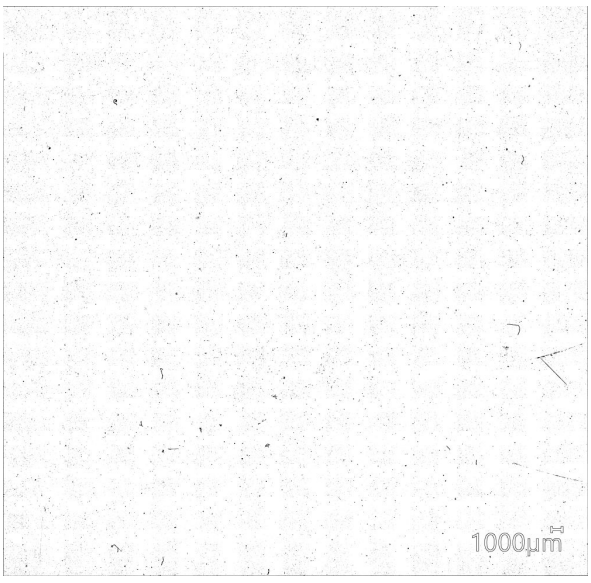

(e) S51 with image processing

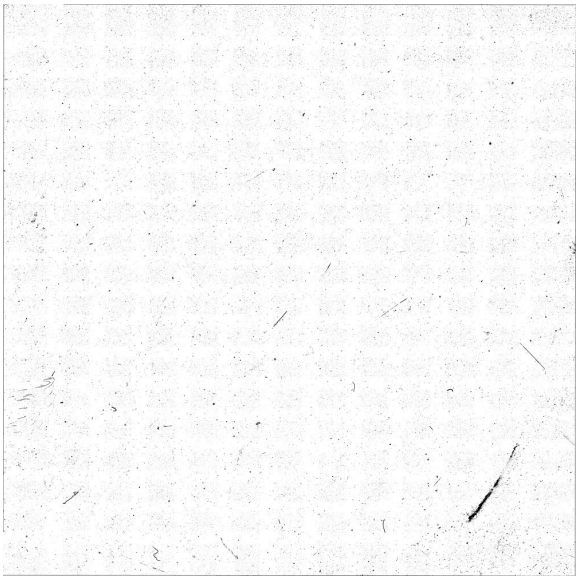

(f) S51 thermal treated with image processing

Figure B.1: Imaged processing of S51 pre- and post-treatment

(a) S55

(b) S55 thermal treated

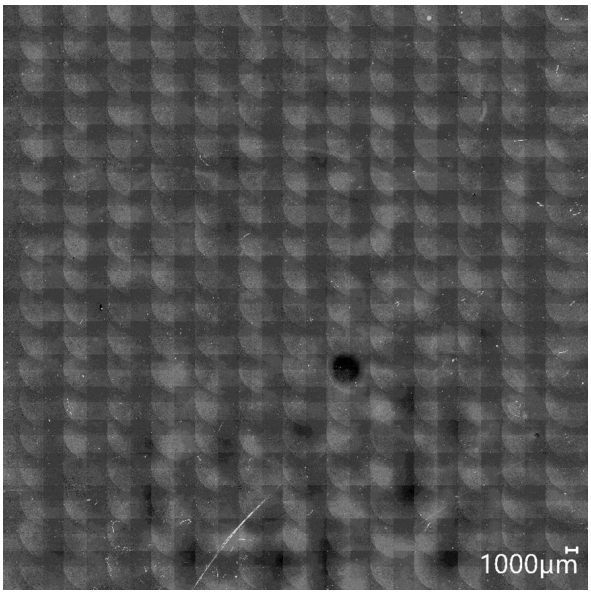

(c) S55 with contrast enhanced

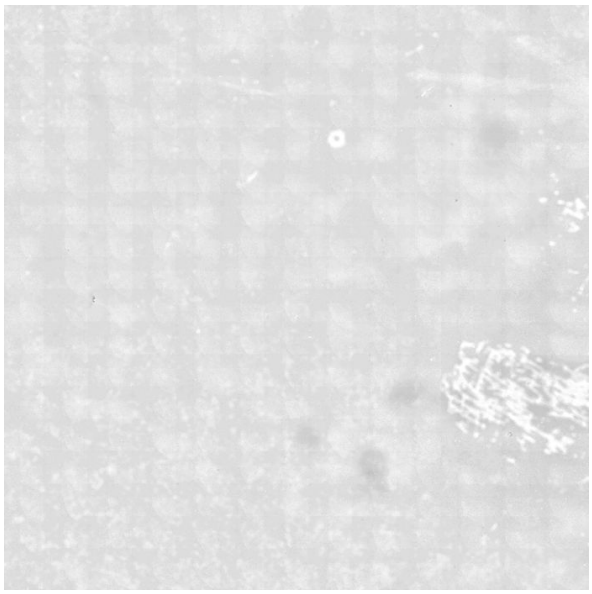

(d) S55 thermal treated with contrast enhanced

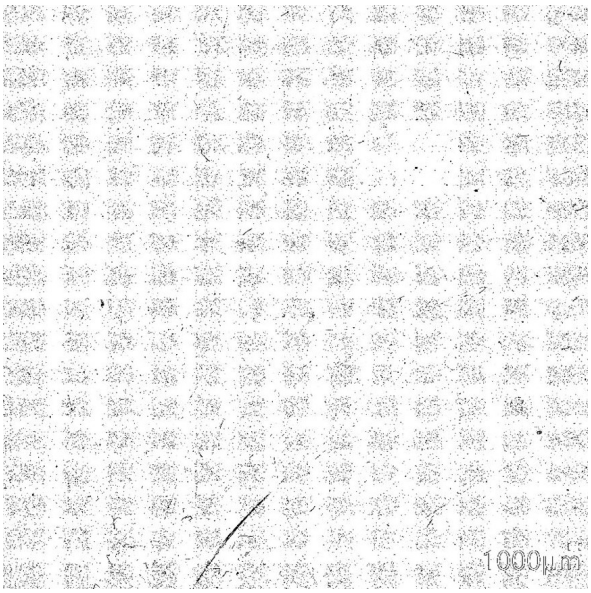

(e) S55 with image processing

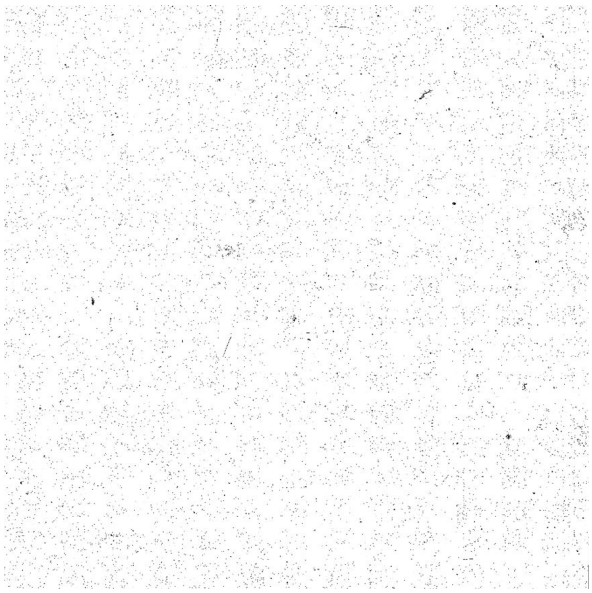

(f) S55 thermal treated with image processing

Figure B.2: Imaged processing of S55 pre- and post-treatment

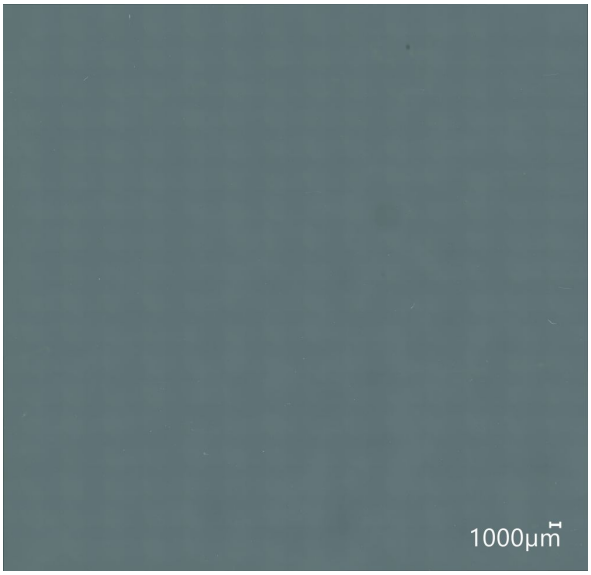

(a) S67

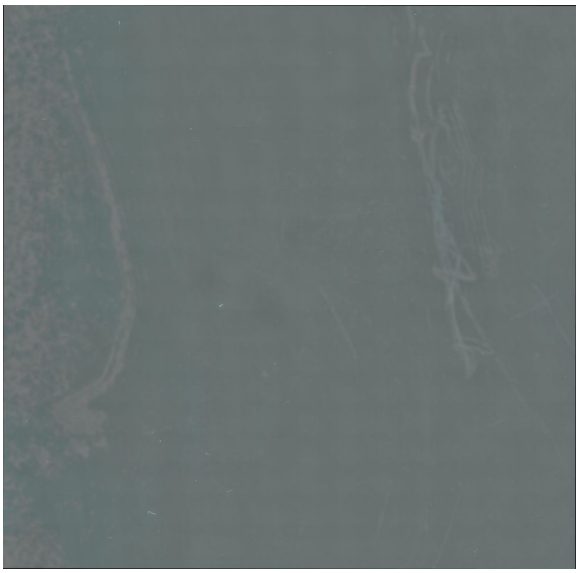

(b) S67 thermal treated

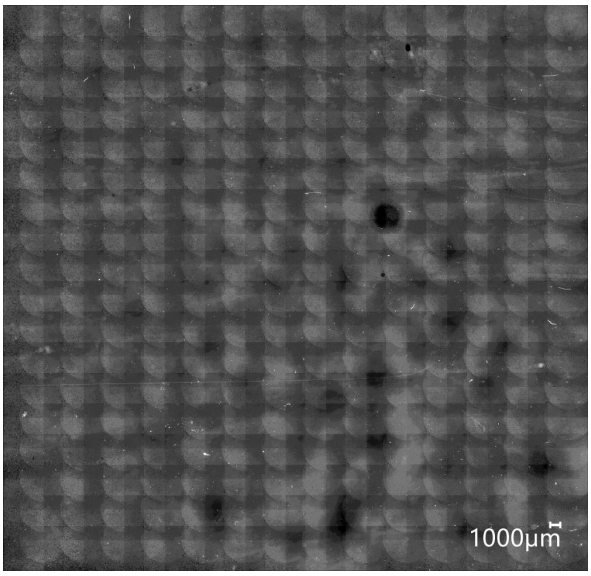

(c) S67 with contrast enhanced

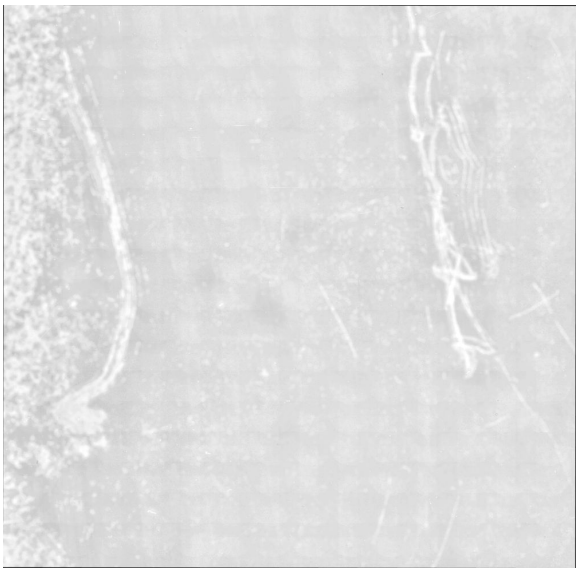

(d) S67 thermal treated with contrast enhanced

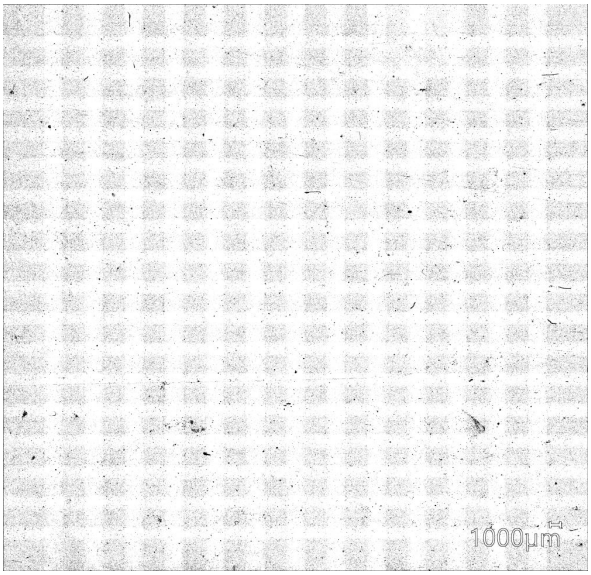

(e) S67 with image processing

(f) S67 thermal treated with image processing

Figure B.3: Imaged processing of S67 pre- and post-treatment

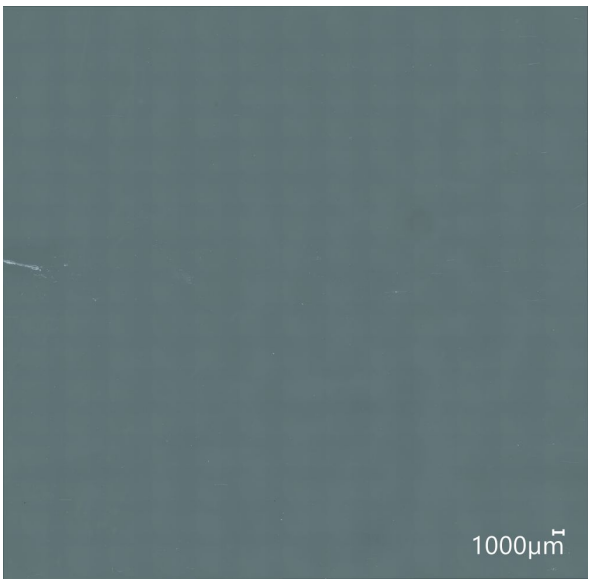

(a) S113

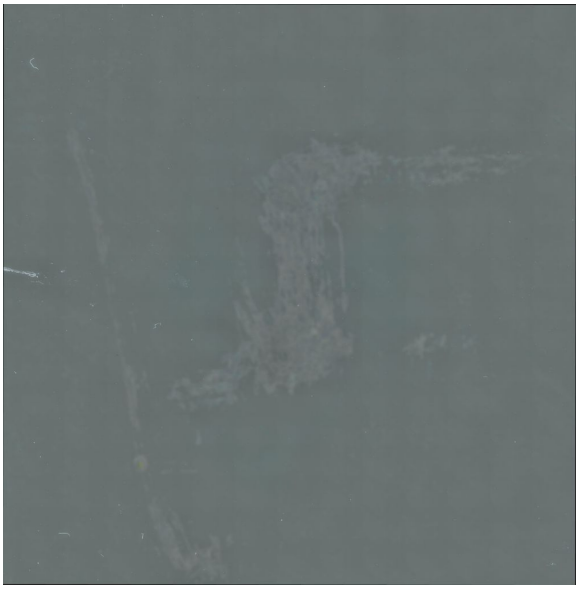

(b) S113 thermal treated

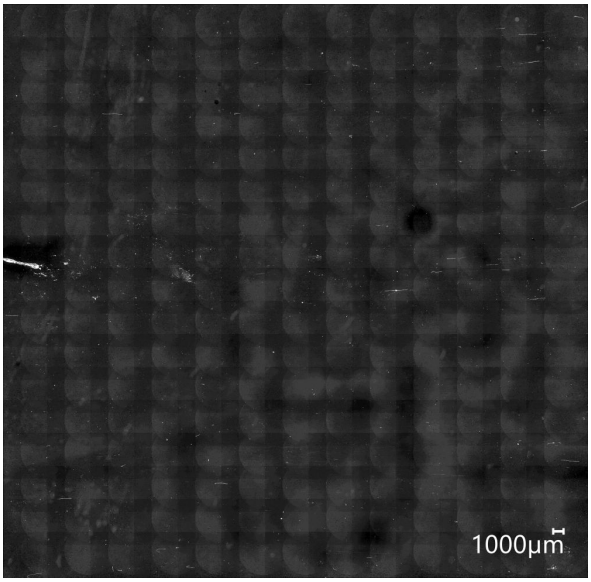

(c) S113 with contrast enhanced

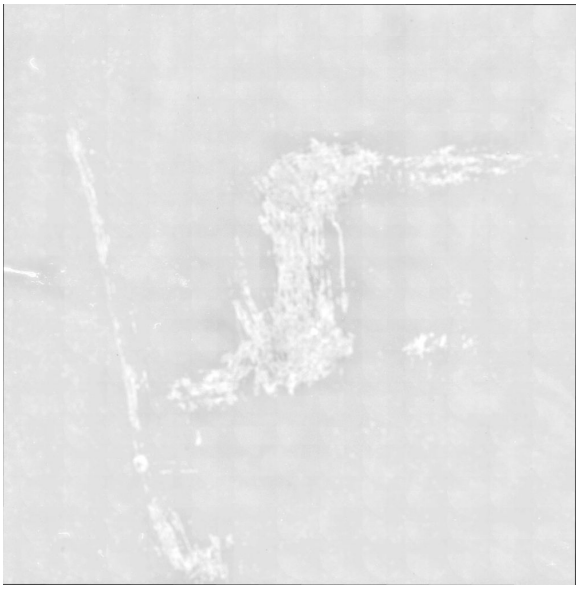

(d) S113 thermal treated with contrast enhanced

(e) S113 with image processing

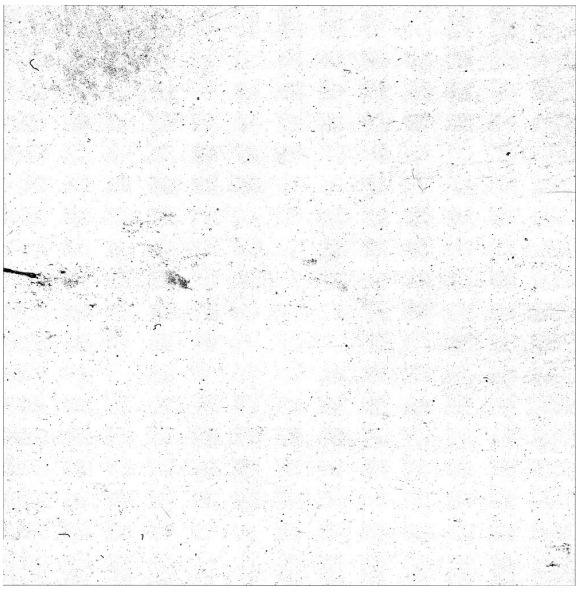

(f) S113 thermal treated with image processing

Figure B.4: Imaged processing of S113 pre- and post-treatment

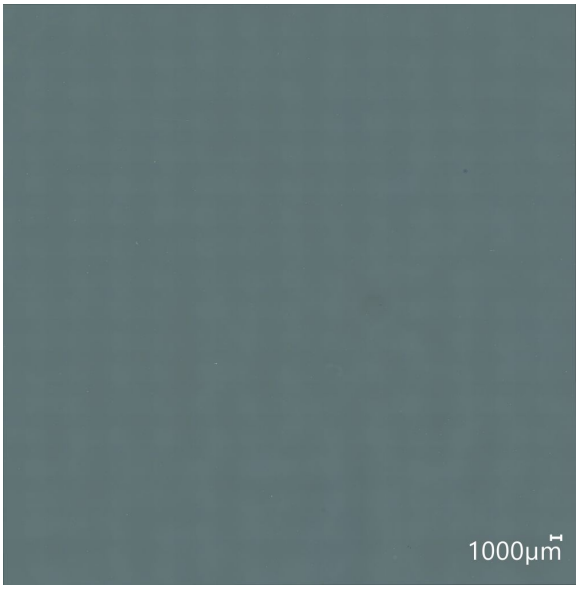

(a) S140

(b) S140 thermal treated

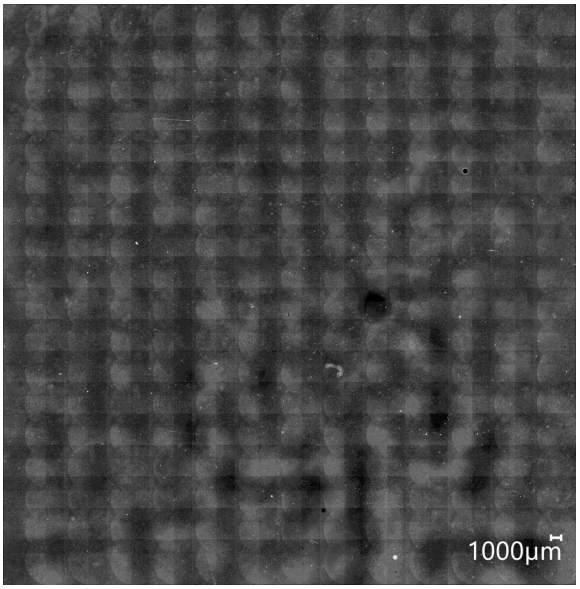

(c) S140 with contrast enhanced

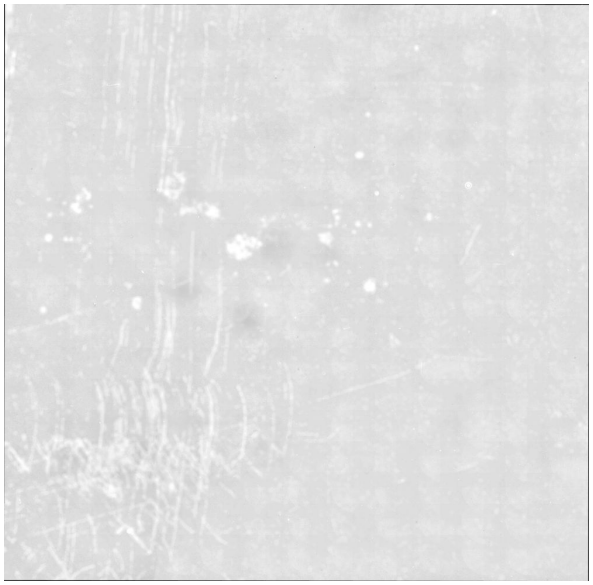

(d) S140 thermal treated with contrast enhanced

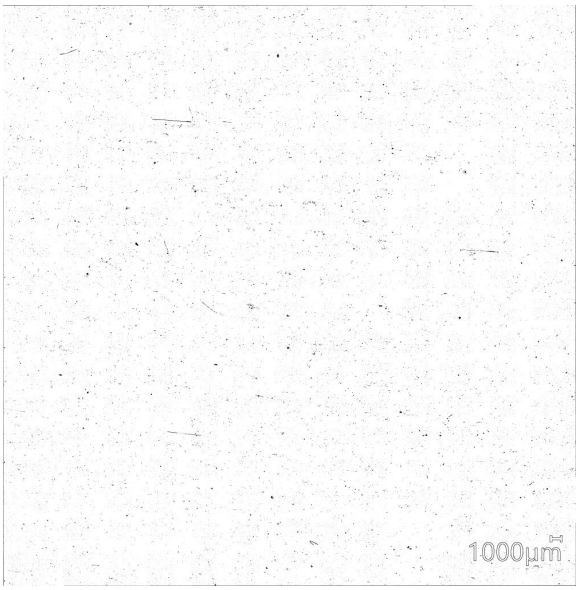

(e) S140 with image processing

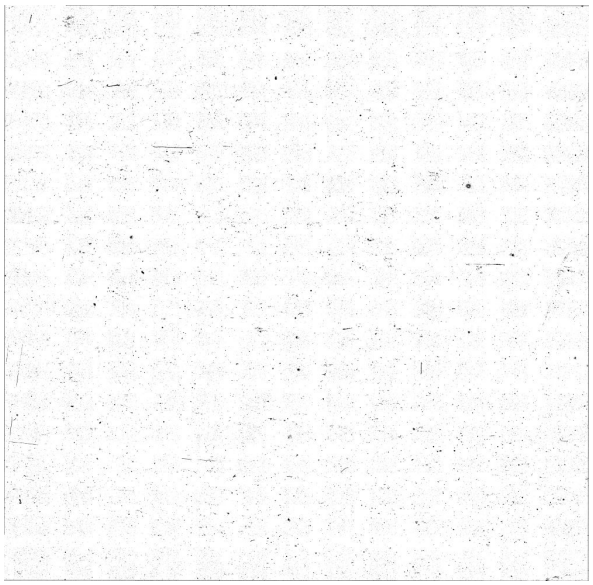

(f) S140 thermal treated with image processing

Figure B.5: Imaged processing of S140 pre- and post-treatment

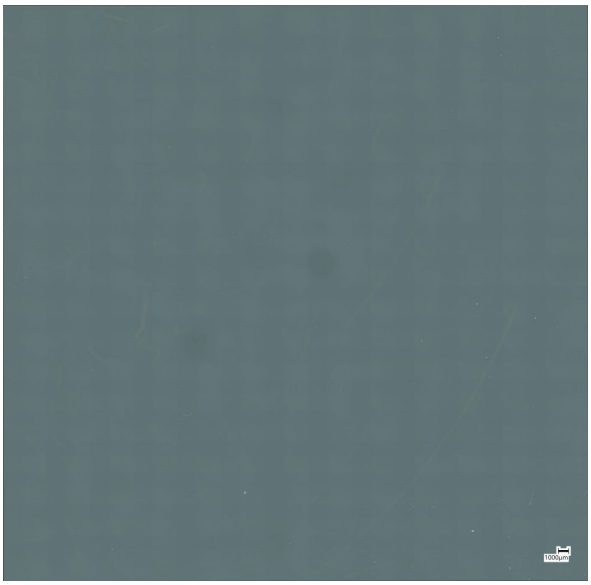

(a) S29

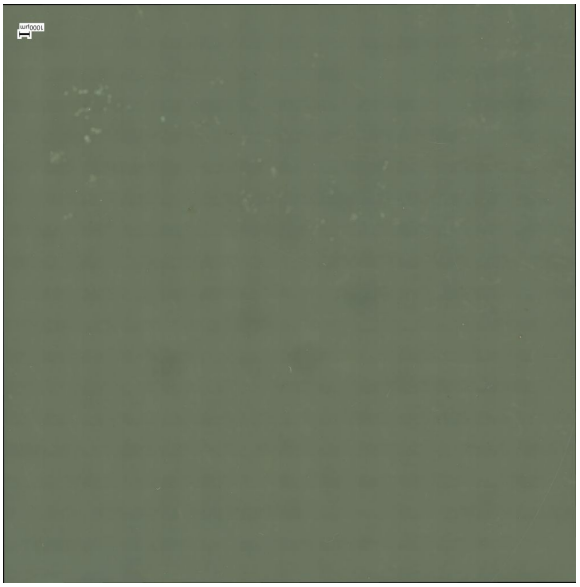

(b) S29 thermal treated

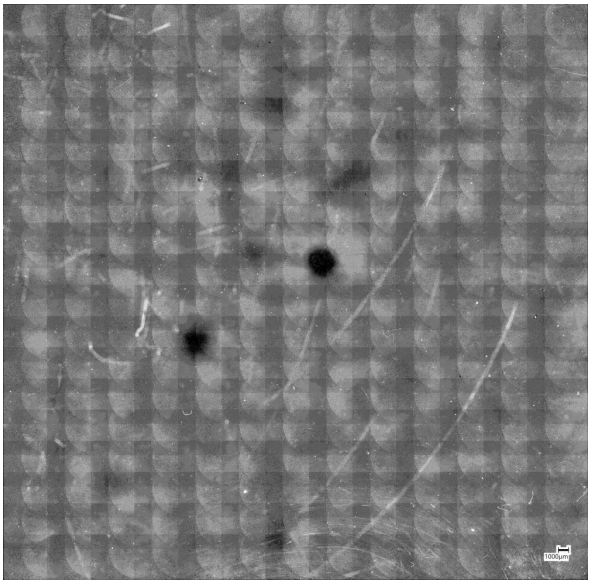

(c) S29 with contrast enhanced

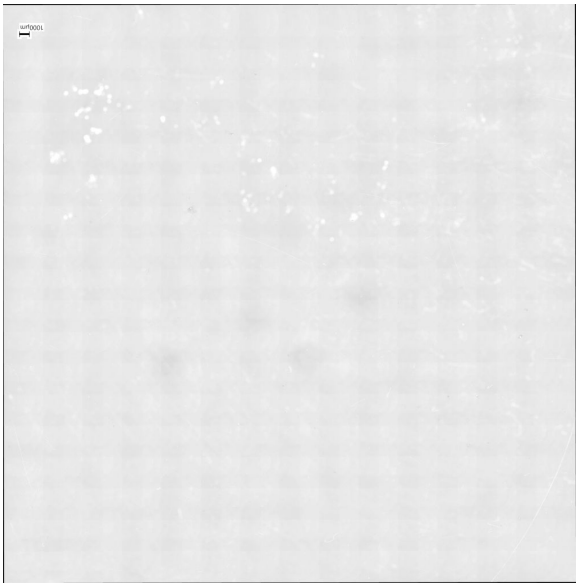

(d) S29 thermal treated with contrast enhanced

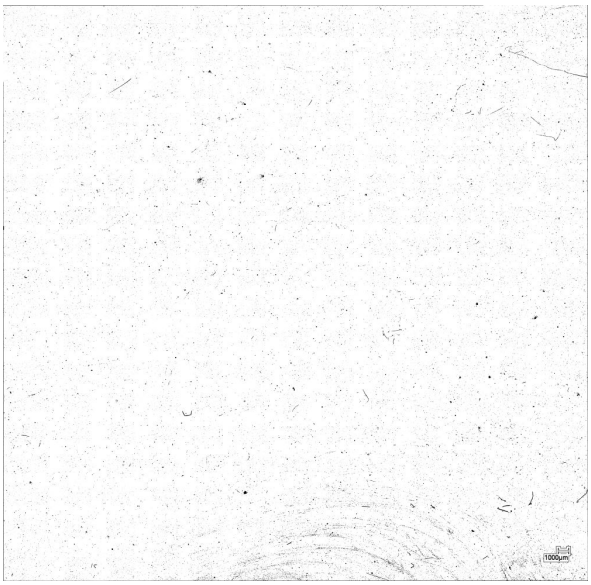

(e) S29 with image processing

(f) S29 thermal treated with image processing

Figure B.6: Imaged processing of S29 pre- and post-treatment

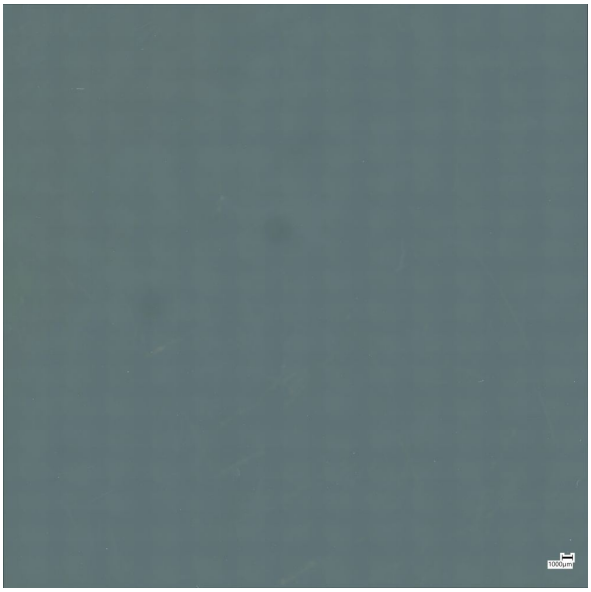

(a) S68

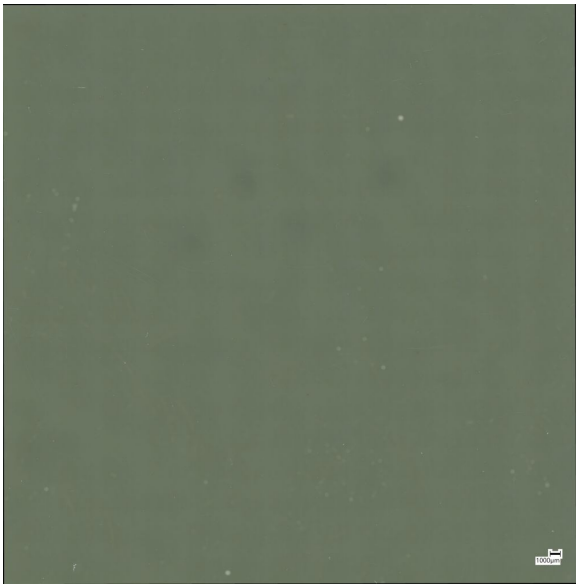

(b) S68 thermal treated

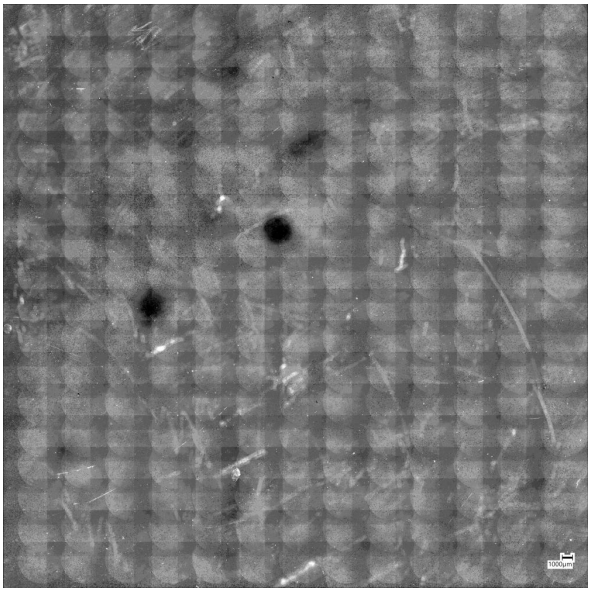

(c) S68 with contrast enhanced

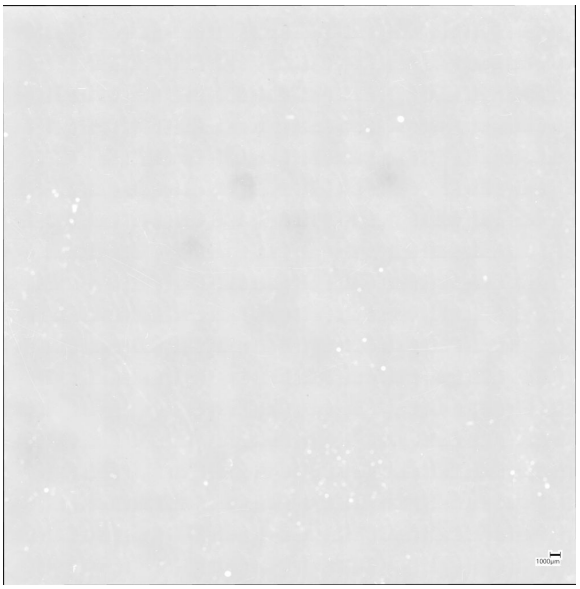

(d) S68 thermal treated with contrast enhanced

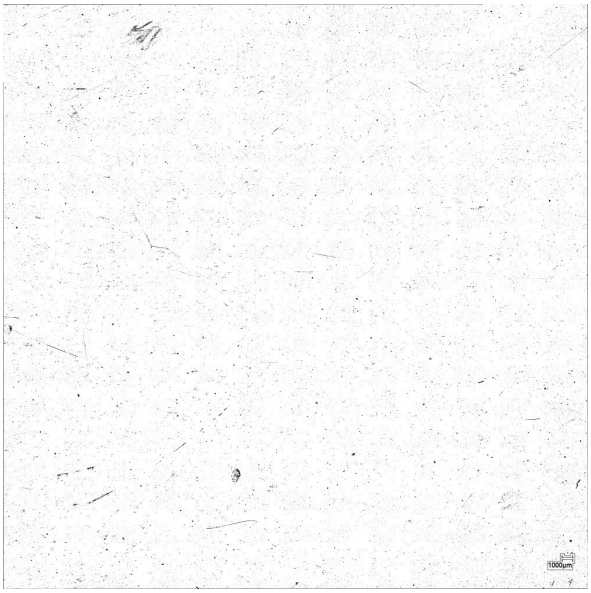

(e) S68 with image processing

(f) S68 thermal treated with image processing

Figure B.7: Imaged processing of S68 pre- and post-treatment

(a) S92

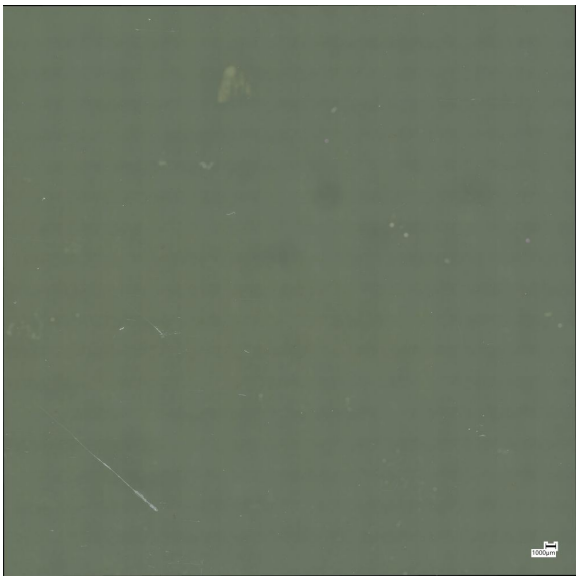

(b) S92 thermal treated

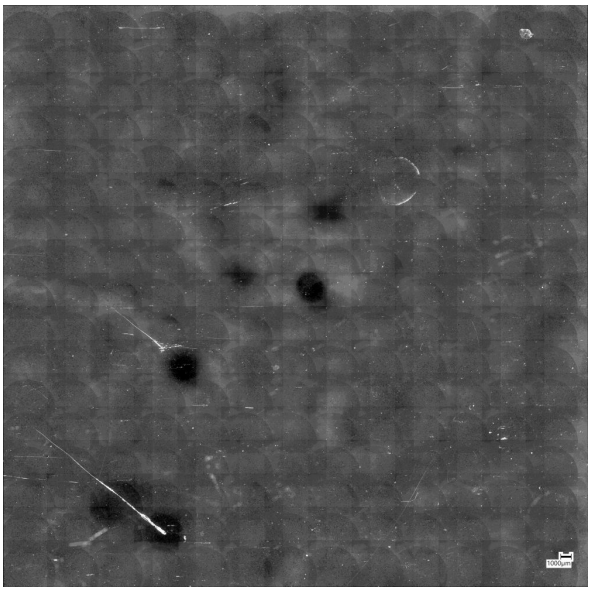

(c) S92 with contrast enhanced

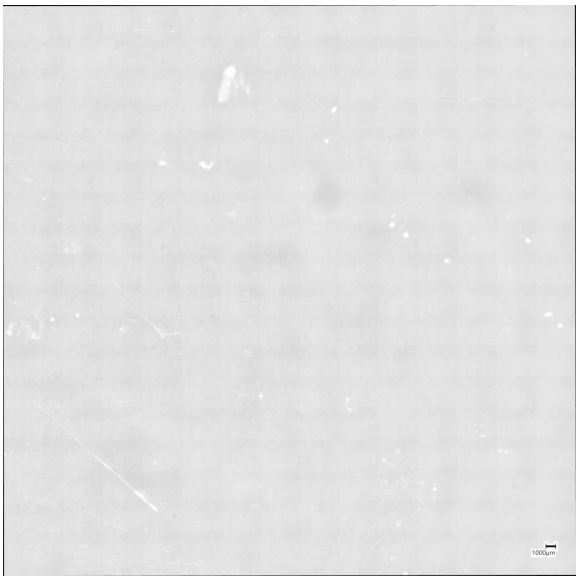

(d) S92 thermal treated with contrast enhanced

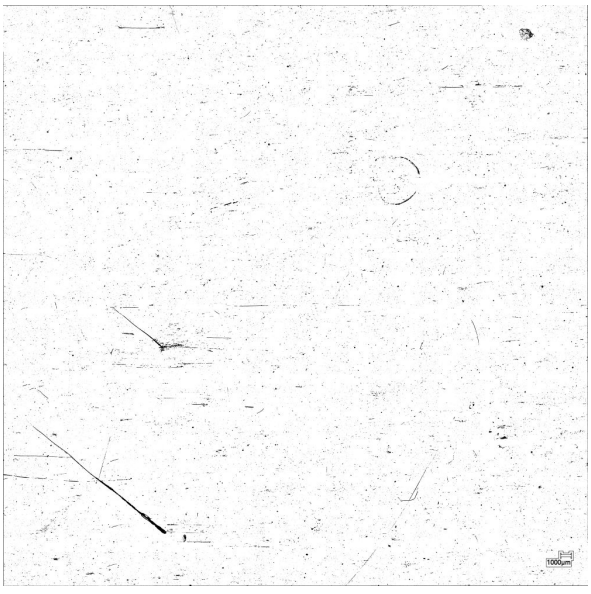

(e) S92 with image processing

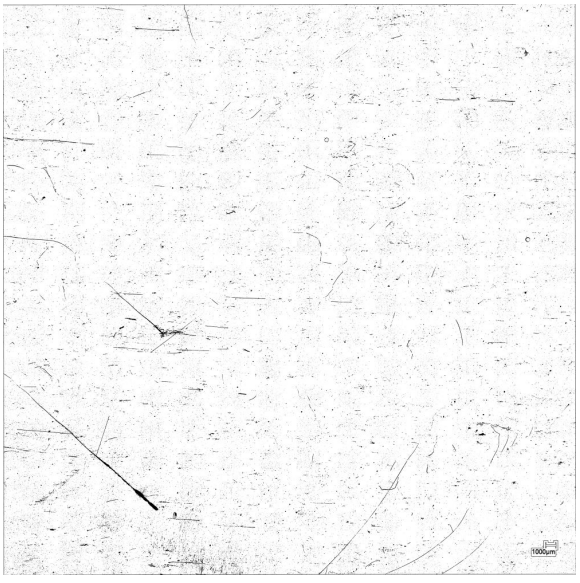

(f) S92 thermal treated with image processing

Figure B.8: Imaged processing of S92 pre- and post-treatment

(a) S124

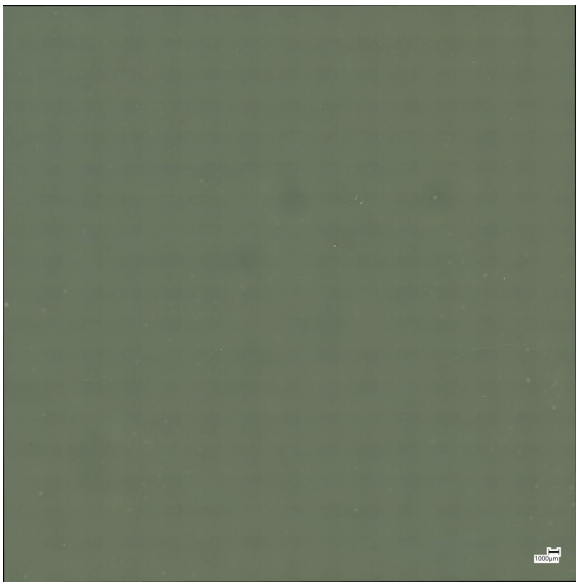

(b) S124 thermal treated

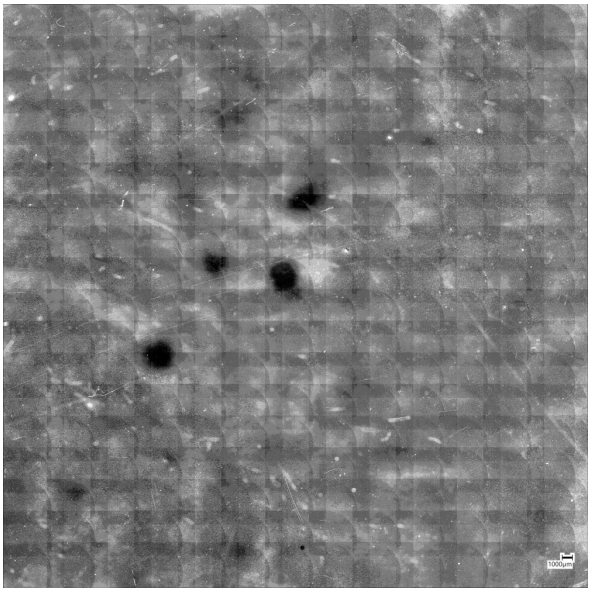

(c) S124 with contrast enhanced

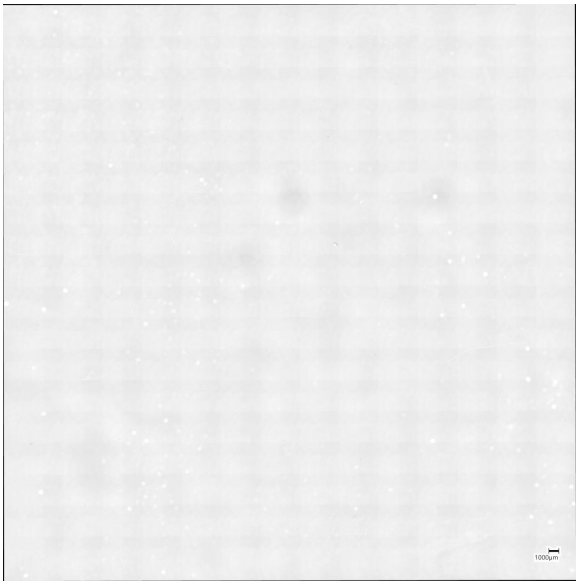

(d) S124 thermal treated with contrast enhanced

(e) S124 with image processing

(f) S124 thermal treated with image processing

Figure B.9: Imaged processing of S124 pre- and post-treatment

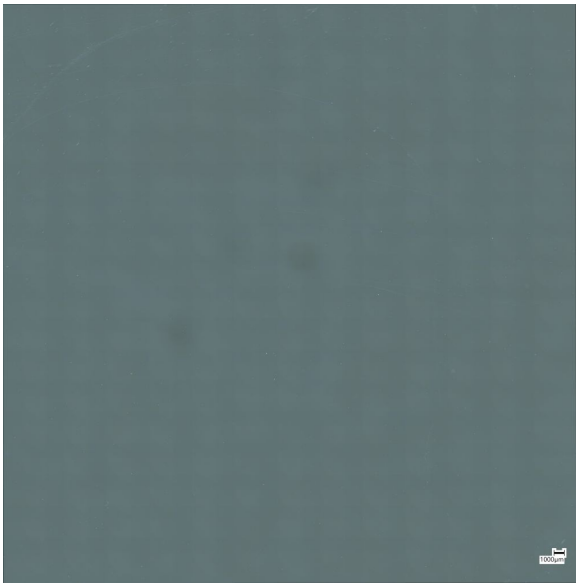

(a) S163

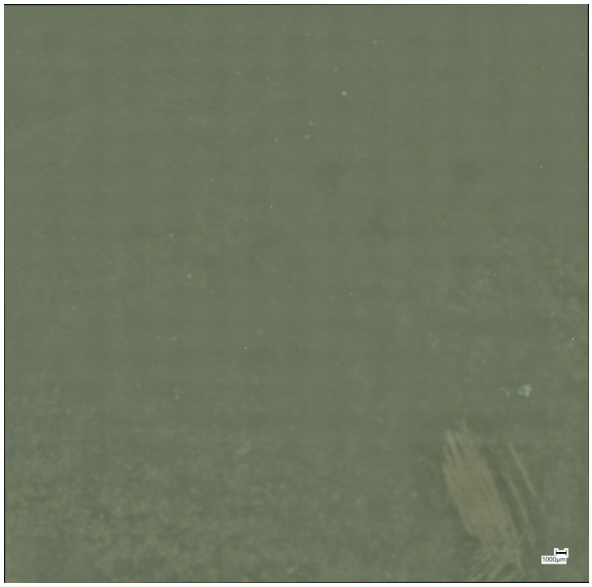

(b) S163 thermal treated

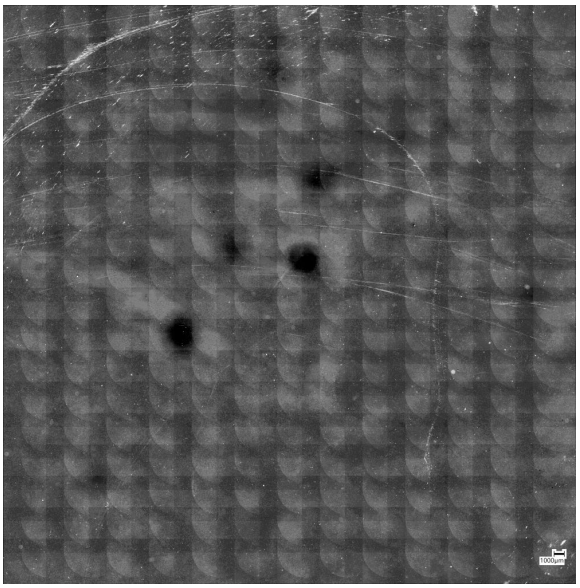

(c) S163 with contrast enhanced

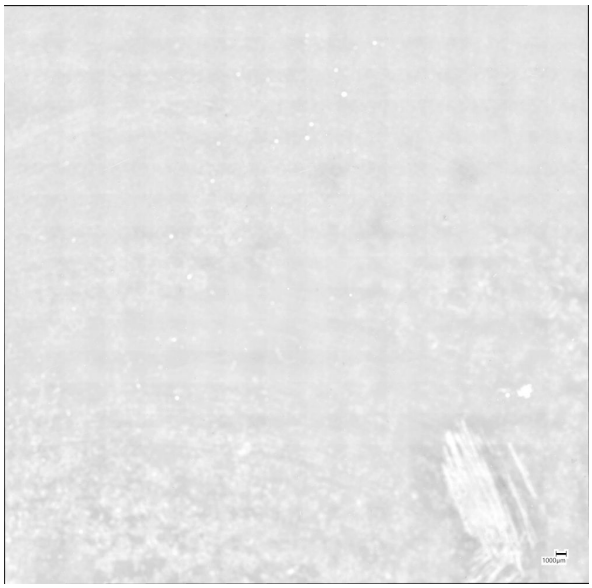

(d) S163 thermal treated with contrast enhanced

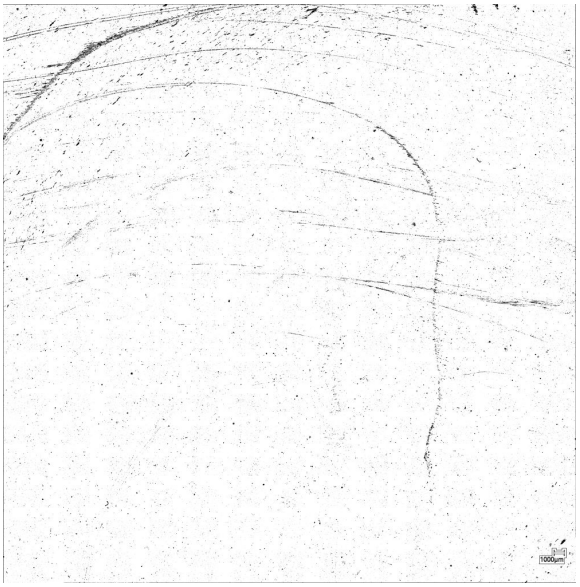

(e) S163 with image processing

(f) S163 thermal treated with image processing

Figure B.10: Imaged processing of S163 pre- and post-treatment

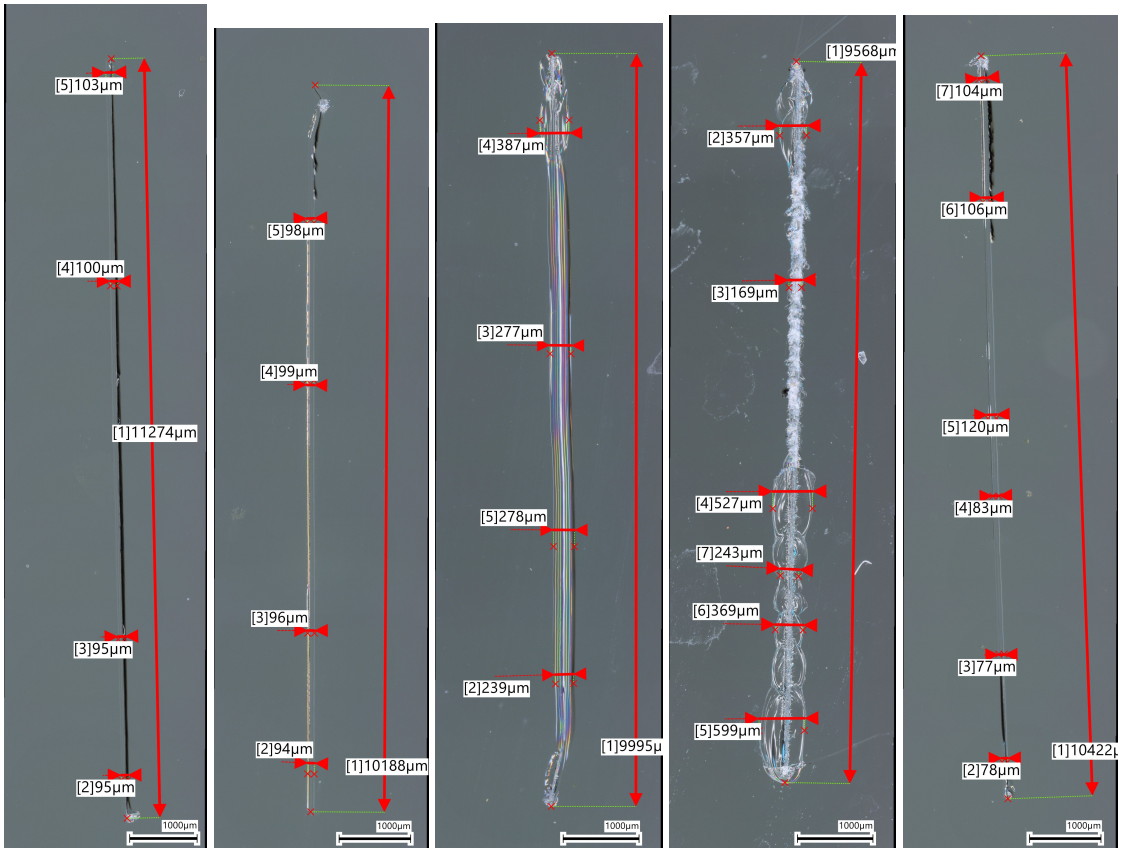

(a) S5 **(b)** S74 **(c)** S81 **(d)** S128 **(e)** S158

Figure B.11: method 5 scratched before thermal treatment

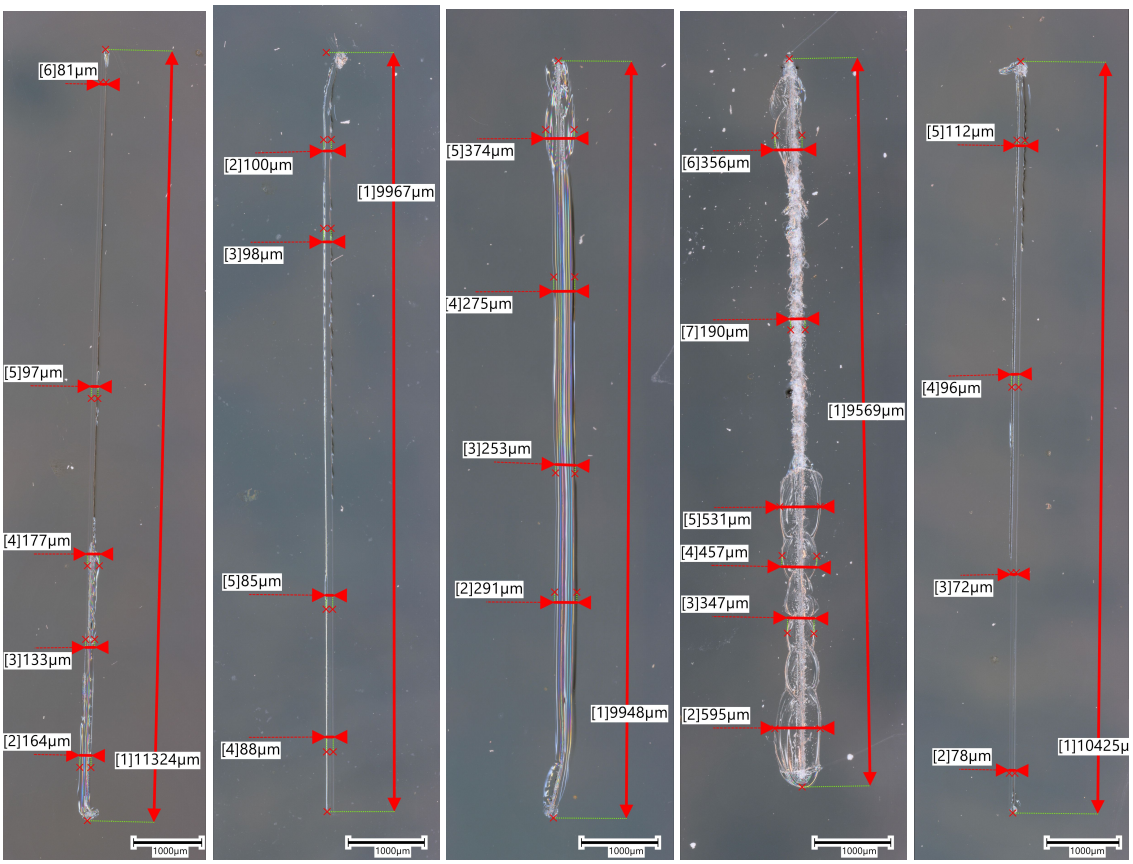

(a) S5 **(b)** S74 **(c)** S81 **(d)** S128 **(e)** S158

Figure B.12: method 5 scratched after thermal treatment

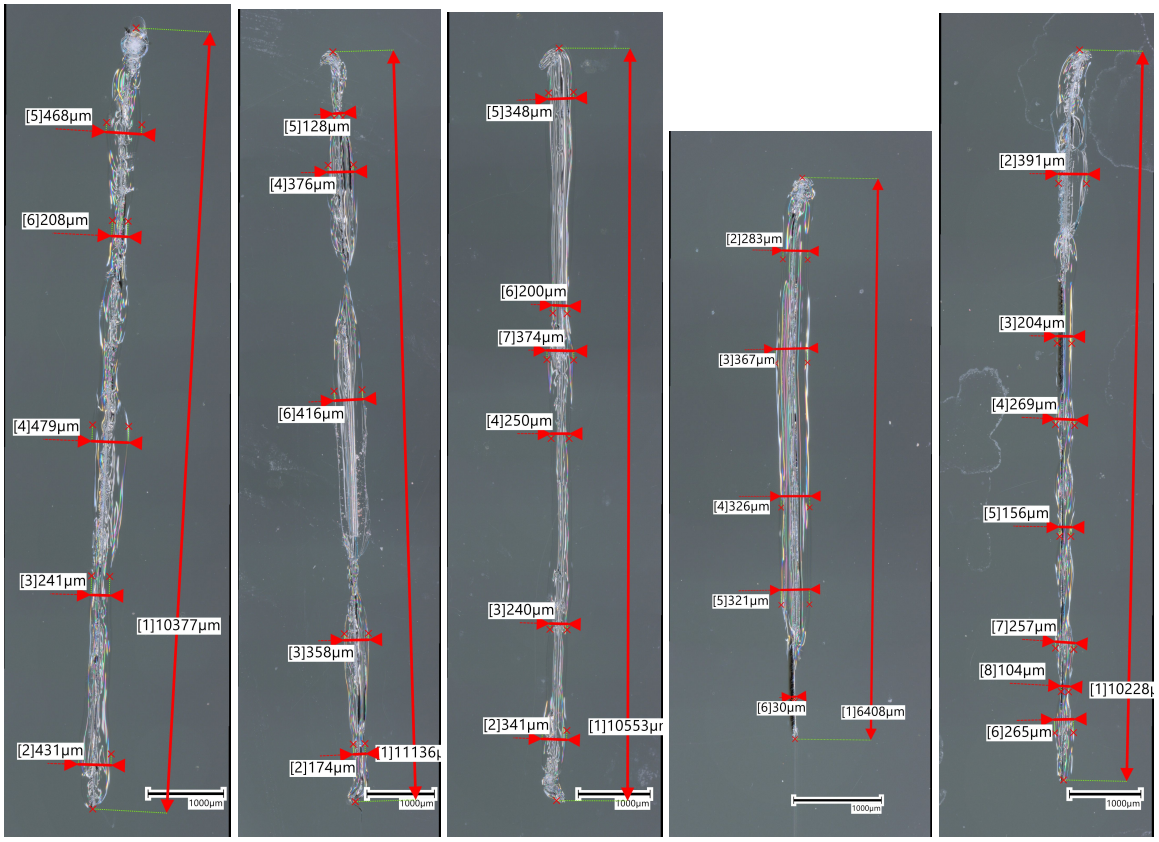

(a) S15 **(b)** S59 **(c)** S71 **(d)** S119 **(e)** S154

Figure B.13: method 6 scratched before thermal treatment

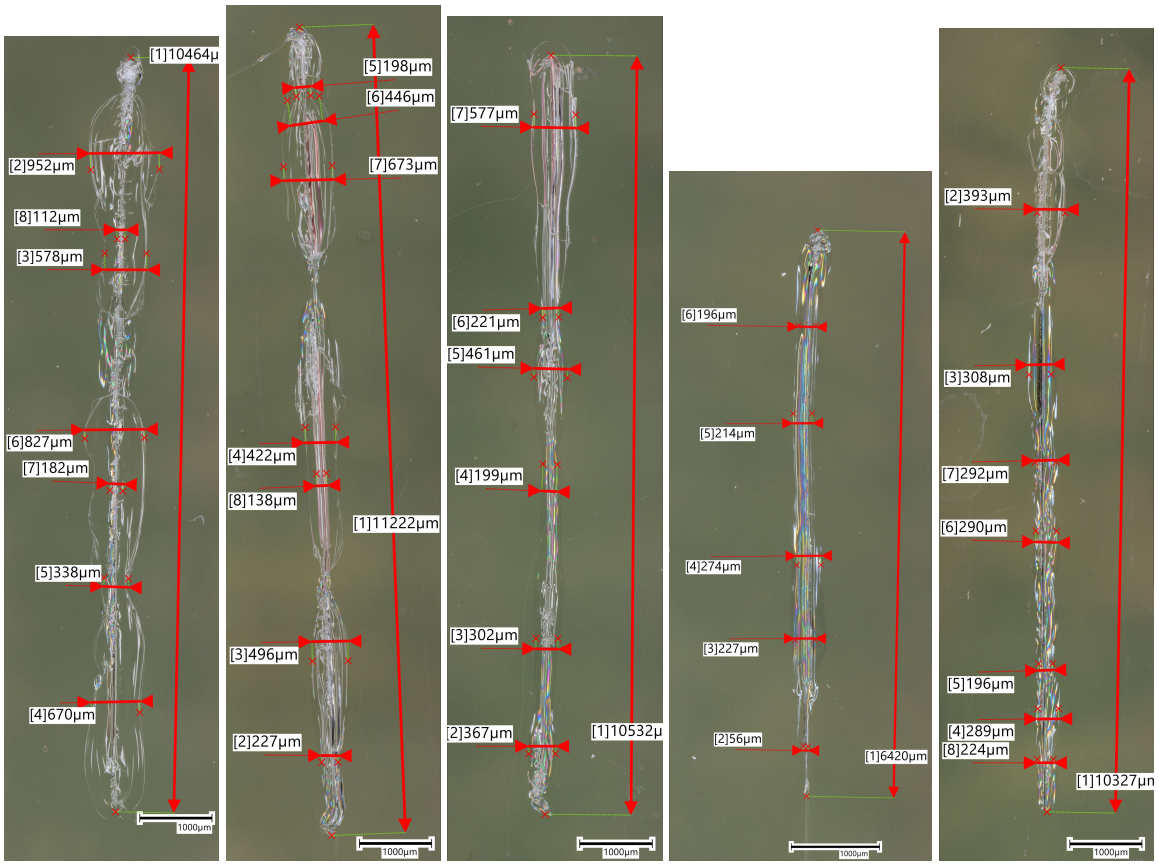

(a) S15 **(b)** S59 **(c)** S71 **(d)** S119 **(e)** S154

Figure B.14: method 6 scratched after thermal treatment

C

Appendix C: Scalp-05 measurement

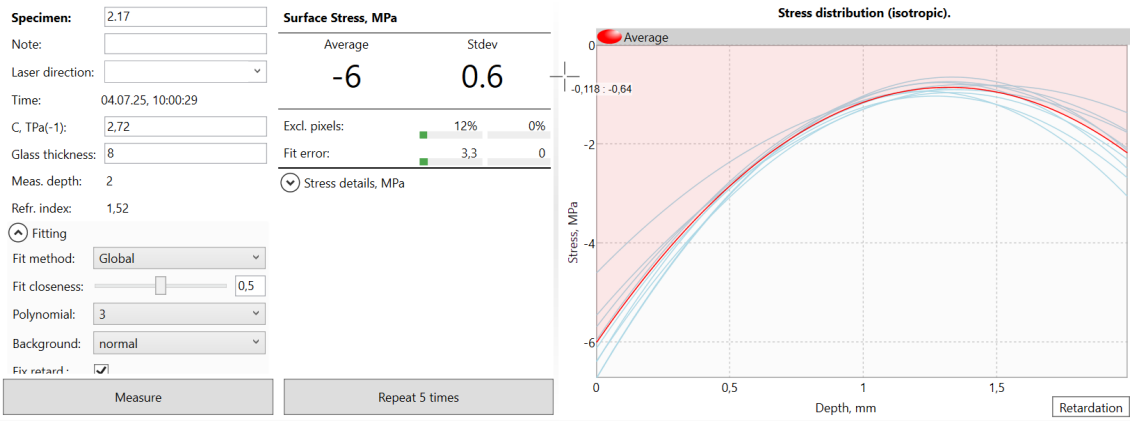

Figure C.1: Scalp-05 measurement S2.17 (No treatment)

Figure C.2: Scalp-05 measurement S2.43 (No treatment)

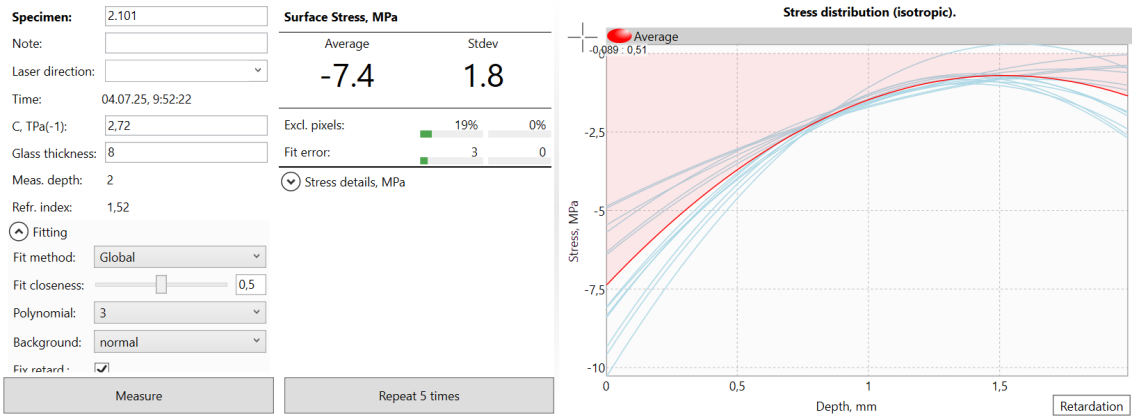

Figure C.3: Scalp-05 measurement S2.101 (No treatment)

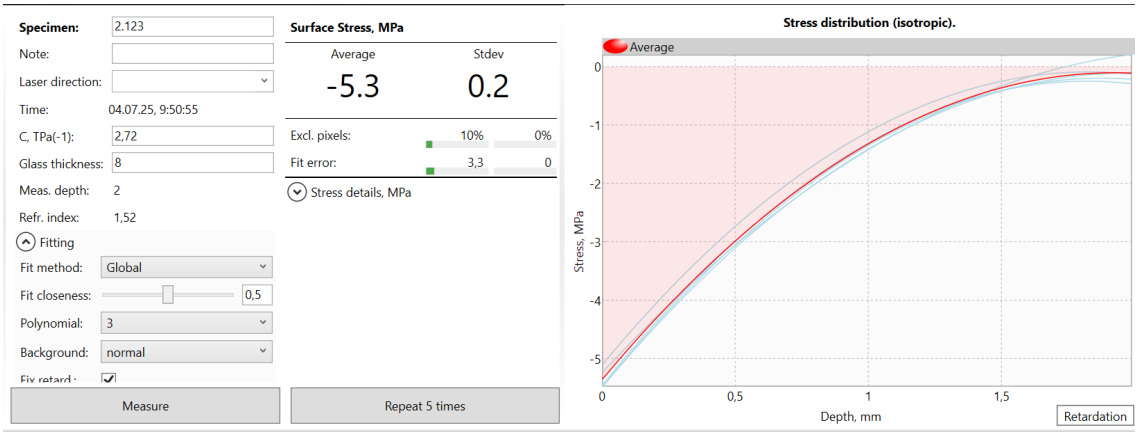

Figure C.4: Scalp-05 measurement S2.123 (No treatment)

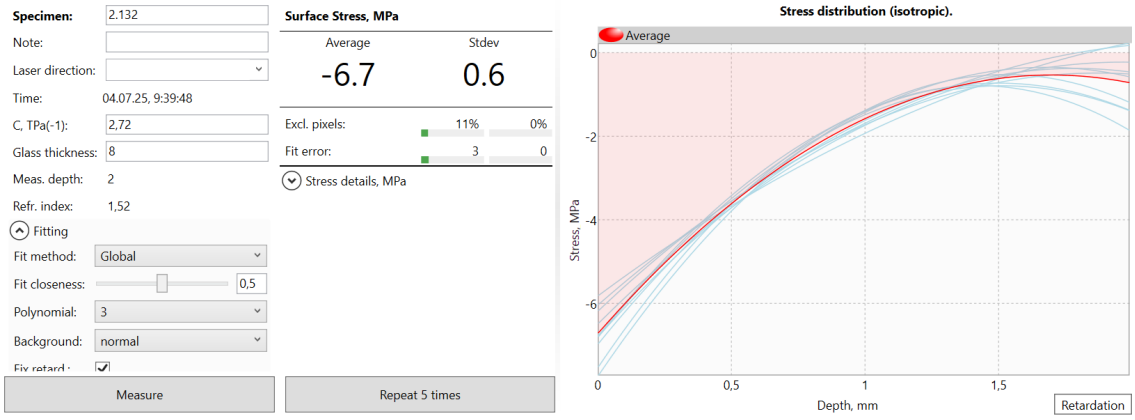

Figure C.5: Scalp-05 measurement S2.132 (No treatment)

Figure C.6: Scalp-05 measurement S2.173 (No treatment)

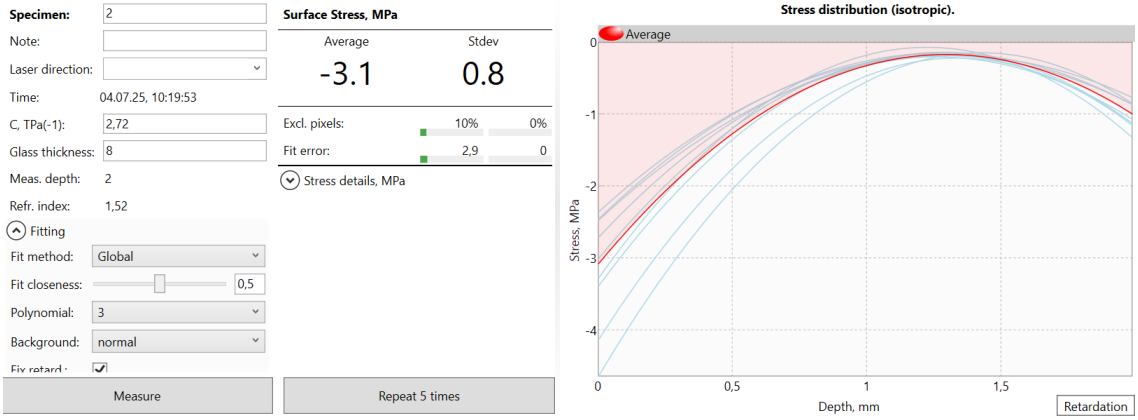

Figure C.7: Scalp-05 measurement S2.2 (500°C)

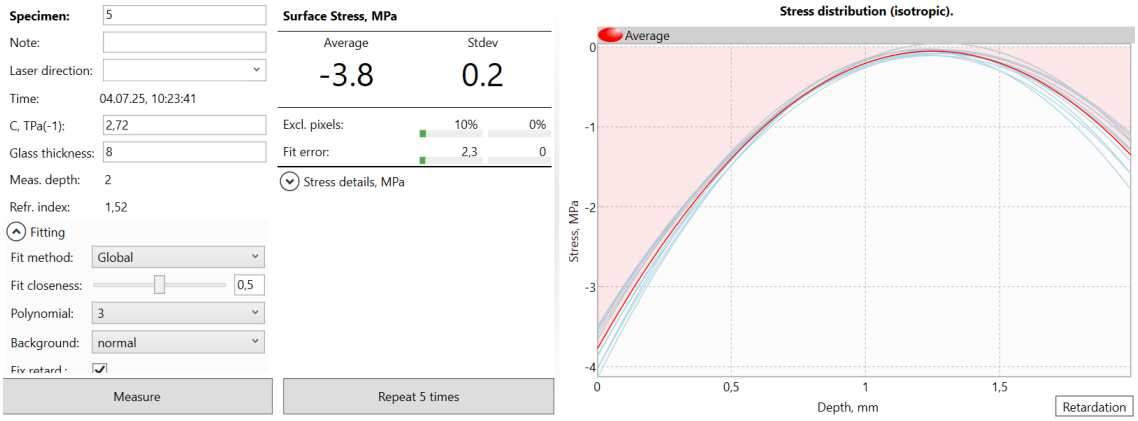

Figure C.8: Scalp-05 measurement S2.5 (500°C)

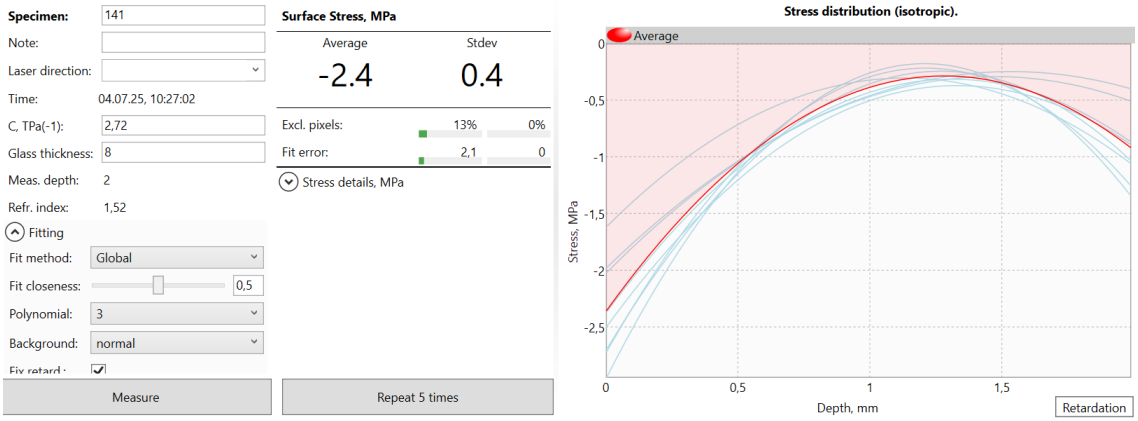

Figure C.9: Scalp-05 measurement S2.141 (500°C)

Figure C.10: Scalp-05 measurement S2.148 (500°C)

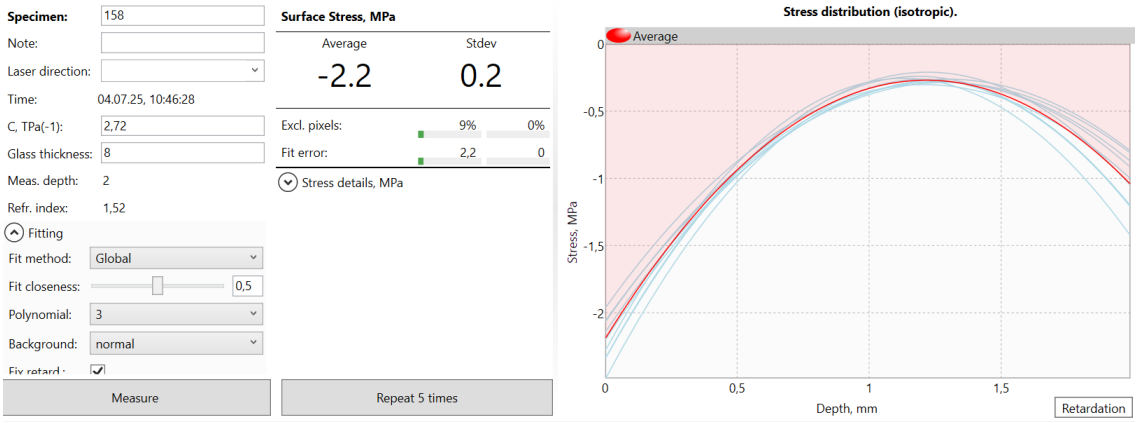

Figure C.11: Scalp-05 measurement S2.158 (500°C)

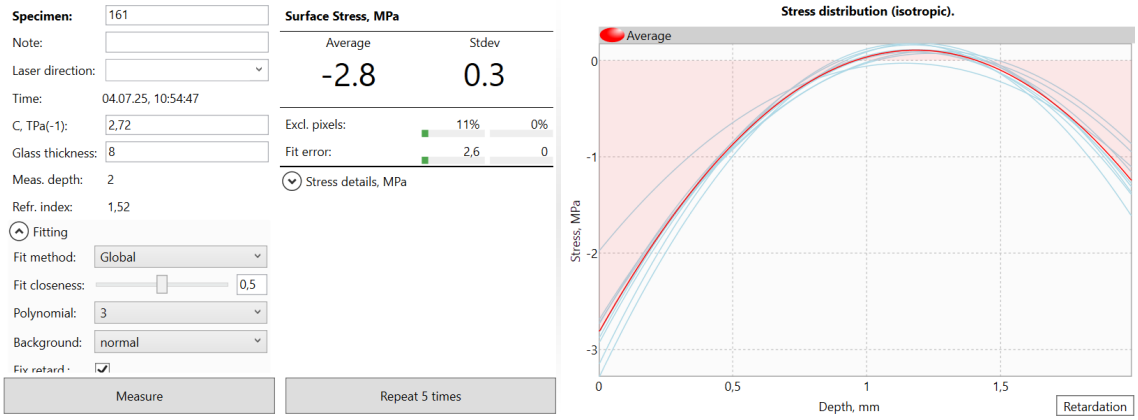

Figure C.12: Scalp-05 measurement S2.161 (500°C)

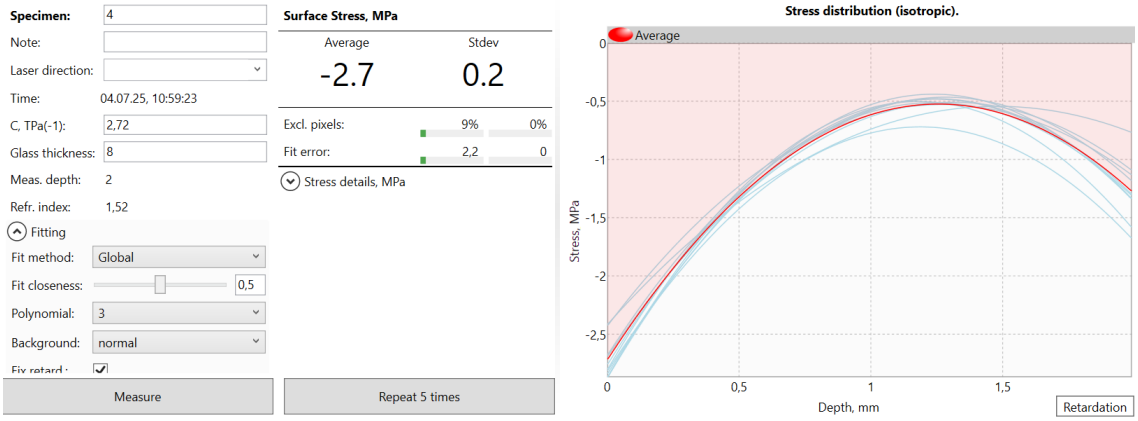

Figure C.13: Scalp-05 measurement S2.4 (600°C)

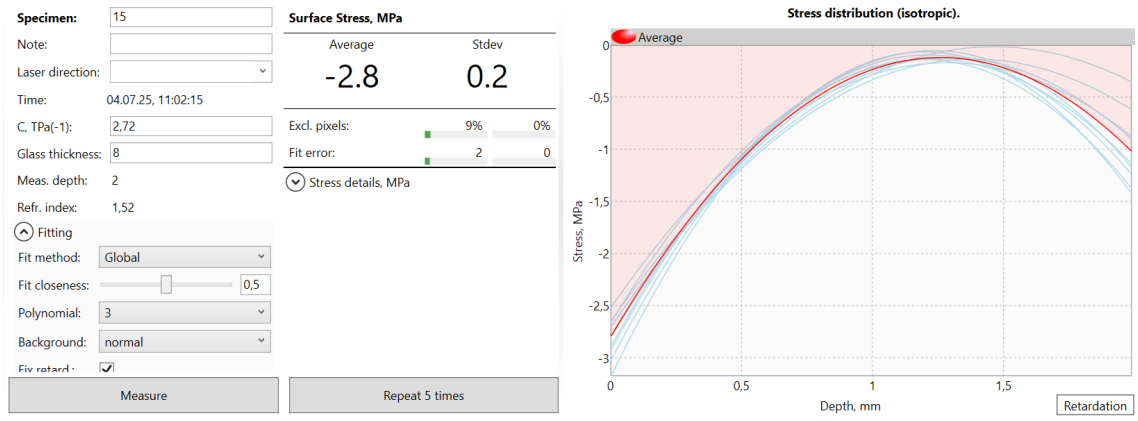

Figure C.14: Scalp-05 measurement S2.15 (600°C)

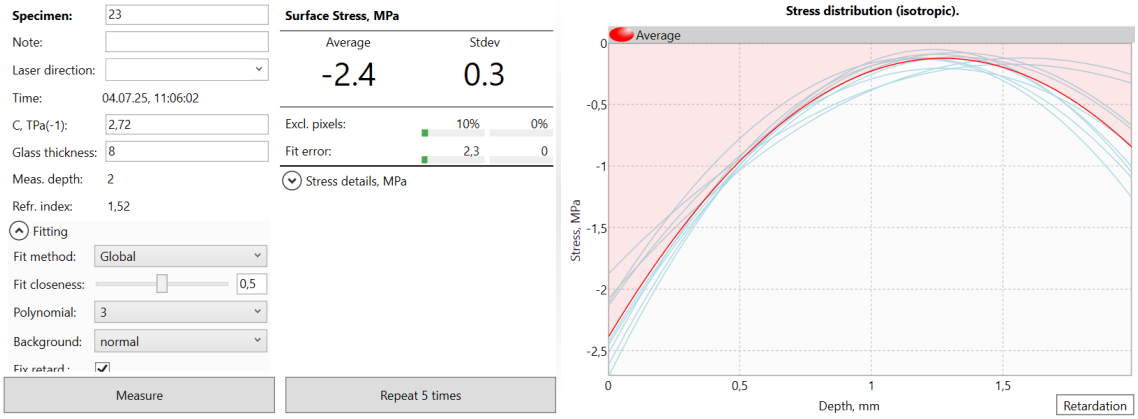

Figure C.15: Scalp-05 measurement S2.23 (600°C)

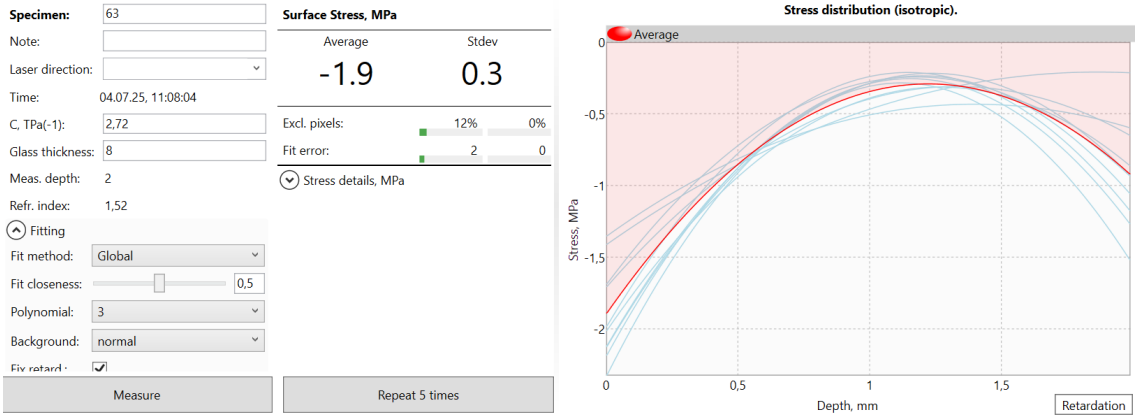

Figure C.16: Scalp-05 measurement S63 (600°C)

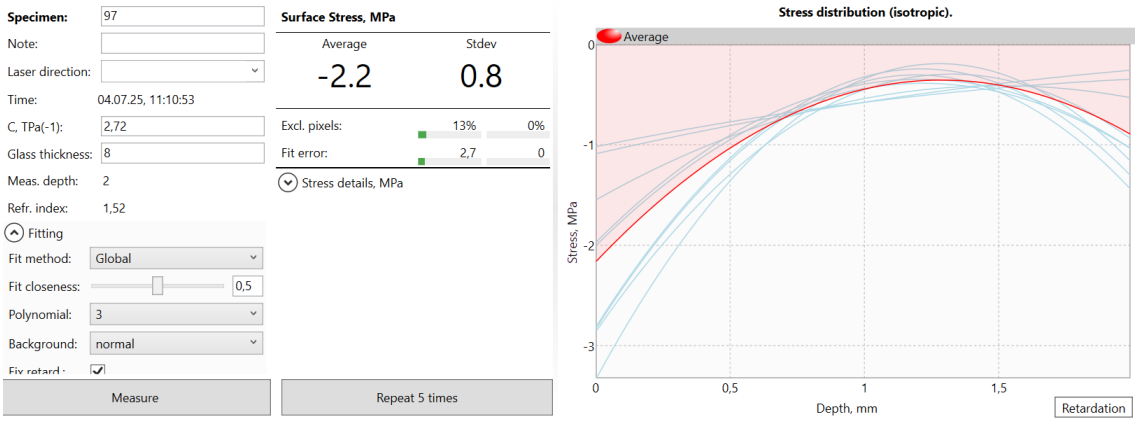

Figure C.17: Scalp-05 measurement S2.97 (600°C)

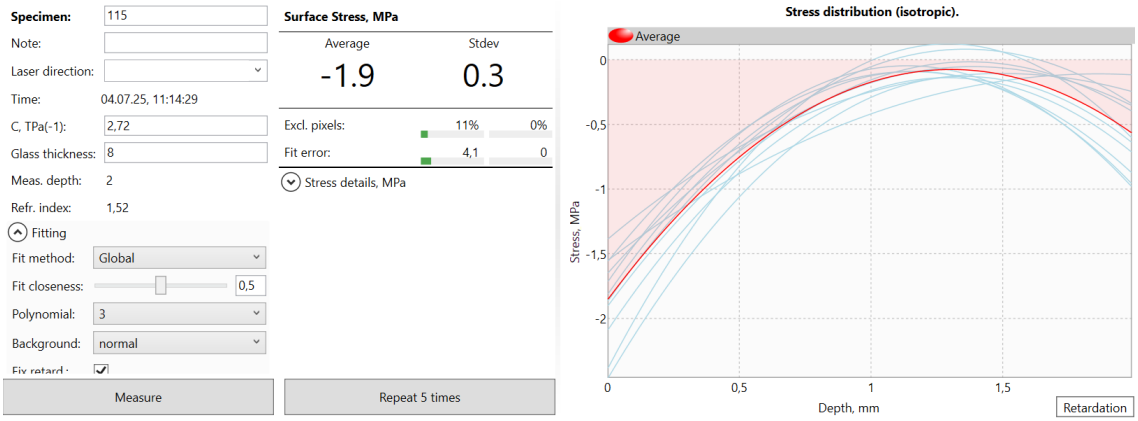

Figure C.18: Scalp-05 measurement S2.115 (600°C)

D

Appendix D: Post fracture images

Naturally aged glass without thermal treatment

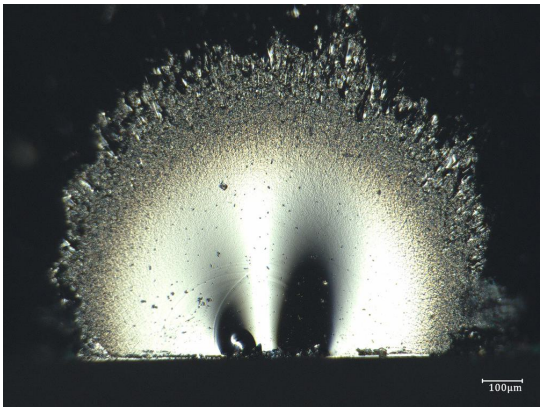

(a) S64 first view

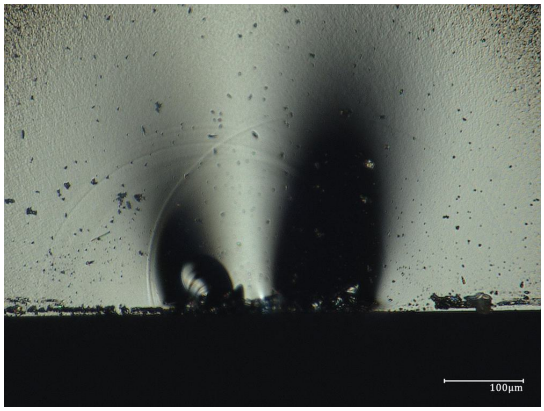

(b) S64 second view

Figure D.1: Different views of S64 (99 MPa)

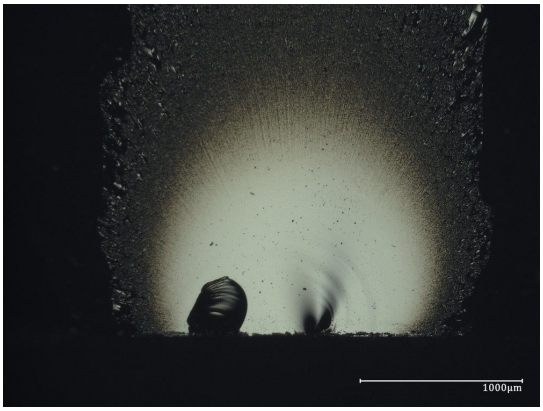

(a) S76 first view

(b) S76 second view

Figure D.2: Different views of S76 (77 MPa)

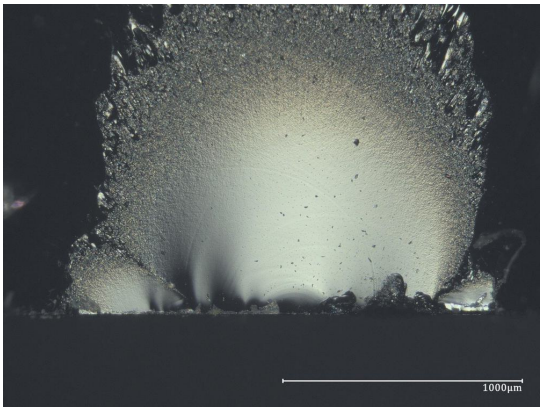

(a) S90 first view

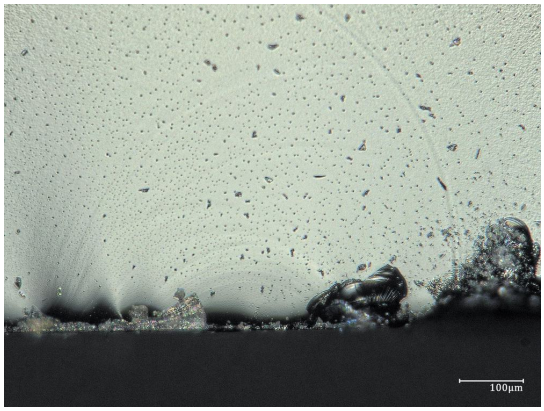

(b) S90 second view

Figure D.3: Different views of S90 (83 MPa)

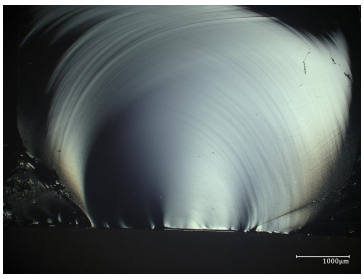

(a) S91 first view

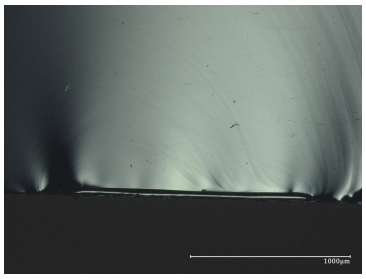

(b) S91 second view

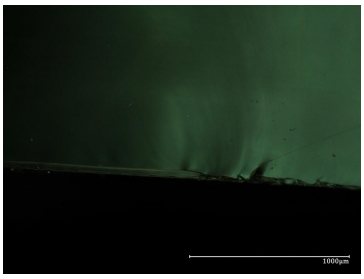

(c) S91 third view

Figure D.4: Different views of S91 (50 MPa)

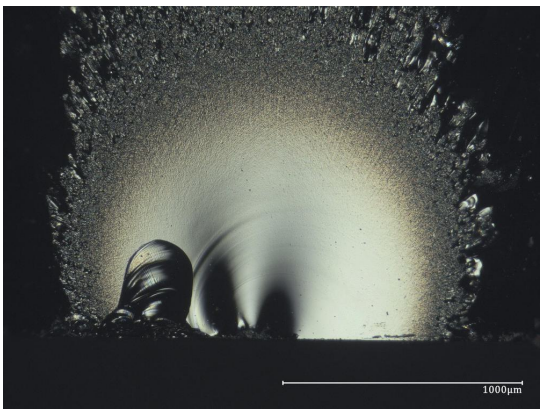

(a) S145 first view

(b) S145 second view

Figure D.5: Different views of S145 (81 MPa)

Naturally aged glass with thermal treatment of 500 degrees

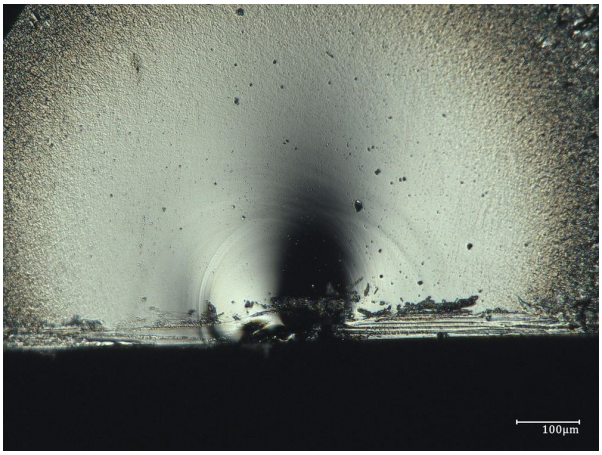

Figure D.6: View of S36 (102 MPa)

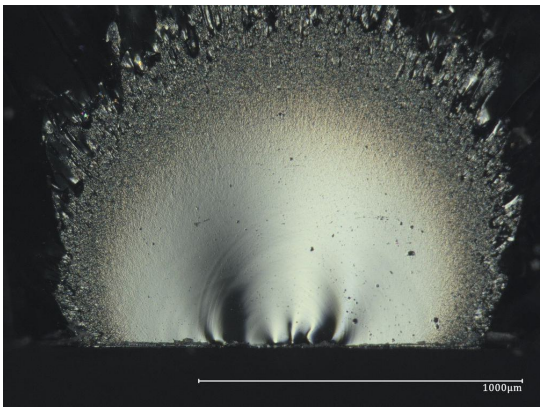

(a) S41 first view

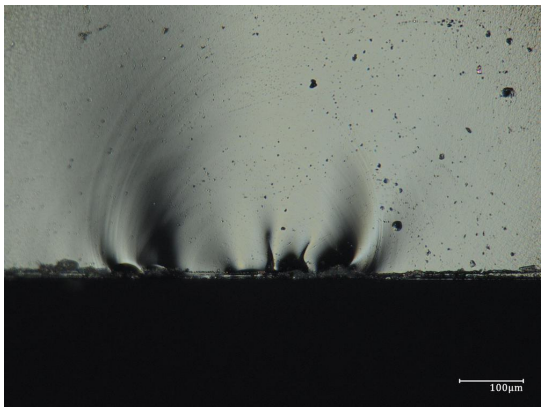

(b) S41 second view

Figure D.7: Different views of S41 (86 MPa)

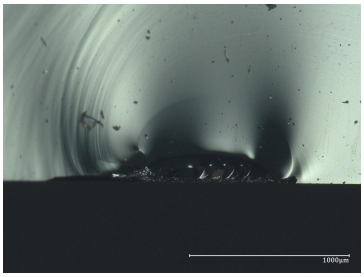

(a) S55 first view

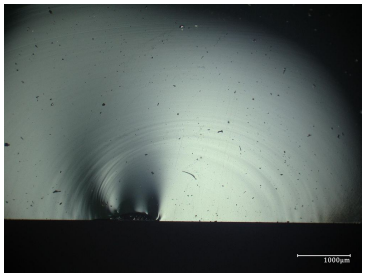

(b) S55 second view

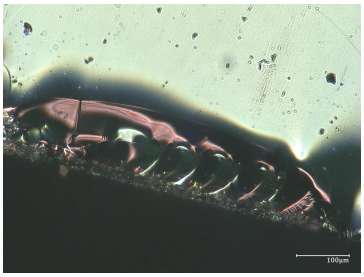

(c) S55 third view

Figure D.8: Different views of S55 (35 MPa)

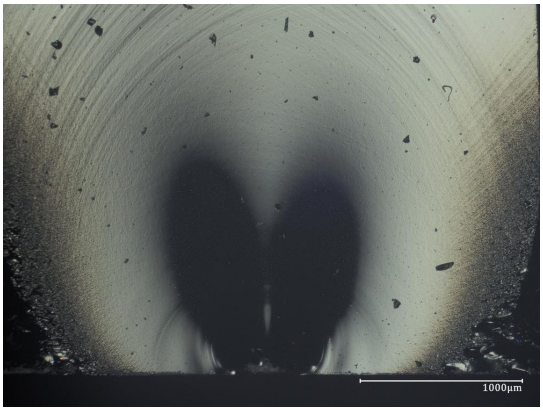

(a) S113 first view

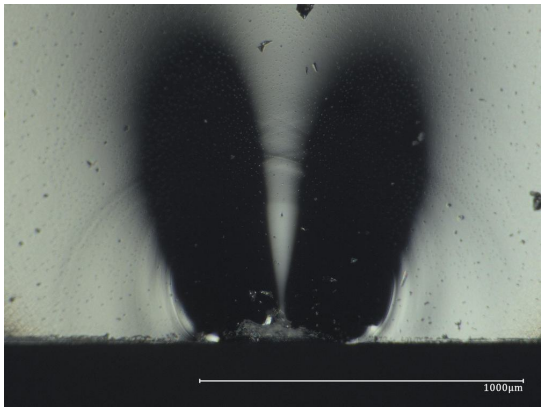

(b) S113 second view

Figure D.9: Different views of S113 (62 MPa)

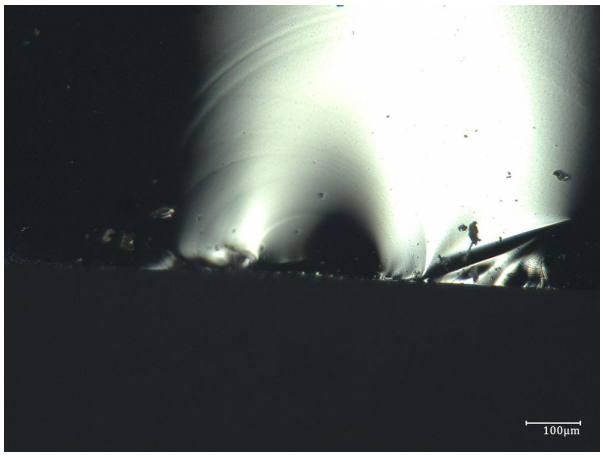

Figure D.10: View of S114 (78 MPa)

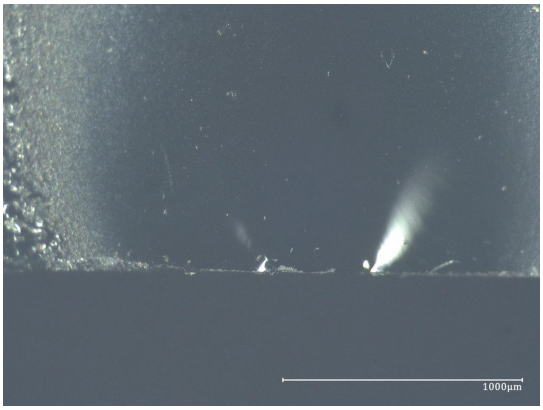

(a) S144 first view

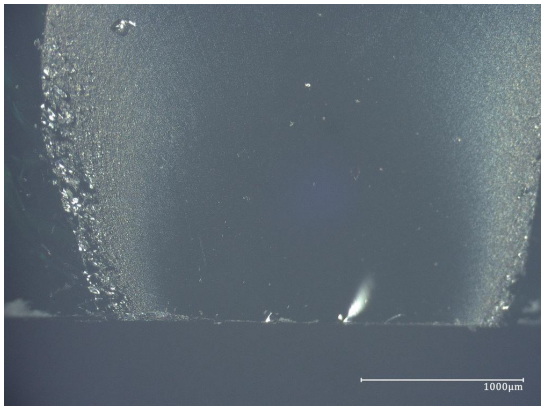

(b) S144 second view

Figure D.11: Different views of S144 (63 MPa)

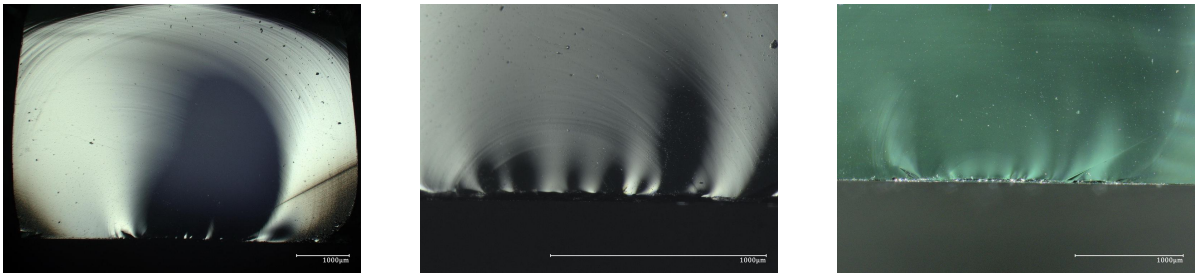

(a) S156 first view **(b)** S156 second view **(c)** S156 third view

Figure D.12: Different views of S156 (43 MPa)

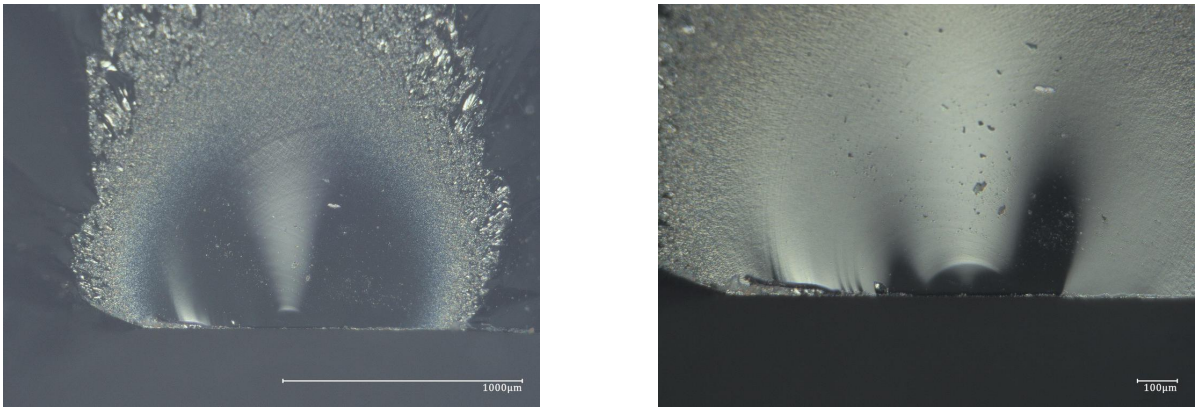

(a) S175 first view **(b)** S175 second view

Figure D.13: Different views of S175 (79 MPa)

Naturally aged glass with thermal treatment of 600 degrees

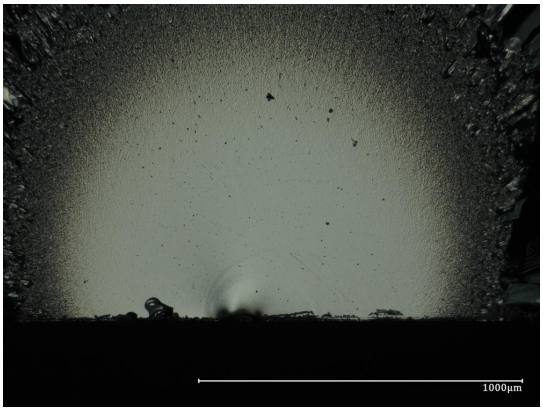

(a) S57 first view

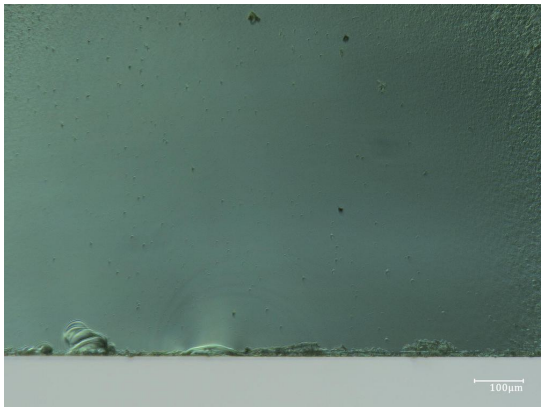

(b) S57 second view

Figure D.14: Different views of S57 (61 MPa)

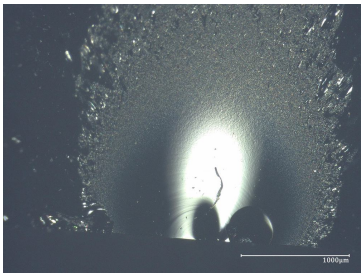

(a) S72 first view

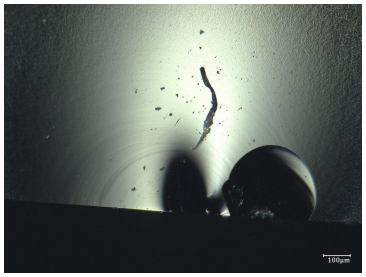

(b) S72 second view

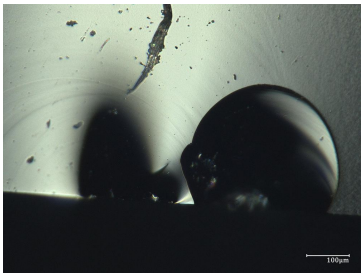

(c) S72 third view

Figure D.15: Different views of S72 (67 MPa)

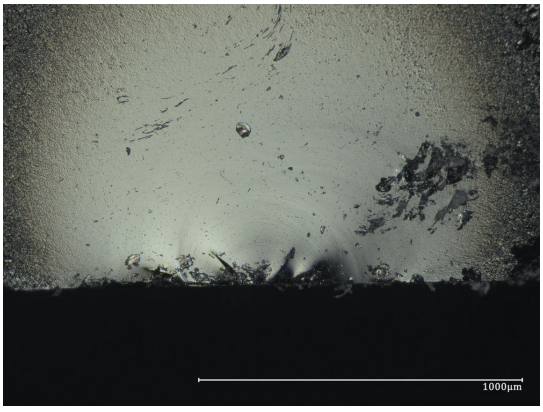

(a) S117 first view

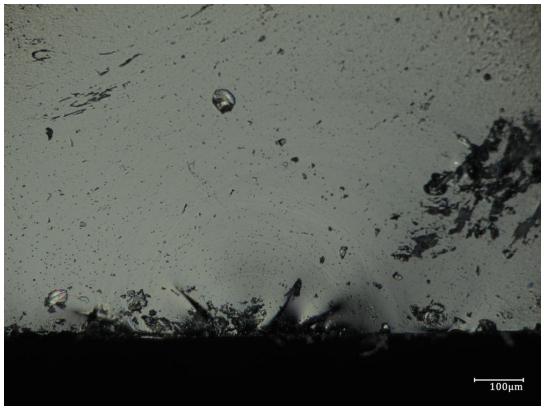

(b) S117 second view

Figure D.16: Different views of S117 (31 MPa)

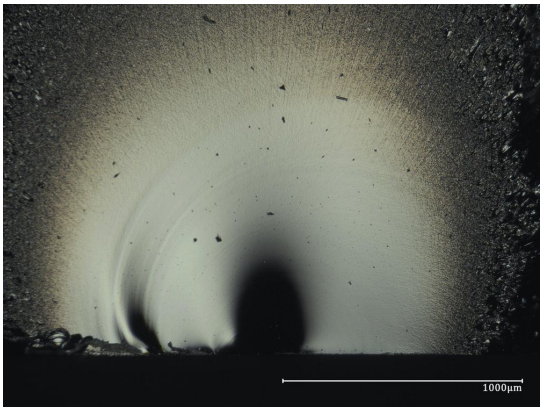

(a) S143 first view

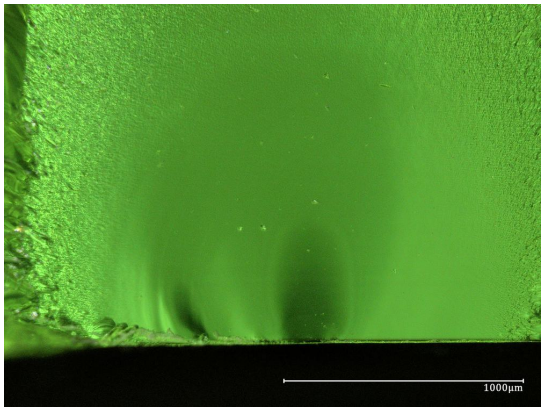

(b) S143 second view

Figure D.17: Different views of S143 (82 MPa)

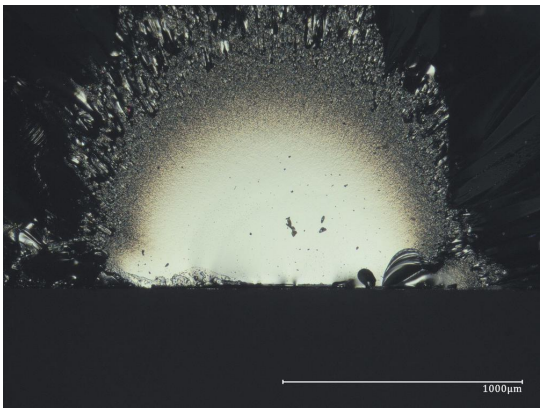

(a) S174 first view

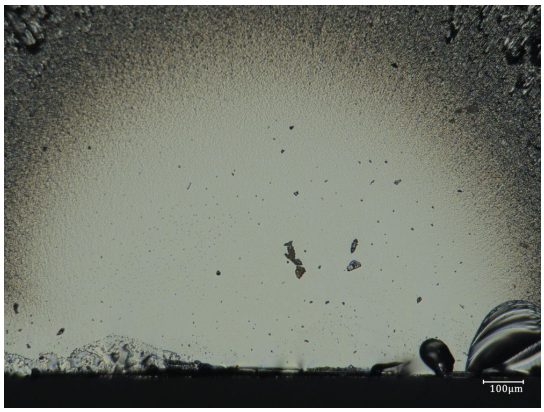

(b) S174 second view

Figure D.18: Different views of S174 (48 MPa)

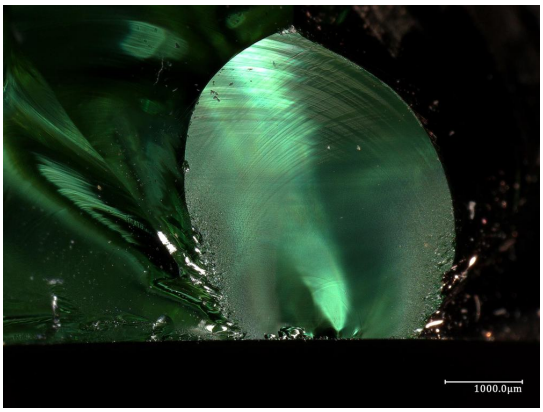

(a) S184 first view

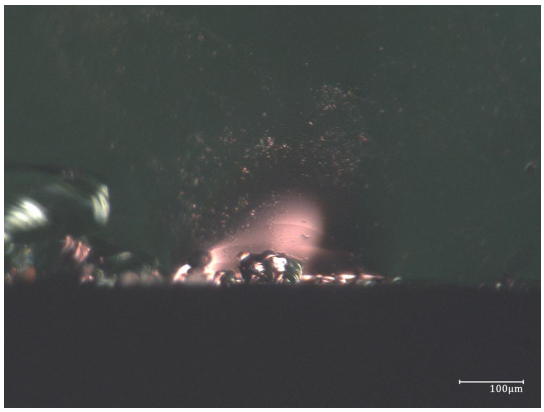

(b) S184 second view

Figure D.19: Different views of S184 (45 MPa)

Artificially aged glass without thermal treatment

(a) S16 first view

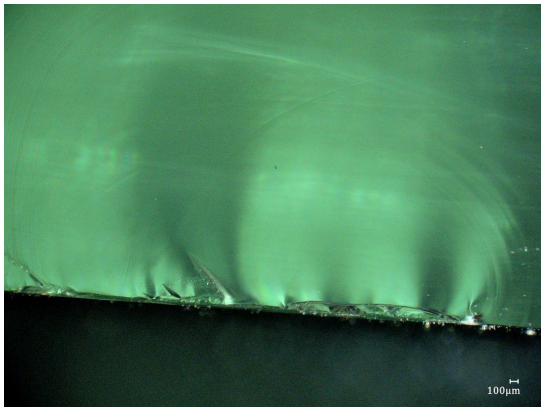

(b) S16 second view

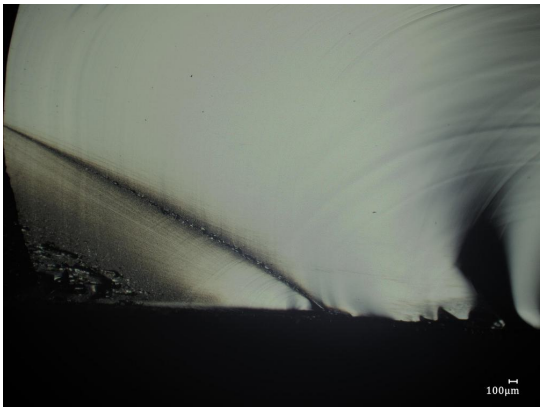

(c) S16 third view

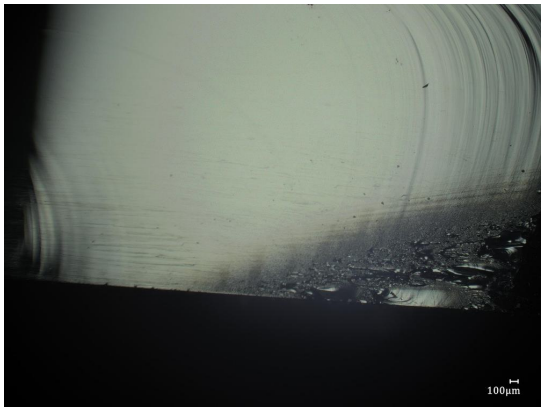

(d) S16 fourth view

Figure D.20: Different views of S16 (36 MPa)

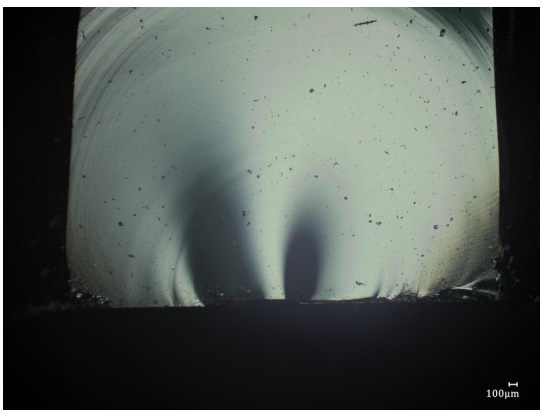

(a) S27 first view

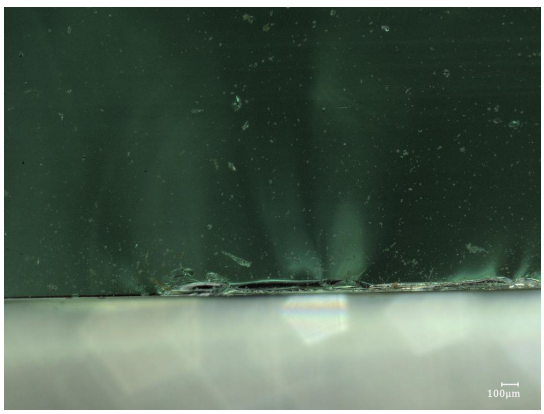

(b) S27 second view

Figure D.21: Different views of S27 (51 MPa)

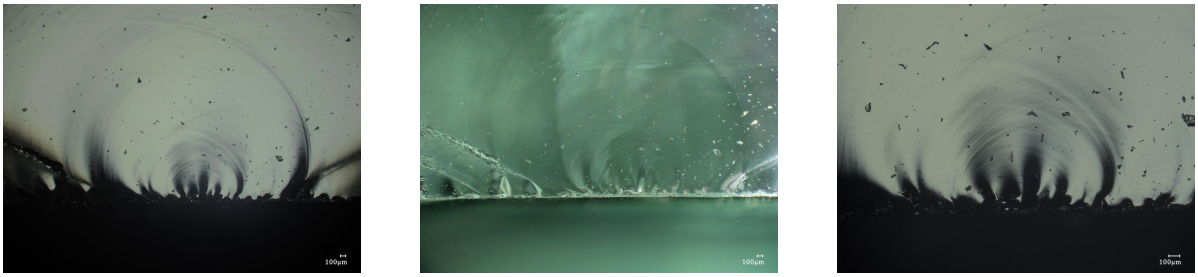

(a) S65 first view **(b)** S65 second view **(c)** S65 third view

Figure D.22: Different views of S65 (46 MPa)

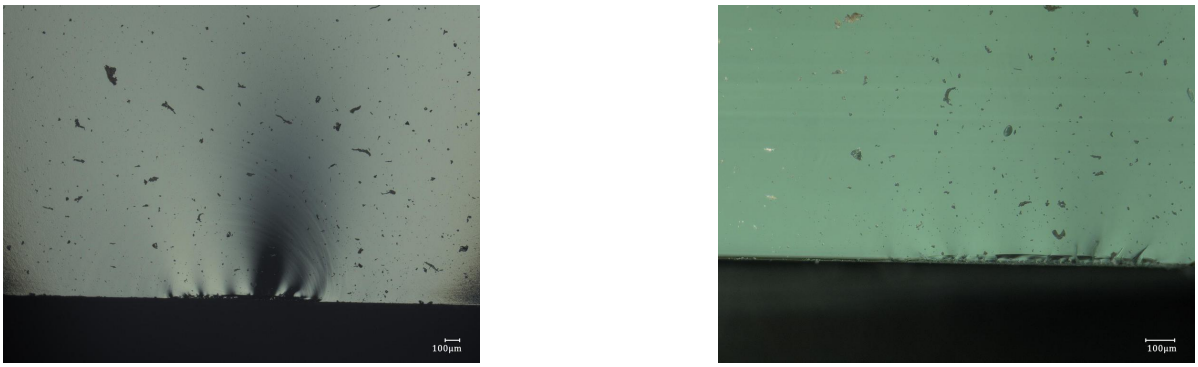

(a) S108 first view **(b)** S108 second view

Figure D.23: Different views of S108 (54 MPa)

(a) S127 first view **(b)** S127 second view **(c)** S127 third view

Figure D.24: Different views of S127 (37 MPa)

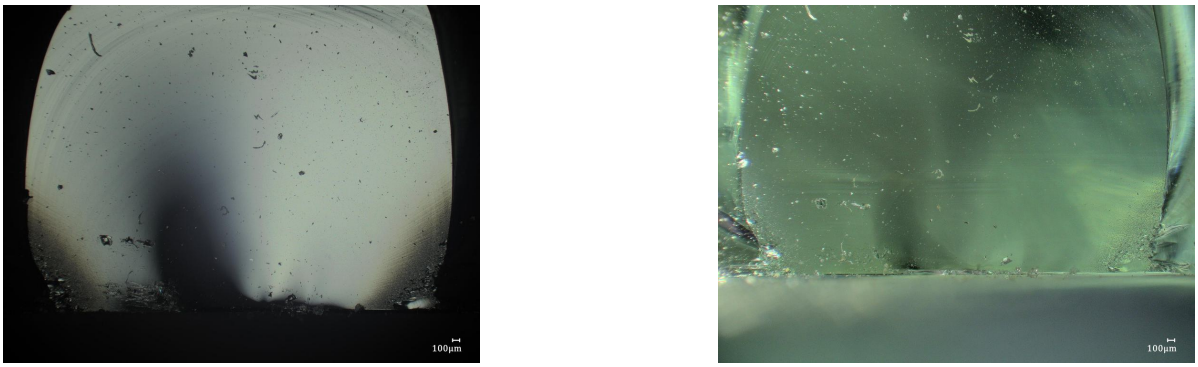

(a) S179 first view **(b)** S179 second view

Figure D.25: Different views of S179 (50 MPa)

Artificially aged glass with thermal treatment of 500 degrees

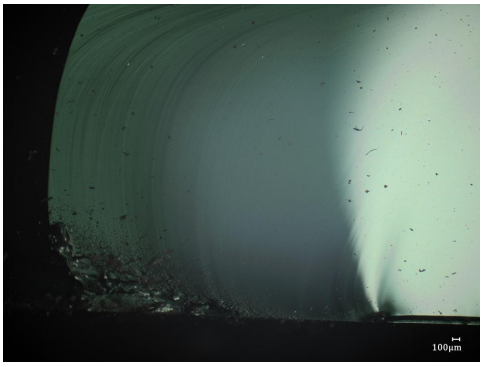

(a) S5 first view

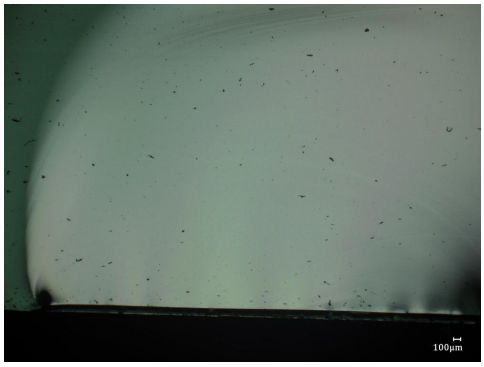

(b) S5 second view

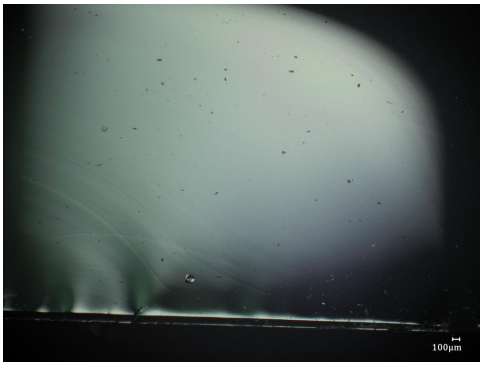

(c) S5 third view

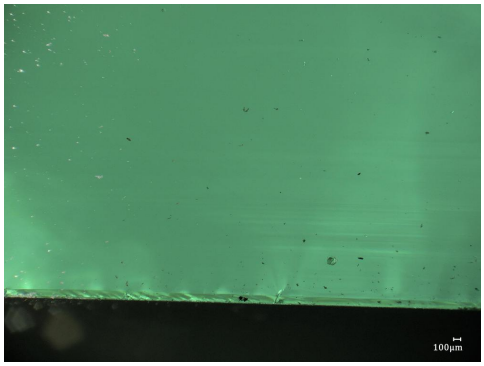

(d) S5 fourth view

Figure D.26: Different views of S5 (33 MPa)

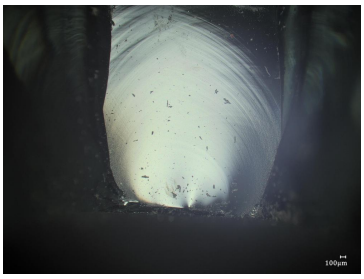

(a) S18 first view

(b) S18 second view

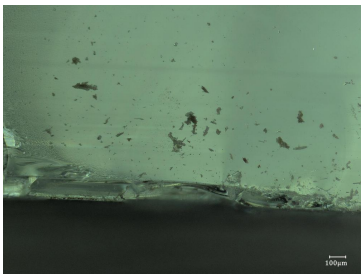

(c) S18 third view

Figure D.27: Different views of S18 (61 MPa)

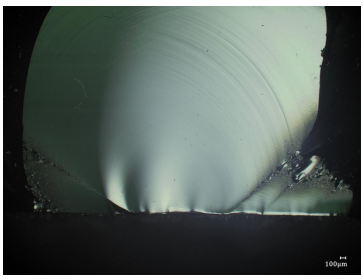

(a) S188 first view

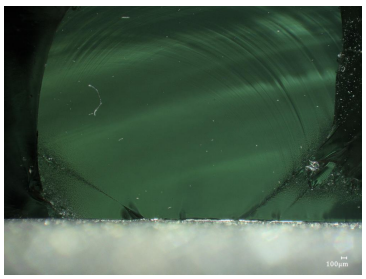

(b) S188 second view

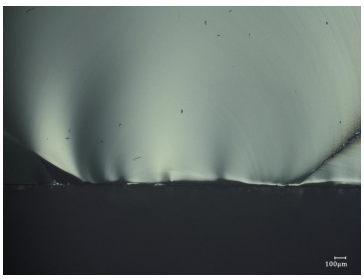

(c) S188 third view

Figure D.28: Different views of S188 (47 MPa)

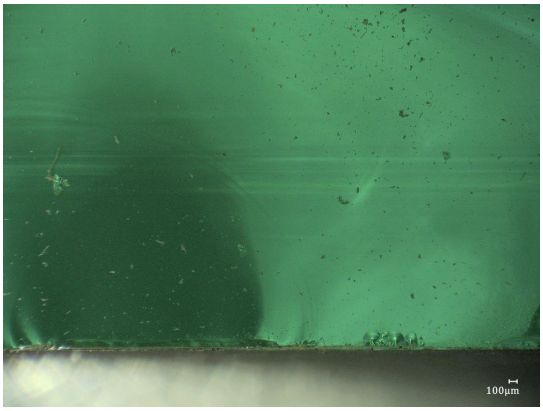

(a) S153 first view

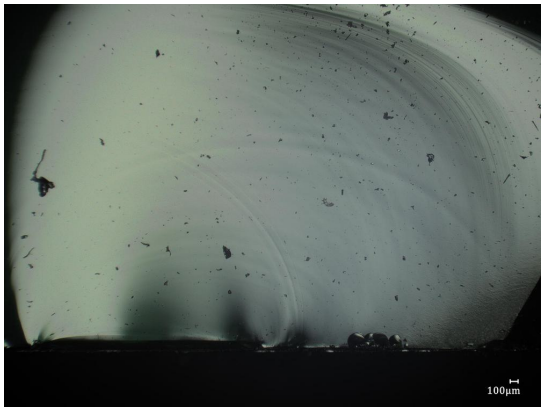

(b) S153 second view

Figure D.29: Different views of S153 (35 MPa)

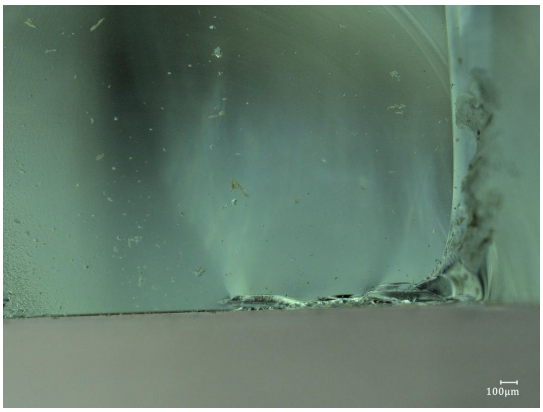

(a) S157 first view

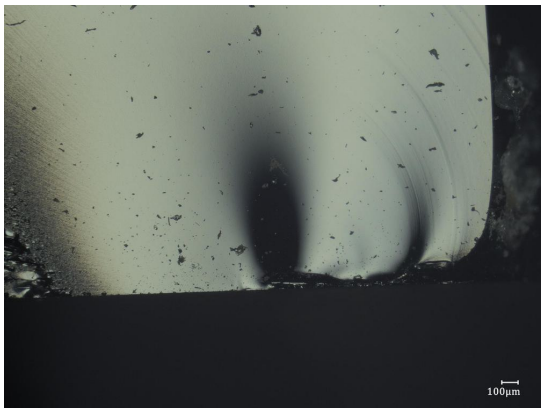

(b) S157 second view

Figure D.30: Different views of S157 (56 MPa)

(a) S185 first view

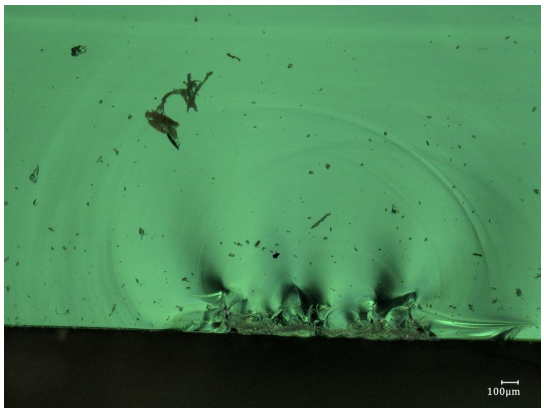

(b) S185 second view

Figure D.31: Different views of S185 (41 MPa)

Artificially aged glass with thermal treatment of 600 degrees

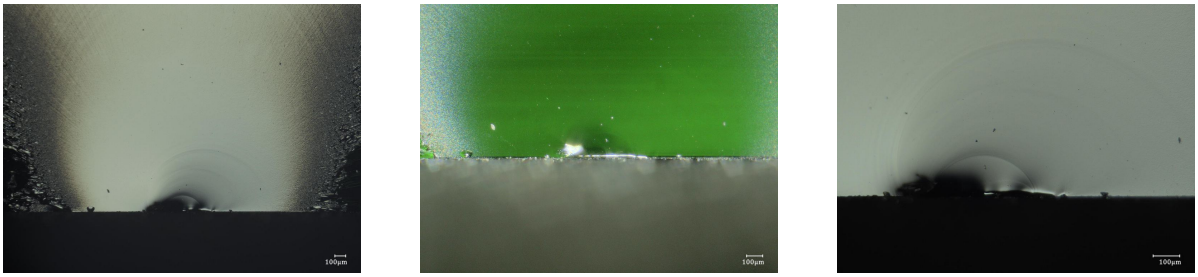

(a) S15 first view **(b)** S15 second view **(c)** S15 third view

Figure D.32: Different views of S15 (28 MPa)

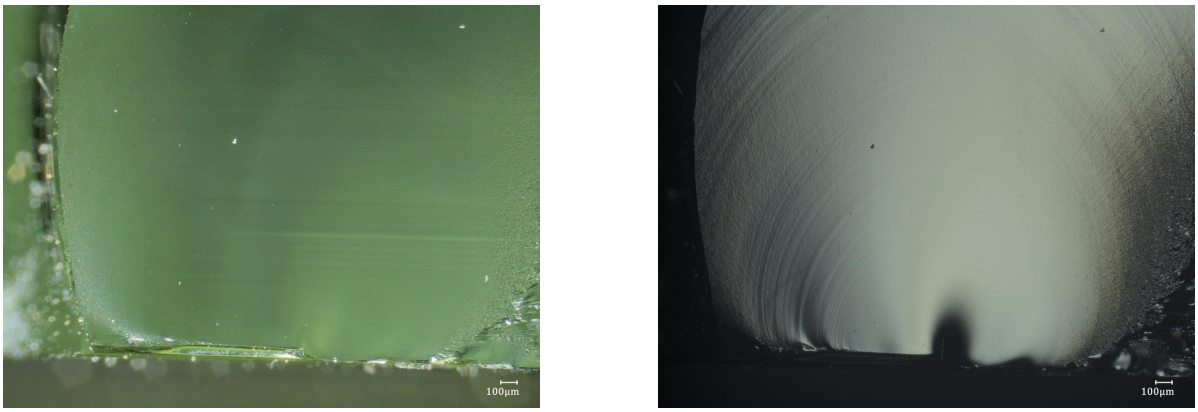

(a) S59 first view **(b)** S59 second view

Figure D.33: Different views of S59 (53 MPa)

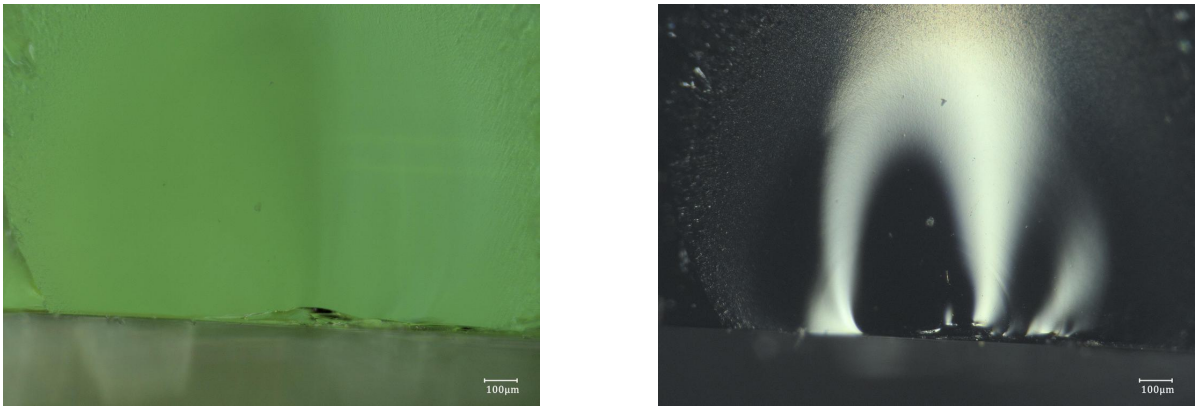

(a) S107 first view **(b)** S107 second view

Figure D.34: Different views of S107 (79 MPa)

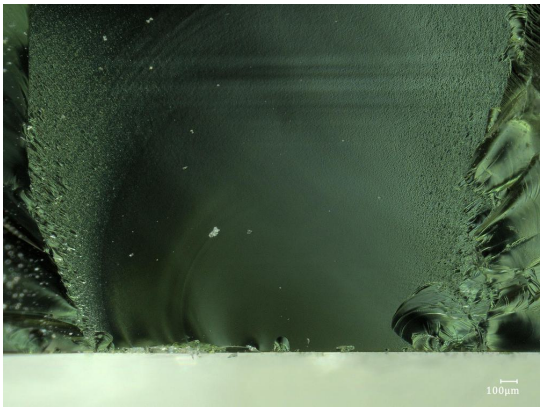

(a) S126 first view

(b) S126 second view

Figure D.35: Different views of S126 (54 MPa)

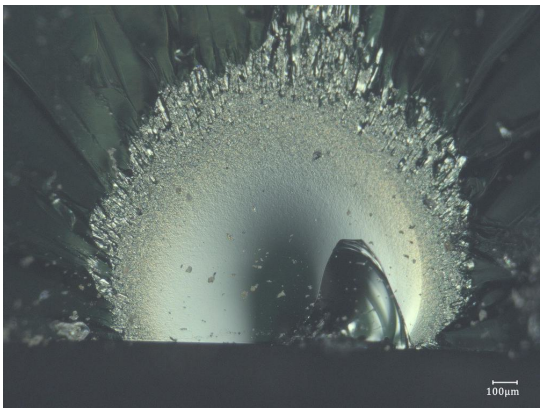

(a) S136 first view

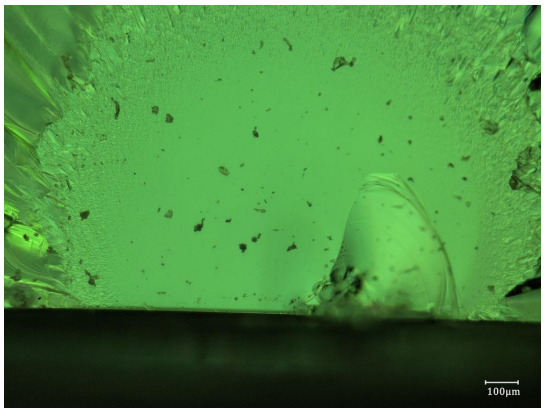

(b) S136 second view

Figure D.36: Different views of S136 (68 MPa)

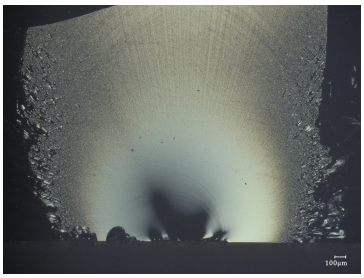

(a) S170 first view

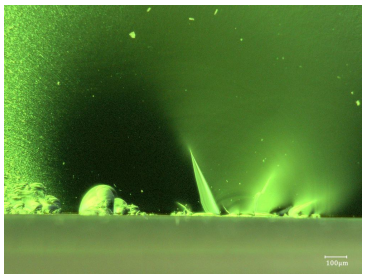

(b) S170 second view

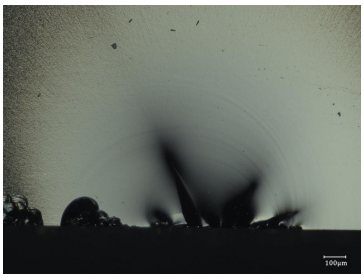

(c) S170 third view

Figure D.37: Different views of S170 (Invalid)

E

Appendix E: Data ring test

Datafile	Location of failure	Fbreakage (N)	$\delta_{failure}$ (mm)	$t_{failure}$ (s)	Stiffness (N/mm)	T (°C)	RH (%)	σ_f (MPa)
M1_S3	IR	14590	0.478	5.44	30520	24.9	38,0	112.99
M1_S6	IR	13435	0.441	5.03	30456	24.9	38,0	103.91
M1_S8	IR	16914	0.555	6.33	30460	24.8	38.2	128.85
M1_S14	IR	14942	0.492	5.59	30347	24.7	38.5	115.27
M1_S39	LR	7921	0.282	3.18	28103	24.6	38.5	61.65
M1_S42	IR	10221	0.336	3.85	30440	26.73	50.22	80.63
M1_S64	IR	12530	0.431	4.9	29106	24.8	39.2	99.29
M1_S73	LR	18518	0.629	7.2	29427	24.8	40,0	146.17
M1_S76	IR	9633	0.343	3.9	28081	24.8	39.9	77.07
M1_S78	LR	6910	0.248	2.81	27830	24.8	40.2	55.21
M1_S90	LR	10392	0.36	4.06	28875	24.8	40.2	82.56
M1_S91	IR	6243	0.225	2.54	27797	24.9	40.2	49.72
M1_S95	IR	11559	0.4	4.52	28890	24.9	40.2	91.53
M1_S96	LR	16977	0.574	6.56	29571	24.9	40.1	135.04
M1_S112	IR	13725	0.462	5.27	29727	24.9	40.1	107.17
M1_S120	IR	12410	0.419	4.8	29652	24.9	40.3	96.96
M1_S122	IR	11515	0.377	4.31	30550	26.7	50.28	89.46
M1_S125	IR	11583	0.394	4.49	29389	24.9	39.9	89.81
M1_S138	IR	14249	0.474	5.38	30088	24.8	39.5	109.86
M1_S145	IR	10600	0.356	4.07	29735	24.8	39.5	81.16
M1_S149	LR	8714	0.302	3.42	28812	24.8	39.4	66.38
M1_S150	IR	12987	0.434	4.97	29909	24.8	39.4	99.5
M1_S159	IR	13188	0.439	4.99	30054	24.9	39.2	100.97
M1_S162	LR	8511	0.279	3.18	30519	26.72	50.61	65
M1_S164	IR	11909	0.396	4.54	30077	24.8	39.1	90.89
M1_S167	LR	13878	0.459	5.22	30222	24.8	39,0	106.12
M1_S180	IR	13559	0.454	5.18	29838	24.9	38.7	104.74
M1_S181	LR	15030	0.501	5.72	29993	24.9	38.4	116.69
M2_S1	IR	15901	0.521	5.95	30530	24.9	40.8	122.36
M2_S22	IR	10351	0.33	3.79	31382	26.75	50.19	79.85
M2_S31	LR	14237	0.473	5.37	30110	24.9	40.6	110.88
M2_S32	OR	12117	0.407	4.66	29776	24.8	40.7	94.07
M2_S36	LR	13075	0.441	5,00	29643	24.9	40.8	102.09
M2_S41	IR	11033	0.377	4.29	29243	24.9	40.8	86.31
M2_S46	IR	7417	0.261	2.96	28400	24.9	40.8	57.58
M2_S51	LR	14008	0.473	5.43	29626	24.7	41.6	110.64

Datafile	Location of failure	Fbreakage (N)	$\delta_{failure}$ (mm)	$t_{failure}$ (s)	Stiffness (N/mm)	T (°C)	RH (%)	σ_f (MPa)
M2_S53	LR	11325	0.394	4.49	28772	24.7	41.5	89.16
M2_S55	IR	4421	0.169	1.91	26218	24.7	41.3	34.99
M2_S58	IR	14706	0.496	5.66	29672	24.7	40.2	115.93
M2_S60	LR	6896	0.242	2.74	28454	24.7	40.3	54.33
M2_S67	IR	7912	0.284	3.23	27874	24.7	40.4	62.73
M2_S80	IR	11209	0.389	4.43	28795	24.7	40,0	88.82
M2_S82	IR	9029	0.303	3.45	29830	26.76	50.56	71.5
M2_S84	LR	13111	0.453	5.16	28932	24.7	40,0	104.69
M2_S100	LR	10973	0.377	4.32	29110	24.6	40,0	86.45
M2_S103	IR	8059	0.282	3.22	28565	24.6	39.9	63.29
M2_S113	IR	7905	0.28	3.18	28245	24.6	39.8	62.28
M2_S114	LR	9953	0.344	3.89	28958	24.5	39.3	77.76
M2_S116	IR	8093	0.262	3.03	30857	26.76	50.96	63.39
M2_S140	IR	15996	0.519	5.96	30810	24.6	39.1	123.64
M2_S144	IR	8105	0.277	3.16	29218	24.6	39.1	62.69
M2_S147	IR	15800	0.513	5.87	30811	24.5	39.5	121.35
M2_S152	LR	12509	0.411	4.71	30419	24.6	39,0	96.02
M2_S156	IR	5539	0.199	2.28	27795	24.6	39,0	42.54
M2_S175	IR	10371	0.348	3.98	29771	24.5	39.4	79.3
M2_S192	LR	9637	0.327	3.72	29500	24.5	39.4	74.11
M3_S7	OR	8353	0.348	4,00	23985	25.14	41.7	64.24
M3_S29	IR	4077	0.302	3.44	13508	25.14	41.96	31.61
M3_S38	OR	7564	0.287	3.26	26373	25.14	42.01	59.17
M3_S44	IR	11039	0.379	4.37	29143	26.77	49.9	86.97
M3_S56	OR	7454	0.275	3.13	27122	25.17	41.9	58.84
M3_S57	IR	7778	0.289	3.28	26940	25.17	41.81	61.4
M3_S66	OR	7077	0.313	3.6	22603	25.17	41.63	55.93
M3_S68	LR	5956	0.326	3.7	18269	25.15	42.12	47.22
M3_S72	IR	8411	0.309	3.51	27212	25.13	42.5	66.95
M3_S92	OR	9422	0.344	3.93	27405	25.14	42.2	74.42
M3_S98	LR	11590	0.412	4.72	28131	25.17	42.21	91.02
M3_S99	OR	8165	0.387	4.46	21108	26.77	50.06	64.33
M3_S104	LR	5816	0.283	3.22	20540	25.14	42.58	45.7
M3_S106	OR	6304	0.308	3.5	20442	25.13	42.58	49.66
M3_S117	IR	3923	0.347	3.92	11291	25.1	42.52	30.71
M3_S124	IR	9382	0.316	3.59	29677	25.11	42.68	72.89
M3_S139	IR	8023	0.295	3.39	27231	25.13	42.47	61.78
M3_S143	LR	10655	0.377	4.28	28233	25.15	42.3	81.94
M3_S146	OR	6864	0.278	3.18	24692	26.76	50.29	52.59
M3_S160	LR	14266	0.491	5.58	29031	25.18	42.42	108.75
M3_S163	OR	11828	0.44	5.01	26863	25.19	42.6	90.16
M3_S165	IR	6219	0.266	3.03	23384	25.14	42.95	47.35
M3_S166	LR	11892	0.424	4.86	28040	25.16	42.48	90.82
M3_S174	LR	6242	0.312	3.55	20015	25.17	42.66	47.82
M3_S184	IR	5786	0.243	2.75	23826	25.19	42.84	44.75
M3_S187	OR	6158	0.376	4.26	16380	25.22	42.62	47.57
M3_S190	LR	6993	0.352	4,00	19861	25.2	43.16	53.95
M4_S13	IR	4586	0.154	1.75	29707	26.65	53.95	35.85
M4_S16	IR	4587	0.154	1.76	29755	26.65	53.8	35.95
M4_S17	ND	3462	0.567	44.32	6100	26.65	54.39	27.07
M4_S25	IR	4627	0.156	1.78	29748	26.65	54.01	36.36
M4_S27	IR	6518	0.218	2.48	29936	26.63	53.94	51.09
M4_S40	IR	5109	0.175	1.99	29269	26.59	53.87	40.46
M4_S43	IR	4362	0.151	1.69	28954	26.57	53.9	34.54

Datafile	Location of failure	Fbreakage (N)	$\delta_{failure}$ (mm)	$t_{failure}$ (s)	Stiffness (N/mm)	T (°C)	RH (%)	σ_f (MPa)
M4_S50	IR	4897	0.17	1.9	28860	26.55	54.29	39.08
M4_S54	IR	4936	0.169	1.91	29268	26.55	53.87	39.49
M4_S65	IR	5751	0.199	2.27	28831	26.55	54.76	46.25
M4_S75	IR	5158	0.185	2.05	27909	26.54	54.22	41.7
M4_S77	IR	4988	0.176	2,00	28308	26.55	54.55	40.32
M4_S83	IR	6457	0.227	2.57	28464	26.58	54.76	52.2
M4_S88	IR	8643	0.292	3.33	29576	26.61	54.32	68.97
M4_S101	IR	4061	0.141	1.61	28703	26.61	54.54	32.24
M4_S102	IR	5498	0.186	2.09	29556	26.65	54.48	43.43
M4_S108	IR	6847	0.234	2.65	29281	26.64	54.53	54.08
M4_S111	IR	5596	0.19	2.14	29391	26.68	53.9	43.97
M4_S121	IR	5005	0.171	1.92	29215	26.72	54.19	39.03
M4_S123	IR	4325	0.149	1.68	28975	26.72	54.69	33.9
M4_S127	IR	4799	0.161	1.84	29720	26.73	54.45	37.33
M4_S132	IR	3942	0.139	1.54	28424	26.77	53.6	30.82
M4_S133	IR	5065	0.17	1.93	29807	26.78	53.63	39.1
M4_S134	IR	5459	0.183	2.07	29834	26.81	54.53	42.14
M4_S142	IR	4431	0.154	1.73	28853	26.83	53.6	34.38
M4_S172	IR	4525	0.155	1.74	29185	26.83	53.64	34.76
M4_S173	IR	4822	0.162	1.84	29692	26.83	54.55	36.85
M4_S179	IR	6450	0.214	2.41	30142	26.85	53.83	49.54
M5_S2	IR	4106	0.178	1.99	23088	26.58	54.23	31.78
M5_S5	IR	4207	0.143	1.62	29482	26.62	53.81	32.64
M5_S18	IR	7841	0.263	3.01	29859	26.62	53.97	61.15
M5_S28	IR	6612	0.222	2.51	29745	26.64	54.27	51.69
M5_S49	IR	6348	0.222	2.51	28629	26.64	54.36	50.27
M5_S61	IR	6511	0.226	2.56	28788	26.66	53.49	51.82
M5_S62	IR	5245	0.187	2.1	28060	26.68	53.4	41.64
M5_S74	IR	5525	0.194	2.21	28433	26.68	54.08	43.98
M5_S79	IR	4728	0.169	1.9	27976	26.69	53.46	38.12
M5_S81	IR	5336	0.188	2.13	28402	26.7	53.74	42.69
M5_S87	IR	4800	0.17	1.93	28167	26.72	53.79	38.3
M5_S94	IR	5927	0.208	2.33	28502	26.71	53.73	47.3
M5_S109	IR	4828	0.165	1.85	29196	26.72	53.72	38.04
M5_S110	IR	5498	0.187	2.11	29477	26.71	53.9	43.2
M5_S118	IR	6258	0.212	2.38	29519	26.7	54.5	48.93
M5_S128	IR	5623	0.189	2.13	29737	26.7	54.39	43.85
M5_S129	IR	6317	0.211	2.38	29892	26.7	55.01	49.51
M5_S141	IR	4461	0.148	1.67	30173	26.7	53.91	34.7
M5_S148	IR	5089	0.169	1.9	30133	26.72	54.51	39.19
M5_S153	IR	4518	0.148	1.69	30461	26.7	53.83	34.88
M5_S157	IR	7365	0.239	2.69	30862	26.7	54.08	56.43
M5_S158	IR	4495	0.151	1.7	29677	26.71	53.9	34.52
M5_S161	IR	4937	0.165	1.88	29834	26.72	53.76	37.82
M5_S177	IR	8256	0.264	3.01	31252	26.72	53.62	63.73
M5_S182	IR	5346	0.18	2.03	29751	26.71	54.16	41.37
M5_S185	IR	5282	0.174	1.95	30419	26.72	54.19	40.98
M5_S188	IR	6080	0.201	2.26	30306	26.73	53.6	47.41
M5_S189	IR	7108	0.234	2.63	30360	26.74	54.08	55.29
M6_S4	IR	4162	0.302	3.47	13768	27.01	52.39	32.13
M6_S15	IR	3651	0.314	3.68	11608	27.04	52.15	28.33
M6_S23	IR	5423	0.214	2.46	25354	27.19	50.65	41.97
M6_S26	IR	8140	0.303	3.45	26885	27.16	50.88	63.8
M6_S30	IR	7209	0.268	3.08	26921	27.08	51.2	56.36

Datafile	Location of failure	Fbreakage (N)	$\delta_{failure}$ (mm)	$t_{failure}$ (s)	Stiffness (N/mm)	T (°C)	RH (%)	σ_f (MPa)
M6_S37	IR	6609	0.282	3.25	23409	27.07	51.87	51.8
M6_S52	IR	7505	0.266	3.04	28206	27.06	51.56	59.58
M6_S59	IR	6709	0.281	3.23	23840	27.06	51.82	52.99
M6_S63	IR	5739	0.242	2.77	23714	27.03	51.81	45.92
M6_S71	IR	8852	0.347	3.96	25514	27.02	52.1	70.82
M6_S85	IR	7319	0.431	4.95	16980	26.96	51.89	58.41
M6_S86	OR	7536	0.32	3.68	23584	26.93	51.79	60.14
M6_S97	OR	9086	0.366	4.2	24850	26.9	51.62	71.77
M6_S107	IR	9980	0.377	4.31	26506	26.9	52.18	79.03
M6_S115	OR	5865	0.337	3.89	17393	26.92	51.39	45.97
M6_S119	OR	6642	0.309	3.55	21509	26.95	52.29	51.67
M6_S126	IR	6954	0.257	2.97	27076	26.94	51.4	54.23
M6_S131	IR	7273	0.312	3.57	23301	26.98	51.01	56.43
M6_S135	IR	7093	0.278	3.22	25547	27,0	51.69	54.75
M6_S136	IR	8642	0.327	3.76	26464	26.99	50.51	67.74
M6_S151	IR	8906	0.334	3.82	26638	26.97	50.65	68.75
M6_S154	IR	4904	0.337	3.86	14545	26.97	50.37	37.76
M6_S169	IR	6625	0.301	3.44	21982	26.96	50.39	51.14
M6_S170	OR	7538	0.268	3.1	28078	26.95	50.12	58.19
M6_S176	IR	8612	0.293	3.39	29368	26.94	50.32	66.31
M6_S178	IR	7433	0.327	3.76	22739	26.93	50.42	57.09
M6_S186	IR	6484	0.278	3.2	23316	26.93	50.13	50.18
M6_S191	IR	6508	0.288	3.29	22570	26.93	50.19	50.49